

Faculty of Engineering of the University of Porto



FEUP

**Dynamically adhesive micropatterned substrates for studying and
controlling cell adhesion and migration**

Ana Catarina Laly Águedo

PROVISIONAL VERSION

Dissertation developed within the framework of the Integrated Master in
Bioengineering
Major - Biomedical Engineering

Coordinator: Prof. Dr. John Connelly
Co-Coordinator: Dr. Patrícia Costa
Co-Coordinator: Prof. Dr. Pedro Granja

September 2015

Abstract

Wound healing is a restorative and complex process essential for human survival and typically triggered when an injury occurs. In the case of skin this process is especially important since it is the largest organ of the body and performs a wide range of fundamental and physiological functions in order to preserve human homeostasis. When an injury occurs the capacity of the skin to heal is triggered. However, in some cases, abnormal wound healing leads to an inefficient regeneration of the skin. In fact, chronic wounds, or wounds that do not heal, are among the major health concerns in the modern world, being more prevalent in the elderly, a rising age group. To provide a better understanding about wound healing processes and to facilitate discovery of new clinical approaches a large number of assays have been developed. Due to the inefficiency of *in vitro* assays, a relevant part of these assays are *in vivo* assays, thereby implicating a significant amount of sacrificed animals. For these reasons it is important to develop efficient advanced *in vitro* wound healing studies in order to foster wound healing research while reducing animals' suffering.

The present work was aimed at creating new *in vitro* high throughput strategies for cell migration and wound healing studies. Based in a previously established technique by this team, two different formats were designed, both using dynamically adhesive micropatterned substrates with either a 400 or a 200 μm islands pattern. For the first format, consisting in a 50 well silicone approach, several optimizations were performed including cell seeding density, as well as brushes photoactivation efficacy and consistency along the wells. Brushes photoactivation showed to reach a peak with a RGD-BT concentration of 2.5 mg/mL, while consistency along the wells showed to be reasonable. Five cell lines were studied with the help of scratch assays, allowing to select HCA2 as the ideal cell line to use in further studies. A wound closure assay was performed correlating RGD concentration with HCA2 cell migration rate, demonstrating that between 2 and 3 mg/mL cells did not exhibit significant differences. An inhibitors assay was performed both with and without polymeric brushes and cells showed to react differently to distinct inhibitor concentrations, although wound closure could not be correlated with inhibitors. Regarding the 96 well plate approach, after a design development phase, necessary materials were selected and initial optimizations were performed. The final phase of the present work was focused in the development of InCell imaging and respective protocols for automated analysis of cell processes. We anticipate that these new *in vitro* strategies can bring new insights in cell migration studies, reducing animals in research while providing an efficient method to compare different conditions.

Acknowledgements

My first and biggest thanks goes to John Connelly. Since the day he gave me the opportunity of joining his group until now he has been helping me building my path being a true mentor and support at the same time. Without his guidance none of this could be possible.

Another special thanks goes to Patrícia Costa, for teaching me patiently (almost) all that I needed to develop my work letting me learn from my own mistakes and showing me that companionship can rise from anywhere. To Filipe Almeida, thank you for your friendly criticisms and for helping me reach solutions without telling them. To the other not less important Connelly group members, Fiona Kenny, Roanne Jones, George Theocharidis and Alex Kao, thank you for sharing your experience and friendship during the last eight months. Another special thanks goes to Luke Gammon for his help with the InCell Microscopy.

To Professor Pedro Granja, I would like to thank for the inspirational classes he gave us some years ago that opened my eyes (and heart) to research as well as for his support during this final step of my Integrated Master.

To my little Cousin Beatriz (you will always be little for me), thank you for always giving me strength with your innate joy and love. Since you turned me your role model all decisions have become more important. To my parents and aunt, you are the reason why I am what I am today. Thank you for believing in me and giving me all the opportunities that I needed in order to reach my achievements. It is true that nothing can be compared to a family's support and I am very thankful for having you with me every day. To Foxy, my four legs soulmate, for bringing more humanity to my life. To my grandparents, Maria e Abílio, wherever you are, thank you for making me feel your hugs in the worst moments transmitting me your perseverance. To my brother and Patrícia, thank you for keeping me on track and showing me that everything is possible. To my second family, Família Santos, thank you for making me one of your own. Beatriz, Nicole, Miguel, D. Ruth e Sr. Joaquim, your support was more than essential for bringing this project together.

To Márcio, not even a million words could describe how much I have to thank you. Thank you for your patient, love, laughs, companionship and everything that you did to make this path more colourful even being so many kilometres away. You are my daily support, my best friend and my other half. Without your patient and love I would not be able of bringing this together, so this is your achievement too.

Another special thanks goes to Sofia Ribeiro for all her patient and support during these last months. Your help and friendship showed to be priceless.

To my other two *companheiros do crime* Nuno and João, I would like to thank for being part of this journey and for making it more “liveable”. This last three years would not be the same without you.

To Rita, thank you for being my home during the last months and for showing me that friendship can turn into sisterhood very easily. To Raquel, thank you for being there since the first day of this last eight years, growing by my side. To Kika, João and PV, thank you for sharing your friendship with me and making me laugh even in the worst moments. To all my other friends, Alexandra, Ana, André, Cláudia, Clara, Diogo, Francisca, Helena, Inês, Isabel, Joana, Joel, Lourenço, Luísa, Mélanie, Miguel, Pedro, Ricardo, Rita, Sara, Sílvia, Vasco e Vera, thank you for being present in my life. Your constant friendship and support made this a better journey.

Index

Chapter 1 Literature Review	1
1.1 Skin Structure and Wound Healing	1
<i>Types of Wound Healing</i>	2
<i>Abnormal Wound Healing</i>	5
1.2 Cell Migration	8
<i>Integrin Receptors</i>	12
<i>Contractility</i>	16
1.3 Migration Assays	19
<i>Scratch Assay</i>	19
<i>Cell Exclusion and Fence Zone Assays</i>	20
<i>Transwell Migration Assay</i>	21
1.4 Dynamic Systems	23
<i>Dynamically Adhesive Micropatterns</i>	24
<i>Caged RGD</i>	28
<i>High-Throughput screening strategies</i>	28
Chapter 2 The Project	33
<i>Aim</i>	33
<i>Context</i>	33
Chapter 3 Materials and Methods	35
3.1 Antibodies, Solutions and Inhibitors	35
3.2 General Patterning and Photoactivation	36
<i>Glass cleaning and gold covering</i>	36
<i>Photolithography and stamp preparation</i>	37
3.3 Micropatterned POEGMA brushes	38
<i>Photoactivation process based in thiol-ene and thio-yne reactions</i>	39
3.4 Assay Assembly	39
3.5 Cell Culture.....	39
<i>Micropatterned substrates</i>	40
<i>Scratch Assay</i>	40
<i>Inhibitors Assay</i>	41
3.6 Immunostaining.....	42
3.7 Cell Imaging and Analysis	42
3.8 Statistical Analysis	43
Chapter 4 Results	44

4.1	Optimization for new patterns and cells.....	44
4.2	New assemblies design	46
4.3	50 Well silicone approach optimization	50
4.4	96 well plate approach optimization	54
4.5	Scratch assays.....	55
4.6	Cell migration in photoactivated polymeric brushes.....	59
4.7	InCell microscopy and analysis.....	66
Chapter 5 Discussion.....		68
Chapter 6 Concluding Remarks and Future Work		74

List of Figures

Figure 1 - Skin structure [7].	1
Figure 2 - Integrin heterodimer schematic view [78].	13
Figure 3 - Different integrin dimers combination [79].	13
Figure 4 - Example of a scratch wound assay using MDCK (Madin-Darby Canine Kidney) cells infected with Cytomegalovirus (CMV). At right (a) it is exemplified the technique while at left (b) it is possible the results 0, 6 and 12h after scratch performance [170].	19
Figure 5 - Exclusion Zone (EZ) example with "Stopper" appliance [171].	21
Figure 6 - Transwell Migration Assay [172].	21
Figure 7 - Commercial culture insert kit available in the market (AutoMate Scientific).	22
Figure 8 - Brief scheme of photolithography process. A) SU8 deposition on top of wafer placed in the spinning disk; b) First 5 minutes baking; c) window, mask and wafer assembly under UV curing; d) secondary baking; e) SU8 rinsing; f) Final master with desired pattern.	37
Figure 9 - Stamped patterns used during the present work with a=400 μm and b=200 μm .	38
Figure 10 - Scratch assay example with red circles marking imaged sites of each assay.	40
Figure 11 - 400 μm islands with HeLa cells before (left) and after (right) optimization. Images were acquired 24 hours after cell seeding. Both scale bars are 100 μm .	45
Figure 12 - Cell seeding density optimization for all four cell lines in both patterns. Images were acquired 24 hours after cell seeding. On the left is possible to see cells seeded in a 400 μm islands pattern while on the right is possible to see cells seeded in a 200 μm islands pattern. All scale bars are 100 μm . Cells/ cm^2 ratio was calculated assuming a diameter of 1.55cm.	46
Figure 13 - Former approach. A) clean glass coverslip; b) gold covered coverslip; PDMS stamps with desire pattern; d1) microcontact printing - stamps soaked in initiator ink the reagent on the gold surface; d2) half of the coverslip cut in four squares; e) 1cmx1cm squares placed in a 24 well plate. The red dots represent the polymeric brushes islands.	47
Figure 14 - 96 well plate approach. A) clean customized glass; b) glass covered with gold; c) PDMS stamp cut with the desire format in order to fit the glass; d) Microcontact	

printing - this step would require a perfect alignment of the stamps preventing polymeric brushes overlap; e) customized glass attached to the plate and ready to use. The red dots represent the polymeric brushes islands.	47
Figure 16 - 50 well silicone approach. A) cleaned microscope slide; b) gold covered microscope slide; c) PDMS stamp cut according to the size of the microscope slide; d) microcontact printing of the microscope slide; e) Reusable 50 well silicone; f) 50 well silicone placement under microscope slide with polymeric brushes. The red dots represent the polymeric brushes islands.....	49
Figure 15 - Scheme view of the 50 well silicone from Grace Biolabs.....	49
Figure 17 - Real formats of different approaches. At left is the former approach, 24 well-plate format, with 4 1cmx1cm squares disposed in 4 wells. In the centre is the 96 well-plate format upside down, showing the glass adhered to the bottom of the plate. At right is the 50 well-silicone approach with cells already plated in the wells. .	50
Figure 18 - Photoactivated substrates after ethanol (left) and UV (right) sterilization. Both photoactivation were performed with a 1mg/mL RGD-BT concentration. Both scale bars are 100µm.	50
Figure 19 - UV position during polymeric brush photoactivation. UV light placed under (left) and above (right) substrates. Both photoactivations were performed with a 1mg/mL RGD-BT concentration. Both scale bars are 100µm.	51
Figure 20 - Brightness mean value of 400 µm islands after photoactivation using 9 different RGD-BT concentrations. This trend was observed in 2 of 3 independent experiments. The other experiment showed a higher variance between 0 and 0.5 mg/mL. N=6-24 depending on the number of brushes present in each acquired image. Data sets are significant at different levels * p<0.05, *** p<0.001 when compared with 2,5 mg/mL RGD-BT concentration.....	51
Figure 21 - Brightness mean value of 400 µm islands after photoactivation using a RGD-BT concentration of 2 mg/mL along a horizontal line of the 50 well silicone. This trend was observed in 3 independent experiments. This graph represents one of those experiments with n=5. The bottom figure represents the position of each well in the 50 well silicone. The P value between acquired results was 0.0793, considered not quite significant.	52
Figure 22 - Brightness mean value of 400 µm pillars after photoactivation using a RGD-BT concentration of 2 mg/mL along a vertical line of the 50 well silicone. This trend was observed in 3 independent experiments. This graph represents one of those two experiments, with n=5. The bottom figure represents the position of each well in the 50 well silicone. The P of wells 2,3,4 and 5 when compared with well 1 was not significant, however, data sets are significant at different levels * p<0.05, ** p<0.01 when compared with well number 4.	53
Figure 23 - Brightness mean value of 400µm islands according to their position in the well using a RGD-BT concentration of 2mg/mL. Marked with a red line is the region with the four highest values of brightness in contrast with the brushes of the same well. This trend was observed in 2 independent experiments, with an n=1 since brightness of each island was acquired as a whole.	53
Figure 24 - 400 µm (left) and 200 µm (right) islands with cells after cell seeding optimization. Images were acquired 24 hours after cell seeding Black lines in both images are the edge of the silicone wells. Both scale bars are 100 µm.....	54
Figure 25 - HCA2 seeded in clean glass (a) and patterned glass (b) after substrate adhesion to the bottom of the 96 well plate using 3M™ Scotch-Weld™ UV Adhesive	

(a) and punched double faced tape (b). Images were acquired 24 hours after cell seeding. Both scale bars are 100 μm	55
Figure 26 - HCA2 migration after polymeric brush photoactivation with a RGD concentration of 2 mg/mL, using the 96 well plate approach. A red line is marking one pillar coloured in black being closed by migrating cells. Scale bar is 100 μm	55
Figure 27 - HeLa cells migration compared with MDA-Mb231 cells after a scratch assay performance. Travelled distance were measured at 0, 4, 24 and 48 hours after scratching. Number of performed measurements (n) varied between 12 and 16 depending on the accuracy and measurability of each image scratch. All scale bars are 100 μm . Differences between MDA-Mb231 and HeLa migration data sets are highly significant (** $p < 0.001$).	56
Figure 28 - Comparison between MDA-Mb231 and MCF-7 migration after a scratch assay performance. Travelled distances were measured at 0, 4, 8 and 24 hours after scratching, in cells treated and non-treated with mitomycin C. Number of performed measurements (n) varied between 12 and 16 for the non mitomycin c specimens and between 4 and 6 for the mitomycin specimens depending on the accuracy and measurability of each image scratch. Chosen images showed on top are examples of mitomycin C treated cells migration. Regarding significance, data sets showed no significance between mitomycin C treatment and no treatment in the same cell line and higher significance between results of different cell lines (** $p < 0.001$). All scale bars are 100 μm	57
Figure 29 - Comparison between HCA2 and NIH3T3 migration after a scratch assay performance. Travelled distances were measured at 0, 4, 8 and 24 hours after scratching. Number of performed measurements (n) varied between 15 and 16 depending on the accuracy and measurability of each image scratch. There was a high statistical difference between both cell lines at 8 hours (** $p < 0.001$) but no statistical difference (ns $p > 0.05$) between both cell lines at 24 hours after scratching. All scale bars are 100 μm	58
Figure 30 - All preformed scratch assays. Travelled distances were measured at 0, 4, and 24 hours after scratching. Number of performed measurements (n) varied between 5 and 16 depending on the accuracy and measurability of each image scratch. There was a high statistical difference between HCA2 cell line and HeLa, MDA-Mb231 (no mitc), and both MCF-7 lines, at 24 hours (** $p < 0.001$).	59
Figure 31 - Percentage of wound closure 24 hours after photoactivation. The wounds are 400 μm islands of polymeric brushes. This trend was observed in 2 of 3 independent experiments. This graph represents one of those two experiments. There was statistical significant difference (** $p < 0.01$ and *** $p < 0.001$) when comparing all RGD concentrations with 0 concentration. There were no statistical significant difference between pairs of data sets with concentrations between 1 to 3 mg/mL. N= 6-12 depending on the number of brushes present in each acquired image. Regarding the images, at left is an island photoactivated with 2mg/mL RGD being invaded by HCA2, where at right is the control a RGE (1mg/mL) photoactivated brush. Both images were acquired 24 hours after photoactivation. Cells cytoskeleton is stained with green while DNA is stained with blue.	60
Figure 32 - Blebbistatin effect in cell structure when plated in glass (left) and polymeric brushes (right). Left images were acquired 24 hours after photoactivation with a RGD-BT concentration of 2mg/mL. Applied blebbistatin concentrations were: C1=0nM; C2=0.5nM; C3=5 μM ; C4=25 μM and C5=10 μM . Left scale bars are 10 μm while right scale bars are 100 μm . At left, cytoskeleton is stained with green, microtubules with red and DNA with blue. At right, POEGMA brushes are stained with green, cell cytoplasm with red and DNA with blue.....	62

- Figure 33 - Latruculin effect in cell structure when plated in glass (left) and polymeric brushes (right). Left images were acquired 24 hours after photoactivation with a RGD-BT concentration of 2mg/mL. Applied Latruculin concentrations were: C1=0nM; C2=100nM; C3=1 μ M; C4=25 μ M and C5=50 μ M. Left scale bars are 10 μ m while right scale bars are 100 μ m. At left, cytoskeleton is stained with green, microtubules with red and DNA with blue. At right, POEGMA brushes are stained with green, cell cytoplasm with red and DNA with blue. 63
- Figure 34 - Y27632 effect in cell structure when plated in glass (left) and polymeric brushes (right). Left images were acquired 24 hours after photoactivation with a RGD-BT concentration of 2mg/mL. Applied Y27632 concentrations were: C1=0 μ M; C2=100nM; C3=1 μ M; C4=5 μ M and C5=10 μ M. Left scale bars are 10 μ m while right scale bars are 100 μ m. At left, cytoskeleton is stained with green, microtubules with red and DNA with blue. At right, POEGMA brushes are stained with green, cell cytoplasm with red and DNA with blue. 64
- Figure 35 - Nocodazole effect in cell structure when plated in glass (left) and polymeric brushes (right). Left images were acquired 24 hours after photoactivation with a RGD-BT concentration of 2mg/mL. Applied Nocodazole concentrations were: C1=0nM; C2=10nM; C3=100nM; C4=500nM and C5=1 μ M. Left scale bars are 10 μ m while right scale bars are 100 μ m. At left, cytoskeleton is stained with green, microtubules with red and DNA with blue. At right, POEGMA brushes are stained with green, cell cytoplasm with red and DNA with blue. 65
- Figure 36 - Scheme of the 50 well silicone placed above the microscope slide. Blue arrows symbolize measures necessary to set up in cell microscope protocol acquisition..... 66
- Figure 37 - Example of 9 acquired images of the same well after being stitched by the In Cell Analyzer software. Red lines mark previous borders of each individual image. 66
- Figure 38 - InCell Analyzer Software general view (right top image) and examples of the several attempts performed in order to acquire the region of polymeric brushes islands. All scale bars are 100 μ m. Area without cells is colored with yellow, area with POEGMA brushes is colored with green and area without POEGMA brushes is colored with red..... 67

List of Tables

Table 1 - List of antibodies and dyes.	35
Table 2 - List of Solutions prepared for immunostaining development.	36
Table 3 - List of used inhibitors.	36
Table 4 - Final applied inhibitors and their concentration.	41
Table 5 - Chosen materials and suppliers, with description, for the 96 well-plate approach.	48
Table 6 - Comparison between the three developed techniques.	69

Abbreviations

AJ	Adhesion Junction
ATRP	Atom Transfer Polymerization
BSA	Bovine Serum Albumin
CAMs	Cell Adhesion Molecules
CIL	Contact Inhibition Locomotion
CLSM	Confocal Laser Scanning Microscopy
DMAP	Dimethylamine Pyridine
DMF	N,N - Dimethylformamide
DMEM	Dulbecco's Modified Eagle Medium
DSC	N,N disuccinimidyl carbonate
ECIS	Electric Cell-substrate Impedance Signalling
ECM	Extra Cellular Matrix
EGF	Epidermal Growth Factors
EMT	Epithelial to Mesenchymal Transition
ERK	Extracellular signal Regulated Kinase
FA	Focal Adhesion
FAK	Focal Adhesion Kinase
FRET	Fluorescence Resonance Energy Transfer
GFOGER	Glycine-phenylalanine-hydroxyproline-glycine-glutamic-acid-arginine
HDF	Human Dermal Fibroblasts
HTS	High Throughput
JEB	Junctional Epidermolysis Bullosa
LCST	Lower Critical Solution Temperature
MAPK	Mitogen-Activated Protein Kinase
MCP	Microcontact Printing
MDCK-CMV	Madin-Darby Canine Kidney - CytoMegalovirus
MEM	Mammary Epithelial Cells
MIDAS	Metal-ion dependent site

MIMC	Micromolding in Capillares
MLC	Myosin Light Chain
MLCK	Myosin Light Chain Kinase
MMPs	Matrix MetalloProteinases
MSCs	Mesenchymal Stem Cells
MT	Microtubules
mTM	microTransfer Molding
NMP	Nitroxide Mediated p
PAA	Poly(Acrylic Acid)
PCP	Planar Cell Polarity
PDGF	Platelet-Derived Growth Factor
PDMS	Polydimethylsiloxane
PECS	Primary Prostate Epithelial Cells
PGMEA	Propylene Glycol Monomethyl Ether Acetate
PI3K	Phosphoinositide 3-Kinase
PiF	Interstitial Fluid Pressure
PSI	Plexin/Semaphoring/Integrin
PSPMA	Poly(3-Sulfopropyl Methacrylate)
RAFT	Reversible Addition-fragmentation chain transfer
RGD	Arginylglycylaspartic Acid
ROCK	Rhokinase
ROI	Region Of Interest
ROS	Reactive Oxygen Species
SAMs	Sell Assembled Monolayers
TIMPS	Tissue Inhibitors of Metalloproteinases
TLA	Time Lapse Analyser
TLM	Time Lapse Microscopy
UCST	Upper Critical Solution Temperature Systems

Chapter 1 | Literature Review

1.1 Skin Structure and Wound Healing

The skin is the largest organ of the body and is responsible for the formation of the first physical barrier of the human structure and for the performance of a large number of fundamental physiological functions in order to preserve human homeostasis, like permanent moisture, temperature regulation and body lubrication [1], [2]. It provides protection against micro-organisms and other kind of injuries, but also enables passage of helpful substances. Composed by three main structural layers depicted in Figure 1, the skin suffers a constant change of cells that move continuously between those layers [1]. Each one has different cells that perform different functions. Keratinocytes are the most common skin cell type, found primarily in the epidermis, creating a population of self-renewing cells. Collagen fibers are the main component of the dermis, a vascularized area that contains receptors for touch, temperature and pain. Fibroblasts also help in the formation of this layer, secreting laminin and other proteins, under keratinocytes guidance [3].

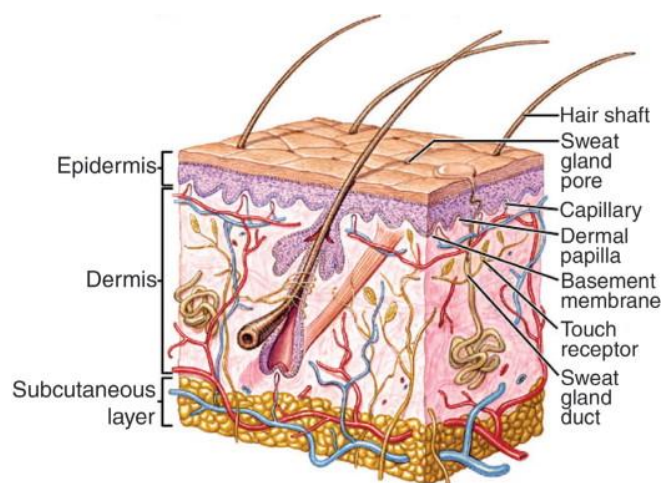


Figure 1 - Skin structure [7].

Normally, this organ is rather undervalued until skin injury occurs. The loss of epithelial integrity, typically named *wound*, can be followed by disruption of underlying normal tissue structure and function [4]. Since cutaneous wounds affect human body equilibrium, immediately after disruption of skin integrity, wound healing starts. This set of events depend on a variety of factors (local wound factors, systemic mediators, underlying disease and type of injury), that combine in order to perform a normal (acute wound healing) or abnormal healing (chronic wound healing) [5]. This restorative process is normally divided in four different but overlapping phases: homeostasis, inflammation, proliferation and remodelling, sometimes followed by scar formation. The coordination of multiple cellular activities makes this a very complex and fundamental process for human survival [6].

Types of Wound Healing

There are several types of wound healing, depending on how their stages are performed. During the first 12-24 hours after an injury, healing by first intention takes place, also called primary healing. Normally connected to acute wound healing, primary healing carries out diverse cellular activities like chemotaxis or Extra Cellular Matrix (ECM) components. Normally, all phases of this healing process are appropriately balanced and fibrosis is predominated by epithelial regeneration but if the wound site is contaminated or poorly delineated, primary healing becomes delayed and the injury is only closed after 3 or 4 days, allowing for phagocytic and inflammatory cells to destroy contaminating cells, with collagen metabolism normally unaffected. When original skin architecture cannot be restored only by epithelial cells regeneration, secondary healing or healing by second intention emerges. In this case, the wound margins pass through an ingrowth of granulation tissue and an accumulation of collagen that leads to an over accumulation of extracellular matrix. This kind of healing has myofibroblasts as its main cells, with properties between fibroblasts and smooth muscle cells. Since it is also a slower process, it can translate into contractures or even functional restrictions. When the injury only affects the epithelium and the superficial part of the dermis we are facing superficial wounds. In such cases, epithelization is the main process, allowing a complete anatomical and physiological restoration [4].

In order to understand why there are delays and how different wound healing processes interact with each other, a brief description of its main stages follows. The first phase, homeostasis, normally has a short span and is essentially focused on blood loss control [6], [7]. When a microvascular injury occurs, an extravasation of the blood in the wound leads to a clot formation and a platelet aggregation with a coagulation cascade.

This will limit further blood loss. Platelets are an important component of homeostasis process since they trap in the clot and release their alpha granules. Besides

platelets, proteins are also important since they begin the attraction and activation of several important cells like fibroblasts, endothelial cells and macrophages by wound healing cascade initiation. Even without haemorrhage, wound healing can occur, being the provisional matrix for cellular migration its clot [4].

The inflammation process can be divided in two phases, according to its duration and the type of cells involved. During the first two days, its named early inflammatory phase, when the wound is infiltrated by neutrophil granulocytes [4]. During this phase, classical and alternative pathways of complement cascade are also activated, being cutaneous injury dominated by inflammatory reactions and mediated by cytokines, chemokines and growth factor actions on cellular responses [5]. The main cells involved are polymorphonuclear leukocytes (which adhere to endothelial cells, performing diapedesis and phagocytosing bacteria and foreign particles) and basal cells (that increase their mitotic activity) [4]. These cells are mainly recruited by membrane-bound receptors [5]. Other redundant cells are excluded from the wound site by extrusion or phagocytosis. After that, until the third day, the late inflammatory phase takes place, when macrophages emerge as a result of blood monocytes phenotypic change. These cells are very important since they help regulate repair by performing phagocytosis, producing growth factors (that help proliferation) and releasing proteolytic enzymes (that help wound debridement). When monocytes and macrophages do not perform their activity normally, severe alterations can occur in wound healing process, mostly by an abnormal debridement of the wound, a delayed proliferation of fibroblasts, an inadequate angiogenesis and a poor fibrosis [4].

Following inflammation, a proliferative stage that can last up to two weeks takes place. It is based on cell migration, extracellular matrix deposition, granulation tissue formation and release of chemical factors [4]. This phase can lead to neo-angiogenesis, the formation of new vessels that will provide blood to the wound site, allowing cell proliferation and re-epithelisation. [5]. The cells that proliferate the most during this stage are fibroblasts, endothelial and epithelial cells [7]. Human Dermal Fibroblast (HDF) are one of the major intervenients in new extracellular matrix construction since they are capable of balancing matrix accumulation and degradation, being attracted to the wound by growth factors. HDF are capable of performing these actions by synthesizing ECM components: firstly fibronectin and hyaluronic acid, in second place proteoglycans and collagen and in third place matrix metalloproteinases (MMPs). For their part, MMPs are proteolytic enzymes capable of degrading all ECM components and regulated by Tissue Inhibitors of Metalloproteinases (TIMPs). Fibroblasts also play a crucial role in mechanical forces development, mainly after differentiating into myofibroblasts, under wound site influence, creating a mechanical feedback loop between cells and their environment. The forces generated by myofibroblasts are very important since they can not only bring

wound edges together but also lead to abnormal wound healing, if not in good physiological conditions [8]-[10].

ECM has also other functions like the induction of cell differentiation and movement, and has other components within such as fibrous structural proteins and adhesive glycoproteins. A specialized basement membrane, that has a direct impact in cell polarity, is also formed during this phase by epithelial, endothelial and smooth muscle cells [4].

Finally, the remodelling phase arises as the stage where the extracellular matrix is reshaped [6], [7]. Starting in the first week, with possible several weeks' duration, the remodelling phase initiates with granulation tissue development, where MMPs, neutrophils and macrophages at the wound site, help collagen degradation, allowing cell migration and proliferation [4]. Granulation tissue formation takes place by basement membrane of parent vessel proteolytic degradation, forming a 'capillary sprout'. This formation depends on endothelial cells migration, proliferation and maturation, mainly due to angiogenic stimulus and organization into the capillary tube [4]. On the other hand, epidermal keratinocytes perform re-epithelisation by their migration, proliferation and differentiation into the wound site from the edges, covering the wound surface with a layer of epithelium. This process is only possible after fibroblast proliferation, collagen matrix formation and the rising of new vessels [2]. The tissue remodelling phase can last up to 2 years with time-dependent and spatial modification of expression patterns, regulating a variety of proteases that coordinate wound healing. These same proteases have an activity and conformation change caused by the wound bed due to 'physiological conditions' modifications, like changes in pH [11].

Besides being regulated by complex biochemical and cellular events, there are other factors that can influence wound healing. Some of those factors are oxygen supply, new capillary development, edema, and mechanical forces, that affect wound healing through mechanochemical transduction processes [12], [13]. Intrinsic and extrinsic mechanical stimulation are very important in wound healing since they help stimulating tissue granulation, by affecting mainly the fibroblasts, myofibroblasts, endothelial cells and epithelial cells [14]. In addition to being affected by mechanical stimulation, myofibroblasts are also responsible for tensile force generation, during tissue remodelling [15]. The primary influence of extracellular and intracellular tensile stress takes place in wound closure since contraction absence can lead to cutaneous regeneration failing [12], [16]. Apart from those factors, it is also essential to mention cells and other biological organelles that can help or delay wound healing, like platelets count, growth factors, gap junctions, neural inputs and cell population [17]. Neutrophils emerge as markers for infections since they migrate to injury site with the premise of removing wound necrotic tissue by releasing specific enzymes [18].

A wound is considered healed when the skin recovers its function and anatomical structure, by re-epithelisation and tissue repair [4]. Sometimes, cutaneous repair can result in scar tissue. Different in appearance and function from original skin, this simple stratified epithelial covering appears after full thickness skin loss. The major difference between this covering and original skin is the absence of epidermal appendages that can lead to thermal dysregulation, for example [2]. In adult mammals, the tissue does not heal completely after an injury because it loses the original architecture and molecular signals released by wound trigger scar repair, instead of regeneration [2], [19].

The ability to regenerate a certain wound is innate in humans. Even so, those capabilities can become dormant, when responsible signalling pathways are inactive. Keeping this in mind, one possible way to improve human regeneration capabilities is to discover those factors and get a better understanding about such signalling pathways, so as to ascertain the major differences between adult and fetal skin [20]. Pathogen and Pattern Recognition have a major importance in wound healing since they are responsible for cellular environmental change detection, triggering specific responses that promote the restoration of tissue function [21], [22].

As already stated, wound healing can be largely influenced by a great number of different factors. Some studies showed that psychological stress, behavioural factors and anger can induce wound healing impairment mostly because skin permeability can be affected by those conditions [23]. Also, Epidermal Growth Factor (EGF), is another example of a crucial player in cutaneous repair since it facilitates cell regeneration by stimulating keratinocytes proliferation and migration. Besides this, they also promote granulation tissue formation and fibroblast motility [24].

Abnormal Wound Healing

Some wounds have problems healing and remain without an effective treatment, like open wounds or infected wounds. In the first case, their management is a problem since they cannot be closed primarily. Normally, open wounds treatment is done by applying constant tension, stretching the skin and expanding it, leading to phenomena such as mechanical creep and stress relaxation [25]. Since cutaneous repair is a crucial process to human permanence after skin injury or surgical procedures, when it is badly conducted, it can lead to infections and consequently prolonged hospital stays, higher patient discomfort and a delayed return to daily life activities [23]. A chronic wound can be the result of a failure during the anatomic and functional integrity production process or in establishing a sustained anatomic and functional result, during an appropriate length of time (approximately three months) [26]. There are several causes that can lead to non-healing wounds like alterations in important components of the healing process (e.g.: growth factors), or even specific condition factors such as those of neuropathy in

diabetes. Predisposition to chronic wounds is also connected to changes in cells profile and activity, ECM composition alterations, epithelisation failure and free radicals or micro-organisms presence. Typically a chronic wound site has a high presence of chronic inflammatory cells, like macrophages, and a defective ECM [4], [24].

One of the major characteristics of this kind of wounds is the unbalanced proteolytic activity, triggered by a combination between an increased protease expression shown by cells and high levels of Reactive Oxygen Species (ROS) produced by wound bacterial bio burden. Besides that, ROS can selectively affect signalling pathways, activating some transcription factors like pro-inflammatory cytokines or membrane type MMP, that are up-regulated in chronic venous ulcers. In its turn, pro-inflammatory cytokines help inducing MMP expression and down-regulating TIMP expression, creating an excessive MMP activity environment. Therefore a delay in re-epithelisation, fibroplasia and angiogenesis occurs due to matrix degradation [27]. Besides those delays, fibroblasts and growth factors also have a different morphology, migration capacities, proliferation and responsiveness in chronic wounds [28]. One example are chronic ulcers whose susceptibility to infection make them especially difficult to treat, leading to patient long term suffering. These kinds of ulcers are very common worldwide, being a large cause of morbidity, with increased incidence, mostly because of lifestyle changes and population aging [18]. According to the United Nations, Chronic wounds in general are a management challenge and a major burden to society, affecting 1% of European population and spending 2% of health budgets. Within chronic ulcers, one of the most common types is the foot ulcer, present in 25% of diabetics and a leading cause of non-traumatic amputation in developed countries [29]. In a diabetic foot, one of the causes of chronic wounds is the hypoxia created by bacteria that consume oxygen in excess, with one solution: affected tissue debridement [30]. In short, 70% of chronic wounds are associated with chronic venous stasis, pressure necrosis, diabetes mellitus and other well-defined clinical entities [24]. On the opposite side of chronic wounds is excessive healing that can lead to scars and keloids formation [4].

Nowadays there are some strategies induced to improve wound healing, mostly applied after studying wound aetiology and status, and establishing a management plan according to it [18]. Those strategies include the application of EGF [24], PDGF (Platelet-Derived Growth Factors) [31], MSCs (Mesenchymal Stem Cells), moisture [4], [5] and negative pressure, to the wound site, all of them with several advantages and disadvantages [32]-[35].

Other significant discoveries were the management of wound infections with anti-microbial agents, like silver and iodine, skin graft and hyperbaric oxygen therapy. Although there have been achieved several new therapies, wound management remains very difficult to treat due to its subjectivity, healing process complexity and patient

variability. In order to respond to these features, a new kind diagnostic tool was created - smart dressings - based on sensors that work similar to point of care technologies, that can be placed into or near wound dressings [18]. Other approaches involve polymers, with a conformational change (in contact with gram negative bacteria) and growth factors pH-dependent release and antimicrobial properties [36]-[38].

Even with these new treatments and approaches, as already stated, most countries continue to spend millions treating patients with non-healing wounds, showing how crucial it is to develop novel strategies to better understand and treat more effectively wound healing, reducing costs, time and patients' discomfort [18]. In fact, chronic wounds are currently a major problem for health care systems, with the United States spending more than 25 billion dollars per year and the United Kingdom reaching annually the 3.1 billion pounds mark [39], [40]. The cost rises not only because of long term hospitalization and number of affected individuals, but also due to world population aging, leading to more chronic wounds patients a consequence of poor sleep, loss of mobility and social isolation, typical traits of that age group [41].

Regarding European statistics, wound prevalence is approximately 4/1000 people, leading to an annual incidence of 4 million individuals. This high incidence translates into a large number of occupied hospital beds (25-50%), and is mainly due to surgical wound infection and pressure ulcers developed during hospitalization time [42].

In order to diminish these numbers it is crucial to try new strategies and treatments. However, since wounds are complex and difficult to study, the best way to study its dynamics is by having the whole wound, allowing multiple target therapies [18]. Normally, it is hard to get those kind of wound sites using controlled conditions, which leads to the typical use of animals and, in a second stage, human experiments, with long clinical trials. According to Great Britain 2012 statistics, in the year of 2012 there were performed more than 4 million animal procedures, with an 8% increase since 2011. Since most of those trials are not successful or do not lead to any new established strategy, at least in a short term, it is easy to conclude that there are a lot of animals used in vain. Taking in to account that long term trials are required to achieve new treatment strategies and that we are now in a new scientific and technological era, it is now possible to create new kinds of mathematical and engineered model systems with the aim of reducing animal burden and clinical research costs. This brings new improvements in the attempt of reaching not only new information about wound healing but also new types of treatment developments [7].

1.2 Cell Migration

As stated during section 1.1, cell migration is one of the most important processes of wound healing. Furthermore, it is also essential to accomplish several other vital phenomena like embryonic development or even tumour metastasis. In order to initiate migration, cells need to form an adhesive complex, stabilized with the help of protrusions present in the leading edge of the cell. With time, this complex gives cells a necessary traction forcing them to move. However, to continue moving forward on the substrate, there is a coordination needed between the formation of further adhesive complexes and the release of rear ECM adhesions. Cell migration as then a highly dependence on the strength of cell-substrate adhesions, primarily mediated by integrin receptors. These heterodimers will be further discuss in this section.

Cell migration has been described in many studies, including an *in vitro* study performed in Zebra fish during the year of 2005. Here, Blaser *et. Al.* showed that cell's motility behaviour vary between three different phases. The first phase shows an absence of detectable protrusions in cells. Second phase is characterized by a change of cell morphology and an emersion of cell protrusions in all directions, with the cell keeping still. Lastly, in a third phase, protrusions start being directional and cells initiate migration. Once reaching the site of interest, cells stop migrating and lose their protrusions. This final process can be considered as a fourth phase [43]. In the case of keratinocytes, cells need the occurrence of at least four different phenomena. First of all, they need to attach to the underlying substrate. This condition in normally defined by the expression and activation level of integrins, which can directly influence their migration speed [44]. Other phenomena include adhesion receptor coupling to the cytoskeleton, directional cytoskeletal action and coordinated detachment from trailing edge [45]. In the case of biophysical migration properties, the relation between cell features and spatial properties of the ECM is very important with cell size, shape and flexibility has key features. Also, proteolysis and other ECM remodelling phenomena can increase cell migration speed [46]. Epithelial cells typically present apico-basal polarity and its only when they start replacing this polarity by polarized protrusions that they start migrating do to the generation of the necessary traction forces for this process to occur [47].

There are two distinct types of cell movements: collective and individual. One of the major differences between them is the way cells interact with the surrounding environment, sensing and processing directional cues.

Individual cell migration can be amoeboid or mesenchymal. Amoeboid movement takes place with the help of propulsion blebs, eliminating the intervention of focal

adhesion or cell attachments. Normally characterized by actin-rich filopodia, weak substrate interaction and round and ellipsoid bodies, this movement is not only commonly performed by differentiated tumour cells but also present in embryonic cells or even leukocytes [48]. On the other hand, in mesenchymal movement, strong attachments to ECM occur leading to elongated spindle-like bodies formation, with cytoskeletal contractility. This kind of movement is performed by fibroblasts and other types of cells that undergo by Epithelial to Mesenchymal Transition (EMT) [49], [50]. In the case of epithelial cells, EMT is almost essential for them to start individual cell migration, since they acquire fibroblast-like properties, losing their cell-cell contacts [51]. Lamellipodia, present in mesenchymal movement is one type of cell extension that helps this process allowing a directed attachment and forward motion [52].

Cell extensions can be guided by several phenomena. Contact guidance, defined as the capacity of cells to sense, recognize and follow topography, is one example of those phenomena [53]. Other example is haptokinesis, when migration is mediated by specific adhesion receptors, triggered by an anisotropy of the encountered environment [54]. At last, physical (durotaxis) and molecular (haptotaxis) cues, both cause intracellular signal polarity and movement along the gradient. Orientation and directionality of durotaxis can be positive, negative or perpendicular [55].

Coordinated movements and cell-fate decisions are a consequence of guidance cues prioritization and processing by cell groups. Hierarchy is further defined by the relative strength of guidance modalities. For instance, migration of an epithelial monolayer that is closing a tissue defect follows the interface between the underlying substrate and cell-free space until the gap is closed and contact inhibition of migration overrules pro-migratory signaling [56]. Moreover cells also react to other contexts like pillars, substrate rigidity, tensile forces and micropatterned adhesion areas, altering their traction forces, differentiation, growth and apoptosis. Substrate dimension has some influence on migration too, leading cells to a dimensional preference detection during the process [57]. ECM is responsible for those topographical cues, providing a mechanical, biochemical and structural environment. These cues guide focal adhesion orientation, cytoskeleton organization, proliferation and phenotypic expression [58].

In contrast with individual cell migration, where cells can move with an amoeboid fashion, squeezing between ECM components, in collective migration cells have to make changes on the surrounding environment. In fact, in collective cell migration, cells exchange signals not only between them but also with the ECM [47], [59].

Collective cell migration is present in a variety of different cell types able to migrate as cohesive clusters, sheets or chains and in different contexts [47]. In a collective, cells divide between leader and follower populations. The first type of population senses signals and are localized at the front of the group. After sensing signals, they transmit

them onto follower cells through cell-cell junctions, localized at their rear. Directional migration rises from this process triggered by chemical and/or mechanical signalling [54]. Lamellipodia or filopodia are examples of protruding actin-based structures acquired as a leading edge toward the substrate, allowing leader cells to secure front-rear polarity and guidance along or into tissue structures. Lamellipodia, already mentioned in mesenchymal individual movement, form a highly branched network, while filopodia comprise long parallel bundles [60]. In the case of 2D cell sheets, leader cells of the collective inhibit leader cells formation in the neighbourhood by a delta-dependent negative feed-back [61]. 'Cryptic lamellipodia', are protrusions that go underneath neighbouring cells and transmit forces along a longer distance and through multiple cells. Cryptic lamellipodia can also lead follower cells to engage in cell-substrate traction forces [54]. Regarding migration rates, individual cell seems to be faster due to their characteristics, however, recent findings showed the opposite [47]. Collective cell migration quicker mobility can be a consequence of several specific processes. The fact that these cells migrate as a collective increases their capability to respond to outside forces, mainly due to cell-cell adhesions, and to generate force by creating a larger number of focal adhesions and traction forces [62]. Guidance signals interpretation can be another reason for collective migration to be faster. With a large number of cells, the possibility for them to sense weaker signals of guidance molecules becomes higher [63].

Communication between the ECM and leader cells and between leader cells and follower cells can be performed through several ways. Adhesion molecules are one of the possible intermediates of those communications. Three different families of cell adhesion molecules (CAMs) are already well studied: cadherins, integrins and selectins. Cadherins are the ones that determine tissue architecture and cell contact formation. These haemophilic adhesion molecules are linked to the actin cytoskeleton inside the cell via a complex set of cytosolic factors. Characterized as a family of Ca^{2+} dependent adhesion molecules, N-cadherin, on neuronal cells, were the first to be discovered. Those were followed by E-cadherin, present in epithelial cells, and p-cadherin, identified in the mouse placenta. Composed by five typical extracellular domains, cadherins can interact in cis to form clusters and mediate adhesions via haemophilic trans interactions [64].

Back to collective cell migration, as already mentioned, only leader cells need to perceive guidance cues, since follower cells can track them with the help of cell-cell communications [63]. Moreover, cell-cell junctions between follower and leader cells feature tensile forces that help balance anterior traction forces formed when leader cells migrate through the substrate. These cell-cell communications can be also performed by gap junctions, channels present in cell membranes that allow the passage of second messengers, ions and small metabolites [65]. Connexins, gap junctions proteins, help maintain cell-cell communication in moving cell groups [66]. The supracellular adhesion

present in these spots along with polarization and mechanocoupling help signal processing and force transmission between cells, enabling required sense and integration of external guidance cues. Supracellular polarity present in the front to rear is mainly supported by the connection of the actin cytoskeleton across multiple cell bodies along with the help of cell-cell junctions that allow the integration of forces generated by individual cells [54].

The extracellular inputs and downstream intracellular signals that define and maintain leader cells are probably cell-type and tissue-context specific. MAPK (mitogen-activated protein kinase), ERK (Extracellular signal regulated kinase), FAK (Focal Adhesion Kinase), PI3K (Phosphoinositide-3-kinase), Akt, Src kinases, Notch and Rho GTPases are examples of downstream intracellular signals that define and maintain leader cells. On the other hand, intrinsic polarity can arise due to early activation of these pathways [54]. Between these pathways, one of the most important ones is the activation of Rho GTPases, that regulates actin polymerization, actomyosin-based contractility, coupling and force transmission through the anterior cell part in order to stabilize integrin-mediated focal adhesions and thus defining leader cell motility [67]. Moreover, cell-cell junctions and junction-derived signals are retained at the rear of the leader cell, silencing locally Rho/Rock signaling and downregulating actomyosin contractility [68]. Contact inhibition of locomotion (CIL) is one of the processes present in cell-cell junctions and characterized by local minimized protrusions and mechanical coupling, contrarily at the protrusions formed at the leader cell. CIL occurs when migrating cells move apart from each other following an event of cell-cell collision. It may be present in epithelial wound healing as well as being the reason of some invasive properties [69].

Regarding cell migration stoppage, it has been already proven that in specific mechanisms, cells stop migrating once they reach their target location due to different causes. Three of them are: by sensing the high attractant in the area, by intervention of repulsive cues, due to physical impedance caused by specific morphology of the target location, or even a loss of protrusions due to other signalling interactions causing loss of capability to respond to attractive cues [47].

Besides cycles of polarization, migration also includes cell extension, formation of cell adhesion molecule attachment, stabilization of cell adhesion molecules to the cytoskeleton, force generation, cell contraction, adhesion release (with the trailing end of the cell), and adhesion proteins recycling [70]. On adult mammalian skin, keratinocytes are an example of migrating cells that try to restore function and integrity of damaged tissues. During this barrier function restoration, normally called re-epithelisation (already mentioned in section 1.1), fibroblast also show a directed biological movement to the wound area in order to synthesize ECM and express thick actin bundles, as myofibroblasts [71]. By their turn, fibroblasts are used in several studies in

order to understand different guidance mechanisms. Front-back polarity feature of fibroblasts initiates by the emergence of peripheral protrusions where one of the lamella becomes dominant. Following protrusions, fibroblasts initiate small GTPase activity dependent locomotion. GTPases are enzymes capable of regulating actin dynamics, adhesion organisation and protrusions formation. In the case of strong adhesion in the cell rear, tension increases leading to stretch-activated Ca^{2+} channels opening. With the entrance of Ca^{2+} , proteases become activated and cleave focal adhesion proteins [60]. Four cyclical steps characterize fibroblasts migration after polarization: protrusion formation, substrate adhesion, cell body contraction and rear retraction, in a directional fashion [60]. Random migration is normally caused by dominant lamella position changes due to high levels of activated Rac-1 GTPase. It is possible to reduce the number of protrusions to a single axial by lowering Rac levels [72].

To provide additional information about cell response to all mentioned conditions several studies mimicking physiological and pathological events have been carried out. These studies have been performed in 2 and 3-Dimensional spaces, covering confined and unconfined migration [73]. In section 1.3 some of the most well-known migration assays and some new approaches will be analysed.

Integrin Receptors

Cell migration, among other functions, needs the assistance of specific transmembrane receptors that, through adhesive processes, act as mechanosensitive receptors and detect changes in the mechanical environment of the cell. Integrin receptors, present in cell-matrix adhesive contacts, are heterodimeric glycoproteins capable of recognising those changes and able to transmit information in the direction of the inner cell body, toward cytoskeleton filaments, with the aim of activating appropriate signalling [74]. Signals that ECM delivers to cells through integrins can control their shape, migration, proliferation, differentiation and survival [75].

Integrins exhibit a ligand binding site in the extracellular region near the cation binding site, composed by two monomers sub-units, one α and one β , that have a relatively short cytoplasmic domain but also have an active role in intracellular signalling cascade [76]. These two subunits are non-covalently bound and form a head and two legs in the ectodomain, spanning the membrane into the end in the cytoplasmic compartment. The extracellular domain is composed by two long legs and a ligand binding head. α sub-units are composed by a seven-bladed head domain, then a thigh domain, followed by calf-1 and -2 domains. Half of the α subunits contain an I domain (which contain the ligand binding site) and a MIDAS (metal-ion-dependent-site) for divalent cations. β subunit is composed of a hybrid domain that connects to b1 domain homologous to the I domain of α subunit plus a PSI domain (plexin/semaphoring/integrin), four EGF domains, a

membrane proximal b-tail domain. In the absence of an I domain, ligands bind to a crevice between the α and β subunits interface. Integrins bind ECM proteins through their

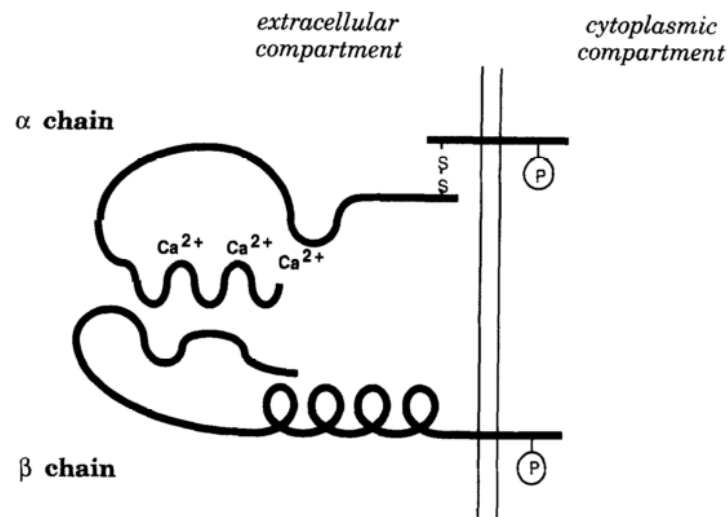


Figure 2 - Integrin heterodimer schematic view [78].

large ectodomain and connect to the cytoskeleton through their short cytoplasmic tail (Figure 2) [75], [77].

There are 24 specific dimers combinations from 18 α and 8 β specific subunits, that show different ligand binding properties (Figure 3) [75], [77]. Three affinity stages are present in integrins: low, intermediate and high [75], [77]. Relative to recognition, not only one ligand can be recognized by multiple integrins but also one integrin can be capable of recognising more than one ligand [78].

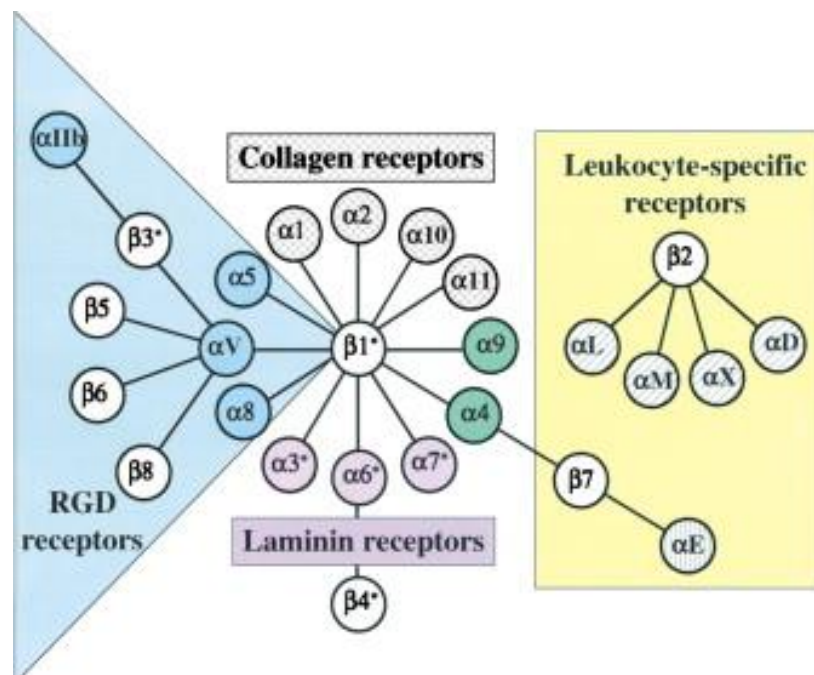


Figure 3 - Different integrin dimers combination [79].

From the 24 different integrins discovered, only 8 are capable of binding to the RGD sequence. Regarding GFOGER (recognition site in type I and IV collagen) triple helical sequence, only collagen-binding proteins can recognize it.

Between the 8 existing β sub-units, $\beta 1$ and $\beta 2$ are the most frequent with the second one being expressed only in leukocytes. In the epithelial cell case, $\beta 1$ and $\beta 4$ integrins are the most common, presenting several receptors for collagen and laminin isoforms as it is $\alpha 1\beta 1$, $\alpha 2\beta 1$, $\alpha 6\beta 1$, $\alpha 6\beta 4$ and $\alpha 3\beta 1$. $\alpha 5\beta 1$ and $\alpha V\beta 3$ isoforms allow the interaction with interstitial matrix or serum proteins ligands via RGD peptide motif. This interaction is held by both α and β subunits exposed outside the cell [79]. These subunits have normally a short cytoplasmic segment, that leads to an indirect interaction with basal actin filaments since it serves as a locus for the assembly of multimeric signalling complexes and actin-binding proteins [79]. Integrin $\beta 4$ is the only subunit that has already been reported has having a long cytoplasmic tail and it seems to only interact with $\alpha 6$ subunits. In keratinocytes this integrin plays an important mechanical role in anchoring cells to underlying tissue, however is associated with intermediate filament instead of actin [80].

When they recognize specific aminoacid sequences, integrins usually convert physical signals outside the cell to chemical ones inside [81], [82]. Mechanotransduction, that conversion of mechanical forces into biochemical signals, it is critical in a large variety of human body processes. With different roles in those processes, integrins can be transmitters of force to other elements, direct mechanotransducers or intermediates on pathways mediated by other receptors [83].

A high regulation occurs at the level of integrin-mediated adhesion with receptor-ligand binding and post-ligation interactions forming complex processes. Focal adhesions (FA), discrete supramolecular complexes containing structural proteins and signalling molecules, are one of the consequences of integrins action, being formed when the transmembrane proteins associate with the actin cytoskeleton and cluster together. FA are then capable of activate signalling pathways which further regulate transcription factor activity and direct cell growth and differentiation, becoming central elements in the adhesion process. For that they function as structural links between cytoskeleton and ECM [84]. FAK, Focal Adhesion Kinase, is one of the signalling molecules that indicate the presence of integrins in Focal Adhesions [85].

In addition, more than 150 proteins are capable of interacting with integrins, allowing them to sense the composition and mechanical properties within the pericellular environment by forming adhesomes (adhesion complex). Among those proteins there are several capable of regulating migration, cell shape as well as other phenomena [86]. Talin is one of the proteins capable of regulating integrin activation or inside-out signalling when bond to the β subunit. This happens do to conformational changes that

increase their affinity to ECM. Kindlin can also enhance integrin activation however talin as shown to be the central regulator of integrin function, linking them to F-actin cytoskeleton as well as to other scaffolding proteins. Vinculin is one of those scaffolding proteins that after being recruited by talin helps linking integrins to F-actin filaments promoting integrin clustering and further formation of nascent adhesions [87].

Integrins can also interact with cadherins. They can communicate through cytoskeleton supported mechanical connections, using travelling signalling molecules or they can start interacting due to a global cellular process as EMT [88]. It was also already stated that cell-cell contact can suffer alterations due to integrin-ECM interactions, impairing or favouring these CAMs actions [89].

Regarding integrin signalling, there are two types of communication: inside-out and outside-in. While in the second case signals are transduced to the cytoplasm from ECM, in the first case affinity regulation takes place inducing clustering (lateral redistribution), and, as a consequence, strengthening adhesion. Only activated and clustered integrins can transmit outside-in signalling regulating cell shape, migration, growth and survival [75].

Moving to integrins studies, since fibroblasts are one of the cell type responsible for regulating dermal tissue and they use integrins as a communicator between cytoskeleton and ECM constituents, they have been widely used *in vitro* in order to understand this transmembrane glycoproteins features. One of the characteristics of fibroblasts that allow those studies is the fact that these cells contract the matrix if seeded in 3D collagens performing fibroblast-mediated contractions with the help of integrin $\alpha 2\beta 1$ heterodimers [90].

Interstitial fluid pressure (Pif), pressure in the ECM fluid of tissues, during edema caused by inflammation, was one of the first *in vivo* phenomena studied to understand function of integrins in skin. After blocking $\beta 1$ integrin monomer, it was possible to watch an increase of edema due to a decrease in interstitial fluid pressure, also showing that this subunit was involved in maintaining collagen network [91]. Other studies suggest that $\alpha 1$ and $\alpha 2$ are important to maintain functions of the skin *in vivo*, but the first one seems to be more decisive. Besides that, in case of the heterodimers conjugation, $\alpha 2\beta 1$ seems to be more important than $\alpha 1\beta 1$ [91]. However, $\alpha 1\beta 1$ appears to regulate collagen synthesis opposite to $\alpha 2\beta 1$ that seems to be able to mediate collagen gel contraction and regulate MMP-1 expression [91]. Also, differences in elastic and viscous element alterations due to blocking interactions between fibroblasts and collagen fibers suggest that $\alpha 2\beta 1$ integrins are capable of regulate the mechanical properties of dermal tissue *in vitro*, being the intermediate of interaction between fibroblasts and collagen [91]. Each integrin domains bind to specific sites, so, for example, ntegrin $\alpha 2\beta 1$ can help dermal fibroblasts to regulate tension which that they can generate mechanical forces. [91].

Junctional Epidermolysis Bullosa (JEB), a human hereditary disorder characterized by blistering of the skin, is associated with the absence of $\beta 4$ integrin, a heterodimer characterized by having a long cytoplasmic domain that binds to intermediate filaments, instead of binding to actin [92]. This can possibly be connected with $\alpha 6\beta 4$ absence, a laminin receptor present in hemidesmosomes. By their turn, hemidesmosomes help stratified epithelial cells to attach to the basement membrane, so in the absence $\alpha 6\beta 4$ they have a fragile or null appearance, leading to the JEB skin disorder [78].

Several other integrins were also already studied in skin of integrin deficient animals. For example, loss of $\alpha 1\beta 1$ revealed not only a higher rate of collagen synthesis and enhancement of collagenase production but also a promotion of fibroblasts survival and proliferation *in vivo* and *in vitro*. Loss of $\alpha 2\beta 1$ generated wound healing failure [93], [94]. These results showed that integrins can have a large influence on fibroblasts through their interaction with tissue. Studies in mice have been considered important since in some cases they reveal the same results as studies performed in human skin, like the integrin $\alpha 2\beta 1$ studies [95]. Nevertheless other studies have been performed in normal skin in order to understand influence of integrins on fibroblast structural and mechanical regulation of the skin, by blocking interactions between these cells and ECM. In keloids, hypertrophic scars and radio-induced ulcers, alteration of $\alpha 1\beta 1$ expression in fibroblasts is one of the examples already studied that proved this integrin can act as an *in vivo* regulator in the dermis [96].

$\alpha 5\beta 1$ are also highly expressed in human fibroblasts, promoting their motility and survival. Together, intermediate levels of expression of $\alpha 5\beta 1$ and $\alpha 2\beta 1$ or intermediate concentrations of ligands (like collagen), leads to an optimum speed of cell migration. As already stated, cell migration is also believed to be direct by ERK, as well as attachment and integrin expression. ERK activation can be mediated by $\alpha 2$ during the formation of focal adhesions [97]

Contractility

The cytoskeleton is a set of structures composed of actin, microtubules and intermediate filaments [98]. Since these filaments are directly connected with cells' mechanical properties and have a large influence in dynamic changes in cell shape, migration and adhesion, changes in their composition and structure can lead to pathological processes. On the other hand, regulation of these properties can be a consequence of microenvironmental mechanical properties [99].

Actin is a protein highly present in contractility processes. This cellular component is kept in equilibrium between two states: G and F-actin. G-actin is characterized by being a globular monomeric state as F-actin is the polymeric filament stat. The passage from

one stage to the other occurs when actin is under physiological ionic strength. Changes between both stages are directly linked to cell motility [100].

Capable of defining modular motile activities, actin cytoskeleton is a cell organelle composed by distinct arrays of actin filaments [101]. It is also assembly and disassembly due to mechanosensitive pathways that trigger those changes according to substrate geometry and variations recognition performed by cells [102].

In actin filaments, all actin subunits share the same polarity defining a barbed end and a pointed end. Polymerisation of polarized actin filaments drives cytoskeletal remodelling allowing changes in cell shape and motility. Actin filaments' barbed end is the regulation point of those transformation, with the possibility of controlling actin dynamics through the binding of certain protein [100]. Cell mechanical activity in response to growth factors and other cytokines changes can be mediated by the Rho-family of small GTPases (Rho, Rac, and Cdc42) [103]. 2D substrates leads to activated Rho in fibroblasts. This stimulates the formation of stress fibers and the development of focal contacts, being these cytoskeletal changes dependent on actomyosin contraction [104]. Increased cell contractility is a consequence of myosin interaction with actin filaments regulated via myosin light chain (MLC) elevated phosphorylation. In its turn, MLC phosphorylation results from the inhibition of MLC phosphatase, derived from the binding and further activation of activated Rho to Rho kinase [105], [106]. E-cadherin plays also a central role in the biogenesis of both cell-cell adhesion and the cortical cytoskeleton. In order to promote the recruitment of Myosin II, Cadherin-based signaling synergizes with F-actin assembly, establishing the apical actomyosin apparatus responsible for junctional tension [107], [108]. E-cadherin adhesion itself can stimulate Myosin II activity via signals such as Rho kinase (ROCK) and Myosin light chain kinase (MLCK) [109]. By its turn, myosin-II contractility mediates the process of cytoskeleton reorganization where the cytoskeleton tensions are involved in the formation of peripheral actin bundles [102].

Mechanosensing may be a consequence of tension created by motor proteins of myosin-family attached to the actin cytoskeleton. Resistance of the substrate to deformation can then cause tension in cells and lead to the integration of the mechanical signal [110], [111]. By its turn, local FA maturation can be promoted by the appliance of an external force on a single-integrin-ECM complex, through recruitment of vinculin, which connects the contractile actomyosin cytoskeleton to the FA complex for mechanosensation [112], [113]. Cortical mechanics by actin regulators drive cell shape changes. By changing biochemical and physical properties of the cortical network, actin regulators determine mechanical properties of the cortex as tension and viscoelasticity. Junctional tension, a participant in epithelial morphogenesis, is produced by the coupling of cortical actomyosin to cell-cell adhesion at epithelial cell-cell junctions [114].

Microtubules (MT) at the leading edge of a polarized cells can be stabilized by activation of FAK, previously activated locally by an integrin. It's also being suggested by some studies that myosin-II-mediated pulling on MT plus-ends at the cortex could lead to centrosome polarization [99]. Nevertheless, how MT pulling plus-ends towards the posterior-end can polarize a centrosome toward the anterior cortex remain unclear mainly because actomyosin redistribution occurs towards the posterior-end of the cell. Actin nucleation factors responsible by localized actin polymerization can be the reason why cell protrusions emerge toward applied load in later stages of polarization. Actin polymerization complex-mediated Arp 2/3 can be activated through signals down-stream of Rac2 and integrin engagement and turn capable of pushing plasma membrane for the leading-edge of protrusions and cell migration [113].

Resistive forces applied by the substrate help balancing internal forces of cells that lead to pre-stress of adherent cells' cytoskeleton. Cell remodeling is normally activated by the redistribution of internal forces due to imposition of physical boundaries and further force sensitive cellular processes activation [115].

It was already proved that assembly or disassembly of cytoskeleton can result from the modulation of tension in proteins through the activation of signaling pathways by the influence of substrate geometry [102]. Myosin is capable of generate sliding leading to a higher tension in α -actin in the bridged or bulged regions and a shear between adjacent actin filaments [116].

Moreover, polarity is a built-in feature of actin and microtubules cytoskeleton, polymers of cells that use energy from nucleotide hydrolysis. This process is divided in several types. Front-back polarity is when cells move in a certain direction towards an attraction. On the other hand, Planar Cell polarity is generated by asymmetric distribution of contents across the epithelial plane. Inherent polarity features are present in the basic building blocks of cytoskeleton. Even capable of being triggered by external factors, polarity is inherently present in actin cytoskeleton. Moreover, certain protein mixtures can also give rise to it with actin polymerization promoting proteins and modifiers [117]. Retrograde flow, a rearward flow of newly assembled actin filaments that polarize migration is created by myosin-II and can act as a clutch, engaging adhesions and driving cells forward by pulling against substratum [117]. When retrograde pulling of myosin against adhesions occurs, the positive feedback signaling formed induce durotaxis, forming gradient of increasing stiffness along cell movement and polarization. However, external diffusible signals are not the only source of polarized migration initiation by contractility networks. With their ends facing apically aiming the delivery of secretory cargo, microtubules tend to span the length of the cell [118].

Another potential player in cytoskeletal repolarization is the Wnt signaling which already showed is capabilities of inducing repolarization of actin and microtubule cytoskeleton and promote asymmetric cell division [119].

1.3 Migration Assays

In order to better understand cell migration processes, several *in vitro* assays were already developed. During the present section three of them will be described.

Scratch Assay

Scratch assay is one of the most traditional 2-dimensional *in vitro* migration assays, with the benefit of being non demanding and very cheap. This assay is performed by “injuring” an area of a confluent layer of a cells, with the help of a sharp object (plastic pipette tip or syringe needle). Then, cells start to migrate into the injured site (Figure 4). Normally it is possible to track the process with a microscope, with events progression being measured through stained assays in a certain point or by time-lapse. Also, manual counting can be replaced by computational methods.

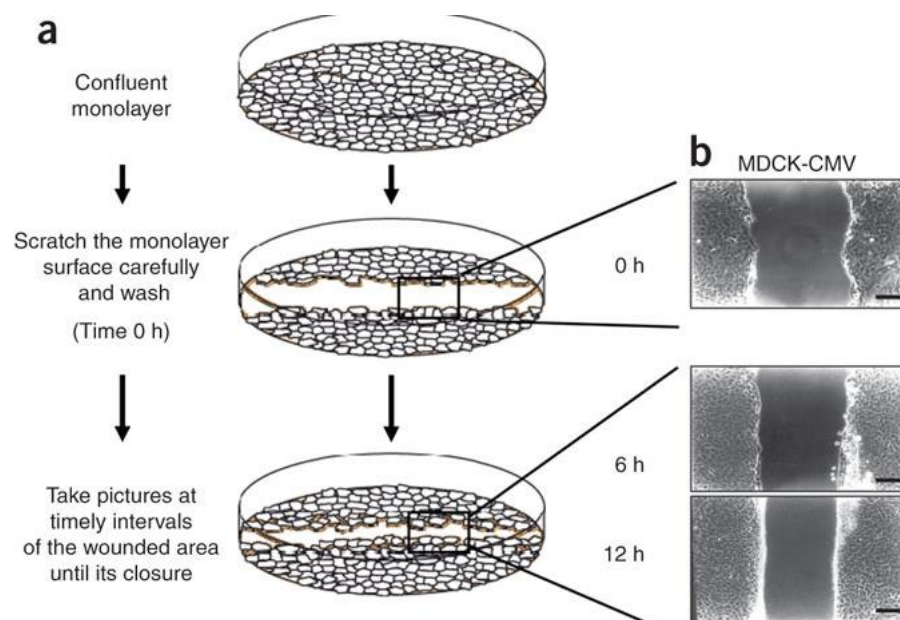


Figure 4 - Example of a scratch wound assay using MDCK (Madin-Darby Canine Kidney) cells infected with Cytomegalovirus (CMV). At right (a) it is exemplified the technique while at left (b) it is possible the results 0, 6 and 12h after scratch performance [170].

This kind of method can be applied in a wide range of substrates and cells, from epithelial to endothelial. Main advantages of this method are procedure time, simplicity, analysis ease and cheapness. On the other hand, the applied scratch can also injure cells and leading to a mechanical cell damage. In order to avoid this secondary effect, wound sites can be created with a confined and reproducible size through, for instance, ECIS (Electric Cell-substrate Impedance Sensing). With this method it is possible to perform scratch assay without interrupting cell mechanical layer and to track migration since wound and re-population have different electric signals. This automated method, also called *Electrical Wounding*, uses electrodes that measure cell impedance, and are also feasible to medium-high throughput assays. Besides *Electrical Wounding* there's also laser ablation. In this case, wound areas are even more well-defined but remnants cell can influence wound healing processes. Major differences between a mechanical scratch assay and an electrical one is in commercial potential. In fact, electrical wounding is reproducible and, therefore, commercial. In contrast, mechanical assay is not currently commercially available since it largely depends on human expertise and appliance [50]. Scratch assay is a valuable tool creating the first insight in how new tissue is formed and the influence of certain components. When this assay is performed, cell-cell contacts break. This leads to an increase of growth factors and cytokines along wound edges. Proliferation and migration also starts, after artificial gap creation. Scratch assays can be carried out both in multi-well plates or individual coverslips. A large range of studies were performed in an attempt to optimize scratch assay. One example is the one performed in order to quantitatively determine fibroblast migration, wound monolayer proliferation and test suitability for crude extracts of medicinal plants, isolated compounds and pharmaceutical preparations. This study had the objective to test Hypericum oil since this compound is normally used in wounds to reduce scar formation. Fronza *et al.* proved that scratch assay is a cheap and convenient method that gives robust and reproducible results related with fibroblasts proliferation and migration through artificial wound site. Hereupon, this method can be performed in order to have a first perception of phytomedicine influence when applied in wound healing [71].

Scratch Wound Assay is then an over-simplified model of re-epithelisation process that was already used with multiple cell types in order to examine compound soluble effects in wound healing [120].

Cell Exclusion and Fence Zone Assays

Cell exclusion is a relatively common wound healing assay. Its concept starts by the creation of cell exclusion zones after cell seeding with the help of an electrical fence appliance or even the use of microstencils. Seeded cells then start to migrate into those exclusion zones in order to close the *wound* and simultaneously allowing cell migration

analysis. It has been reported the use of a tool named *stopper* that has a certain diameter and can be applied prior to cell seeding, replacing mechanical forces appliance and excluding the risk of damaging cells. This *stopper* can be from silicone, a material widely used in epithelial migration assays [50] (Figure 5).

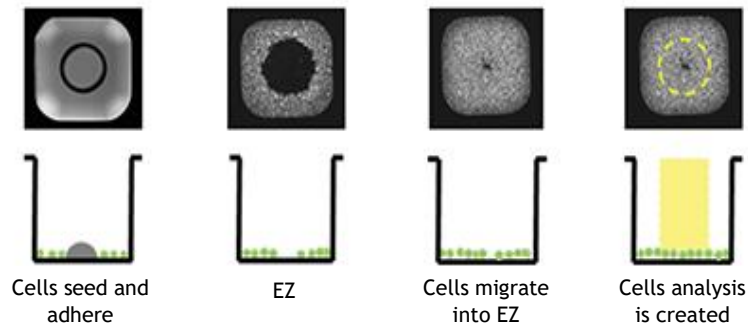


Figure 5 - Exclusion Zone (EZ) example with "Stopper" appliance [171].

Fence assay has the inverse concept of exclusion assay. Instead of performing an *ablation* of an assay's zone, in the fence assay the procedure passes through a restricted cell seed into an inner area of a substrate (Teflon, glass or metal) placed on a standard cell culture dish. This zone is surrounded by a ring device that will be further removed in order for the attached cells to migrate into this outer zone. Cell exclusion and fence assays have similar advantages and disadvantages since both have a similar but inverted concept [50]. These methods were already applied with a wide range of objectives being one of them the study of consequences of changes in paracellular permeability and of the location and function of epithelial tight junction [121].

Transwell Migration Assay

Also named Boyden Chamber Assay, thanks to its creator, the Transwell Migration Assay is either mainly used to assess cell migration and consists of two chambers with different mediums (an upper and a lower one) separated by a porous membrane through which cells transmigrate (Figure 6).

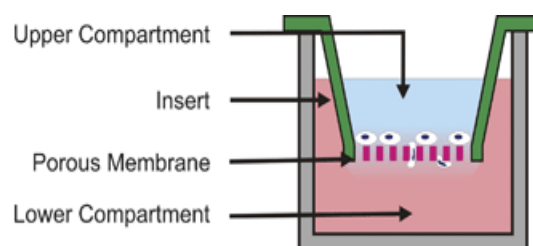


Figure 6 - Transwell Migration Assay [172].

Membrane pores are directly dependent on the size of the chosen cells, being one of the worst disadvantaged since the assay cannot be standardized. Even so, there are currently three methods of detecting and quantifying those migrated cells. The first one is based in cell fixation. After they pass through the membrane cells are stained and quantified. On the other hand, the second method is based in fluorescent markers. Cells that are capable to migrate through the membrane are fluorescently stained, detached and quantified using a fluorescent reader. The third option uses a dark porous membrane which blocks light transmission from non-migrated cells. One of the major advantages of this procedure is the absence of additional equipment besides the culture inserts [50].

Mostly used to culture epithelial thyroid cells, culture inserts were developed in 1986 by Steele et al. This piece allows a free exposure of the basolateral cell membrane to the medium and exhibits two separated compartments becoming more akin to the *in vivo* conditions. Besides thyroid cells this technique can be applied to mouse mammary epithelial cell line COMMA1D, in order to study the influence of substratum nature on biochemical differentiation, and in bovine mammary epithelial cells (MEC) studies, where inserts coated with several components were driven simultaneously in order to determine how they could influence the reorganization of structural features and the maintenance of metabolic functions [122], [123]. Culture inserts technique was also used to test how Planar Cell Polarity (PCP) proteins control the stabilization of endothelial adhesion junctions during lymphatic valve formation. Polarized cell movements are controlled in part by PCP signalling, which helps coordination of collective cell behaviours through acto-myosin-dependent contraction of Adhesion Junctions (AJ) regulation. [124]. Now a days IBIDI is one of the companies that supplies complete solutions for this kind of wound healing technique through a product similar as the one presented in Figure 7.

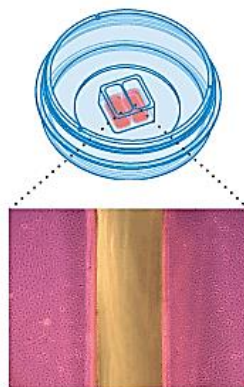


Figure 7 - Commercial culture insert kit available in the market (AutoMate Scientific).

Since the transwell migration is an endpoint assay the optimal time of analysis for each cell has to be tested separately, with a special caution relative to non-invading cells

versus invading cells. Even so, this technique can be applied in order to study a large number of different cell types from epithelial cells to mesenchymal ones [50]. One of Boyden Chamber and culture inserts techniques appliance example was in the performance of chemotaxis assays. In this kind of experiments, one of the most important concerns was to minimize monolayer culture period for diminish possible chances of phenotype loss [52].

Stimulation of Primary Prostate Epithelial Cells (PECs) migration by normal stroma and epithelium of the prostate was also investigated with the help of this type of assay. With Transwell technique it was possible to conclude that the combination of adhesion and motility factors from the prostate stroma is necessary for efficient stimulation of epithelial cell migration. In this study Transwell filters were also used and PEC were placed in the upper chamber unlike migration factors (like collagen) that were placed in the lower chamber [125]. Dental Pulp Stem Cells are another example of cells tested with a Boyden chamber assay. Their migration abilities were tested both in a normal environment and in the presence of inhibitors [126]. Finally, transwell migration assays were used to optimise *in vitro* assays, which predict the sensitivity of dendritic cell migration to applied chemicals. This was the Sens-it-iv EU funded project [127]. Together these assays show that the transwell migration technique is a useful process that can bring new outcomes related with cell migration.

1.4 Dynamic Systems

Since cell migration and wound healing are dynamic processes, it is also relevant to mention dynamic systems created with the aim of better understanding them.

One example of those applications are optical tweezers. As already stated, creating a force responsible for cellular motility emerges when a cell detects a chemoattractant gradient leading to movement towards the source. For the detection of the gradient, receptors play a role in collaboration with G-protein linked signalling proteins. In a study by Yang et al., applying optically trapped microspheres near cells generated a chemoattractant gradient. The authors robotically controlled the trapping of PLGA microparticles that released a specific chemoattractant molecule in a liquid environment, activating polarization and cellular migration [128].

Microfluidic devices are other type of dynamic system, simple and adaptable. Composed by two or more chambers linked side-by-side by a narrow connecting bridge this technique allows the submission of cells to assays with several different aims as co-culture or stimulus studies, under conditions that allow variability. Another advantage of

this application is the high temporal and optical resolution and the possibility of analysing specific cellular responses like the phosphorylation states of signalling proteins [129].

Patterning techniques are an alternative rising method now widely used for cell migration assays. Allowing the imposition of different geometries to cells attached to specific proteins present in previous synthesized surfaces, this method brings a new range of possibilities for wound healing assays [130]. Dynamically adhesive micropatterns will be further described in a more thorough way.

Dynamically Adhesive Micropatterns

One of the first techniques developed for the creation of dynamic surfaces was the appliance of Self Assembled Monolayers.

Self-Assembled Monolayers (SAMS) involve patterning on a gold substrate using an elastomer stamp, followed by selective etching in an aqueous, basic solution of cyanide ion and dissolved dioxygen [131]. This technique emerged some years ago has a method to modify metallic surfaces, being characterized has a spontaneous assembly of molecules arising from a surface. However, one of its disadvantages is the thickness of SAMS, which led to the creation of polymeric brushes, thicker than the initial ones. Polymer brushes, a layer of polymers attached to a surface, are mainly composed by a head-group (attached to that surface), a backbone (mainly an alkyl group) and an end-group (CH₃, OH). The end group has a large influence on surface properties and in the polymerization mechanism applied [132]. Polymeric brushes are highly interesting as they allow the combination of multiple tuneable features with the capability of, for instance, give a stable and conformal coating to biomaterials [133]. The polymeric chain is linked by one end to an underlying substrate, enabling the manipulation of grafting density (density of polymer chain by surface area), chemistry (choice of monomers that will be polymerized as the brush is generated) and coating thickness (via the length of polymer chain and grafting density). A rapid manipulation is also another advantage of polymeric brushes. There are two main ways of creating polymeric brushes. The first one is by anchoring an already set up polymer to a surface, mainly named as “grafting-to”. The second one, “grafting from”, is characterized by the coupling of a molecule to a surface further allowing the growth of the polymer chain. This last method allows the possibility of choosing all architectural features of polymeric brushes, being currently the most used one. There are also several controlled surface-initiated polymerization techniques like the ones based in radical chemistry: ATRP (Atom-transfer polymerization), RAFT (Reversible addition-fragmentation chain transfer) and NMP (Nitroxide-mediated p). Surfaces and initiators have either a variety of options. In the present work, gold was the selected surface, but silica, glass or polyamide are other possibilities. One of the most important characteristics of polymeric brushes is grafting density mostly because it defines their

regime. There are three types of polymeric regimes: “brushes”, when they are extended and partially oriented, “mushroom” or randomly spaced, creating isolated structures [133]. Polymeric brushes conformation is modulated by several parameters being also very dynamic. The way polymeric brushes respond to multiple environmental stimuli is important for understanding, design and properties’ control enabling cell behaviour manipulation [132].

In order to create stimulus responsive brushes, mix polymeric brushes or copolymeric blocks can also be used. When talking about pH sensitive systems, these are based in polymeric acids or basis and show a high degree of swelling, a fully charged state and a high influence in repulsive forces. Regarding temperature sensitive brushes, they are based in polymers with LCST (Lower critical solution temperature) and UCST (Upper critical solution temperature), mainly in aqueous solutions. Responsive systems also emerge with the addition of small molecules to polymer brushes. In these cases, brushes conformation can change and some surface properties can become controllable like protein adsorption.

Large polymers aren’t able to penetrate entirely the brushes, remaining on the superior part of them. This is also an important parameter for the current work since one of the steps is the coupling of RGD to the generated polymeric brushes. When choosing the polymers that are going to adhere to the brushes it is possible to organize simultaneously different polymers as long as they have different sizes [132].

In the case of brushes with high grafting density, Human *et. Al.*, showed that 5 aminoacid peptides are unable to diffuse through the brush, blocking a detectable adsorption in the its inferior part [134]. POEGMA was the first protein-resistance polymeric brush to be discovered, showing an absence of fouling to different medium like BSA (Bovine Serum Albumin), to which it was exposed [135]. However hydroxy-terminated POEGMA brushes showed poorer stability and detachment of the film after prolonged incubation times [136]. In order to turn brushes bioactive, it is necessary to biofunctionalize them with proteins, peptides or small molecules. Even if proteins cannot normally adhere to POEGMA brushes, these can be a platform for protein adsorption since once adhered, proteins remain anchored to the substrate, resisting multiple treatment and maintaining functionality. When presenting hydroxyl groups, POEGMA brushes become POEGMA-OH, hydroxyl-terminated POEGMA. By its turn, DSC, disuccinimidyl carbonate, is an attractive coupling agent mainly because of its availability and is mild reaction at room temperature. Also, it shows a large stability. DSC can serve as a coupling mediator to peptides like biotin [133]. In order to perform cellular adhesion, adhesive peptides can be immobilized in previous described substrates. YIGSRG is an adhesive laminin sequence recognized by integrins [137]. GFOGER (glycine-phenylalanine-hydroxyproline-glycine-

glutamic-acid-arginine) is another peptide, already mentioned during integrin section, composed by 45 aminoacides that can couple to POEGMA-OH [133].

Created in 2001, click chemistry is used to fabricate alkyne and azide functionalized surfaces, presenting mild reaction conditions, high conversions and selectivity. Capable of running with azides or alkynes on surfaces, click chemistry was already used for the functionalization of several different surfaces [138]. By their turn, the synthesis of polymers with the thiol-ene or thiol-yne reactions, a radical mediated addition of thiols to alkenes or alkynes that allow a further efficient chemical coupling in a post-polymerization modification, as became useful. Thiolyne reaction can be complementary to thiol-ene, cu-mediated and alkyne-azide reactions. Thiol-yne reaction was one of the primary synthetic tools in years to come in polymer and material chemistry [139]. It requires only one step to assemble 3 components and further access thermal liquid product, show fast reaction rates, minimum side products, excellent chemoselectivity and functional group tolerance [140].

Functional surfaces can then be prepared by the combination of microcontact printing with thiol-yne/ene chemistries [141]. Between printing techniques there is: MIMIC (micromolding in capillaries), mTM (microtransfer molding) and MCP (microcontact printing). However MCP is the most versatile and cost-effective method, capable of patterning large area surfaces after PDMS being impregnated with ink molecules solution and further maintained in contact with the surfaces. Ink molecule is then transferred accordingly from the PDMS pattern [132]. Propargylamine reaction is normally performed to induce alkyne groups and allylamine is used to introduce alkene pendent groups. On the other hand, RGD is the peptide motif inserted by photoinitiated coupling. Moreover, different surface ligand densities lead to different cell migration speeds. In previous works, Costa *et. al.*, used thiol-ene and thiol-yne chemistry to couple peptides to POEGMA brushes. The functionalization of those brushes was made with allylamine and propargylamine via cysteine residues. Further photoactivation was performed with the help of a photo-initiator, Irgacure 2959. Stimulus responsive brushes along with cell-adhesive peptides sequences, like RGD, allow cell adhesion control and detachment without dealing with protein-brush interactions [141]. Regarding the polymer, POEGMA has several advantages, like excellent reproducibility, and allows the control of micrometer sized features. Moreover, its thickness has a high influence on protein adhesion and cell patterning [142]. A higher substrate protein resistance is favorable for a good cell patterning, however the type of chosen initiator is also important for good results, since by diffusion it can reach outside areas between the stamp and the substrate [142].

However, there are other polymers with important features that can allow the creation of dynamic brushes. Parylene C is a soft polymer that belongs to poly polymers

family (paraxylylene), normally characterized by the substitution of one atom of hydrogen by an atom of chlorine in the aromatic monomer. Being transparent and stable at room temperature, it is largely used as a coating for 3D structures, mainly for anti-adhesion layers in microfluidics. In the past, using this polymer for certain applications used to be difficult as it required chemical functionalization or specific degree of interaction with cells and biomolecules. Nowadays, parylene C surface can be modified, making changes in its wettability due to physical or chemical alterations triggered by exposition to ionized gas. Besides exposure to ionized gas, parylene C can also be modified by pH responsive microgels with the aim of producing biosensors. For this purpose there are two different methods: drop casting a solution of microgels onto the pc samples or micropatterning the surface in order to induce pattern of microgels. Nevertheless, both methods need a previous ionized gas treatment. These are good tools for the creation of smart parylene C surface for biosensing and diagnose application [143]. Stimulus-responsive polymer brushes are other attracting alternative to POEGMA. PNIPAAm brushes, thermally responsive poly(N-isopropylacrylamide) polymers, show a structural transition at a lower critical solution temperature (LCST), of approximately 32°C, making it closer to human body temperature and an advantage for biomaterial application. Depending on the surrounding temperature, its state can be either hydrophilic or hydrophobic [144].

Back to surface modification, between other methods of modifying surfaces there is direct photopatterning, which turns possible the control of brush growth at the micrometer scale and dewetting of macroinitiator, which support the growth of POEGMA brushes and allows the control over protein location on exposed substrates. This last methods leads to the guidance of fibroblasts adhesion inside the dewetted areas. It is scalable and low cost, but doesn't allow control over geometry of the generated patterned [145]. For a patterned cellular assay, brush stability is also important. POEGMA shows chemical stability during storage and cell culture, control of cell spreading, cell shape and control over cell culture size and geometry [142]. Comparing ECM proteins microcontact printing with polymeric brushes micropatterning, the last ones are more resistant. To date, POEGMA brushes have been compared with several other brushes. PSPMA (anionic brushes) and PAA (charged brushes) are other alternatives for cell patterning [133]. One study using adhesive brushes was performed by Connelly *et. al.*, when adhesive islands with different sizes showed that differentiation incidence of primary keratinocyte was directly influenced by a certain pattern morphology. Furthermore, pattern geometry had a direct influence in F-actin remodeling and cell shape, inducing alterations on F- to G-actin balance [146].

Summarizing, micro-patterned polymer brushes allow the study of geometrical adhesive cues and how physicochemical surface properties influence cells. POEGMA biofunctionalization by thiol-ene/yne chemistry leads to the creation of dynamically

adhesive patterns allowing the study of environmental geometric confinement influence on cellular migration and wound healing. Micropatterned polymeric brushes can then generate biological phenomena allowing their further quantification. During this analysis, interface properties can be controlled as well as the appliance of different parameters [133].

To better understand those kind of structures there are already available some techniques, such as atomic force microscopy, neutron reflectometry and contact angle goniometry. Recently, it was proved that polymers can exhibit an intermittent transport mechanism in several interfaces as liquid-solid. Those studies were performed using a unique molecule tracking method capable of studying the dynamics of stimuli-responsive polymer brushes, leading to the determination of individual trajectories [147].

Caged RGD

Nowadays there are several biointerfaces generated with the help of synthetic peptides. Those peptides are capable of mimicking active domains of ECM components and allow the study of the interaction between ECM and cell membrane. As already stated, RGD modified substrates can be dynamic. With that aim, cages were produced. Cages are photo removable protecting groups, light-triggering, that allow an accurate spatiotemporal control and *in situ* regulation of molecular factors involved in signalling pathways. These groups attach to the active site of a biomolecule in order to inhibit its activity. After that, light exposure leads to photocleavage and function is restored. Caged RGD allows the modulation of cell response. This functionality can be activated in different time points by sequential illumination steps and dynamic regulation of RGD [148].

Stimuli-responsive materials react to specific perturbations applied or produced that will further have some influence in cell-material interactions. However these perturbations have to be tolerable by cells. Under UV light, the change from azo-benzene to cis state, covers physically tethered RGD, with the surrounding PEG and other illuminated regions resistant to cell binding. When RGD is caged with an o-nitrobenzyl group, a UV radiation and electrochemical potentials are useful for the fabrication of dynamic scaffolds. However, those effects can be adverse to cells or have unknown effects in cell behaviour. In this case cells stop having the ability of modulating the substrate. Hydrolysis can also make changes in RGD exposure [149].

High-Throughput screening strategies

Quantitative characterization of cell behaviour used to be performed in 2-Dimensional environments through computer-assisted light microscopy. However, some

new automatize methods have been recently developed. The need for those trials emerged due to migration behaviour variations between *in vitro* 2-Dimensions and *in vivo* conditions mostly because cells need different abilities in each of those situations. From the existing techniques the most commonly used for 3-Dimensional imaging is fluorescent microscopy and multi-photon technology typically combined with an automatic cell tracking method. Even being cheaper and easier to apply, phase-contrast microscopy is becoming less used through the years [150]. On the other hand, Time-Lapse Microscopy (TLM), allows cell behaviour characterization through image, including migration patterns analysis, by an automatized observation and it's normally performed with a camera mounted on a microscope located on a built chamber. This microscope takes pictures to certain regions of interest (ROI) upon fixed endpoints, allowing direct insights about cells phenotypic behaviour like migratory potential. However, the presence of manual procedures turn the results obtained very subjective introducing a possible amount of errors. Since most of assistance software is not adapted to high throughput screening, Huth *et. al.* developed the Time Lapse Analyser (TLA). TLA has several different analysis modules suitable for different applications, including wound healing, which can measure directional migration and proliferation. Normally this is also measured with endpoint assays, but in the case of TLA, image processing relies on each frame local entropy, which translates structural information in illumination intensity. TLA provides not only wound area information but also the total length of the edge of the cell, allowing the distinction between wound healing performed by active or passive migration [151].

Automatic cell tracking systems are very important to obtain effective quantitative measures but most of them are based on a wide range of tracking algorithms, making them more difficult to develop. These kind of systems have to be easy and effective for researchers to use and can be continuously improved. Also, measurements of spatio-temporal cell behaviours are extremely important to perform a critic analysis since analysis device can also make changes in culture conditions. Aiming to show the effectiveness of cell tracking system for biological research, Bise *et. al.* presented an automatized cell tracking device for *in vitro* wound healing assay under different culture conditions. In this specific case, three different conditions were monitored through a sequence of phase-contrast microscopy images. This system allowed cell region localisation and a tracking procedure using non-invasive imaging. Bise *et. al.* were able to compute spatio-temporal measurements (cell density, migration velocity, among others), proving that cell tracking for quantitatively analysing cell behaviours is efficient [152]. Confocal laser scanning microscopy (CLSM) is another *in vitro* time-lapse microscopy technique capable of following a cell during an amount of time along a multilayer tissue. CLSM is capable of optically cross-sectioning cells and tissues, thereby reducing out of plane fluorescence and improving sensitivity. In the case of producing a high throughput

analysis for this large amount of image data it is necessary to develop fully automated image analysis pipelines. However, since cells can suffer format changes, this mechanism has to be able to perform cell spatio-temporal correlations. Chakraborty *et. al.* developed a method for automatically tracking individual cells in closely packed developing multilayer tissues, capable of combining spatial and temporal associations between cell slices [153].

In the case of temporal information capture without cell tracking, the approach is based on the sum of absolute differences between the pixels of consecutive photographs, thus detecting cell division events. Cicconet *et. al.* developed a software implementation based in this concept, named CellTracker [154].

As cell migration is a dynamic process, it is highly difficult to analyse since most of traditional image approaches are based in just changing endpoints and quantified. One new technique that has been used in order to suppress this need is Long-term Time-lapse cell imaging that allows a wide screening and covering multiple cell cycles during an extended period of time. Once again, Phase-contrast microscopy was applied, in this case by Debeir *et. al.*, avoiding various disadvantages associated with fluorescent microscopy. When multiple fluorescent excitation is applied to cells, this can bring some drawbacks like photo bleaching and/or photo damage to living cells. This group combined two strategies: phase-contrast time-lapse video microscopy and an adequate analysis method. Debeir and his team acquired an image every 4 minutes over a period of time between 48 to 72 hours. Their method could be applied to low density cell models, allowing a complete cell migration behaviour study. Additionally this analysis was applied to scratch wound healing assays, once again proving its efficiency [155].

Time-lapse main drawback is the time spent trying to segment cells. This kind of equipment should allow simultaneously motion detection within the cell and a quantitative perception of cells morphology changes during cell migration processes. Moller *et al* developed a semi-automatic tracking with minimal user interaction method, based on a two steps algorithm, where the user only has to determine the rough positions of cells in the first frame. This method was able to diminish the high variance between different cells segmentation, traditionally given by manual segmentation because of cell boundaries subjectivity [156].

High throughput screening (HTS) techniques were also applied in order to test certain cellular attributes. Gahemi *et. al.* applied this technique to a MSC microenvironment, with HTS capabilities allowing the study of multiple factors and interactions at once, exploring simultaneously physical, chemical and biological parameters. However, HTS needs an array subdivision method in order to enable multiple factors combination. This lead to the conjugation of other techniques like layer-by-layer construction or ECM printing [157].

Regarding microfluidic chips, one of the most evident difficulties is having an automatized equipment for an automatized deposition of samples on chips. One of existing methods is partipetting, a technique capable of creating hydrogels randomly pipetted in the top of a microwell array, in a way that each individual hydrogel enters in a single microwell [158]. A large range of lab-on-a-chip assays were performed both with ordered and altered configurations. However, a high throughput analysis should be performed in order to take advantage of this sophisticated approach and allowing a complete characterization of the all process [159]. MetaMorph Software is another imaging software capable of controlling automated microscopes, acquire time-lapse images from multiple areas of interest in parallel and track migrating cells in a highly quantitative manner [160]. Finally, InCell Microscope is a high throughput imaging system capable of acquiring images by itself in an entire plate or cover slip, by setting up a specific plate format. After that step, it also enables an automatic analysis of the acquired images based in a previous stablish protocol [161].

In summary, biomaterials have to be functionalized in order to be able to adapt to conditions and cells that are being tested. Even though these approaches are increasing in number and evolving quickly, in order to be effectively used they have to be follow by the correct screening systems. Most of screening techniques have also been improved during the last decade but they are still in the way to become less susceptible to human errors and more automatized thus optimizing all mentioned *in vitro* assays.

Chapter 2 | The Project

Aim

The aim of the current project was to create a high throughput *in vitro* assay for cell migration studies based on a previously established technique by Costa *et.al.* [141].

With this purpose, an initial design of the new assay was performed and several objectives were outlined.

1. First of all it was necessary to learn all the techniques involved in the previous work including cell culture, gold thermal evaporation, photolithography and microcontact printing.
2. The second step was focused on the search for ideal materials in order to assemble the new 96 well-plate approach. Those materials included plates, glass, adhesive, overnight reaction ‘containers’ and petri dishes.
3. The last goal of the project was to optimize the assay settings including cell density, ideal cell line, ideal pattern size, and photo-activation reaction parameters, making it usable for further cell migrations tests.

Furthermore, during the achievement of these goals, another approach emerged.

Instead of the 96 well plate assay, a solution using a 50 well slide showed to be an alternative to the previous design, and the project changed its path to optimize the 50 well slide format.

Context

This project was the result of a collaboration between Faculty of Engineering of University of Porto and Queen Mary University of London, being the laboratory work performed at the Blizard Institute. Funded by Dr. Hadwen Trust Foundation, this project had the aim of creating an alternative to decrease *in vivo* animal assays performed for cell migration studies. In the already established technique, cells were cultured on micropatterned POEGMA brushes, further photoactivated with a peptide using thiol-yne reactions, forcing cells to migrate into previously non-adhesive areas [141]. This *in vitro* assay showed to be promising, however inducing a high number of different conditions with

this technique would be time and material consuming. The present project emerged with the aim of supressing those disadvantages in pursuit of replacing animals in research while providing improved tools for wound healing assays.

Chapter 3 | Materials and Methods

During this section different materials and methods used along this work will be described.

3.1 Antibodies, Solutions and Inhibitors

For the immunostainings performed during the present work, several antibodies and dyes were used as described in Table 1.

Table 1 - List of antibodies and dyes.

Name	Species	Fixation	Stain	Dilution	Supplier
Primary Antibodies					
α -tubulin	Rabbit	PFA 4%	Microtubules	1:100	Cell Signalling Technology
Secondary Antibodies					
Alexa anti-rabbit 555	Goat	PFA 4%	Microtubules	1:500	Molecular Probes
Phalloidin 488	Dye		Cytoskeleton	1:1000	Invitrogen
CellMask™ Deep Red Plasma	Dye		Cell Plasma	1:30000	Thermofisher scientific
DAPI	Dye		Cell nucleus	1:1000	Biotium
Streptavidin FITC	Dye		RGD-BT	1:100	Sigma Aldrich

Besides antibodies and dyes, immunostaining techniques required the preparation of different solutions, all listed in Table 2.

Table 2 - List of Solutions prepared for immunostaining development.

Name	Composition	Supplier
4% (w/v) PFA	4% Paraformaldehyde diluted in PBS	Sigma Aldrich
Triton-X100	0.2% Triton diluted in PBS	Sigma Aldrich
Blocking Solution	10% Bovine Serum and 0.25% Fish Gelatine diluted in PBS	Sigma Aldrich
Mowiol (mounting Media)	2.4 g Mowiol 4-88, 6g glycerol, 6mL H ₂ O and 12mL of 0.2M Tris-Cl (pH 8.5)	Sigma Aldrich

Regarding the inhibitors assays, the ones used are also listed in Table 3.

Table 3 - List of used inhibitors.

Name	Stock Solution [mM]	Supplier
Nocodazole	10	Sigma Aldrich
Blebbistatin	50	Merck Milipore
Y27632	10	LKT Laboratories, inc.
Latrunculin	1	Merck Milipore

Lastly, all other reagents not listed in this tables but mentioned along this chapter were purchased by Sigma-Aldrich (USA), unless stated.

3.2 General Patterning and Photoactivation

Micropatterned polymeric brushes were the primary technology used during this work. Several steps were performed in order to obtain final surface compositions as is described during this section.

Glass cleaning and gold covering

Micropatterned substrates were synthesised on gold (Au) coated glass surfaces. Glass coverslips and microscope slides were cleaned with, at least, 3 cycles of 15 minutes sonication, while immersed in Millipore purified water. Once sonicated, the chosen glass was cleaned individually with ethanol (100%) and dried under nitrogen gas. This overall

step had the purpose to remove dust and oil impurities from the surface, allowing a further deposition of metals.

For the gold covering, an Edwards Coating System E306A (thermal vapour deposition) was used. Since gold adheres weakly to glass, an initial coating of chromium with 1.5nm thickness was performed, followed by a 15nm thickness coating of gold. In both coating processes, the metal thickness was measured by a quartz balance (Intellemetrics IL-150). Final gold coverslips and microscope slides were stored in clean boxes.

Photolithography and stamp preparation

In order to obtain specific patterns of polymeric brushes in previous described gold surfaces, photolithography and PDMS stamp preparation were performed.

Photolithography was used to create a master for the stamp that would further be used to ink the initiator and stamp the gold surface, creating a polymeric brush with the desired pattern. Based in microchem guidelines [162] the procedure started with ethanol cleaning and nitrogen drying of a silicon wafer. 3 mL of SU8 photoresist were placed in the centre of the wafer and spin coated at 3,000 RPM for one minute, followed by a 5 minute pre-exposure bake at 100C. Once baked, a window and a mask were placed on the top of the wafer, with the help of lateral clips. This mask had the inverted desired pattern. After conventional UV curing (350-400 nm) for 8 seconds, another 5 minutes baking was performed. Finally, SU8 not cross-linked by UV was rinsed twice with PGMEA for 30 seconds, dried with nitrogen gas and kept in a petridish until PDMS casting. A brief scheme of the photolithography process is shown in Figure 8.

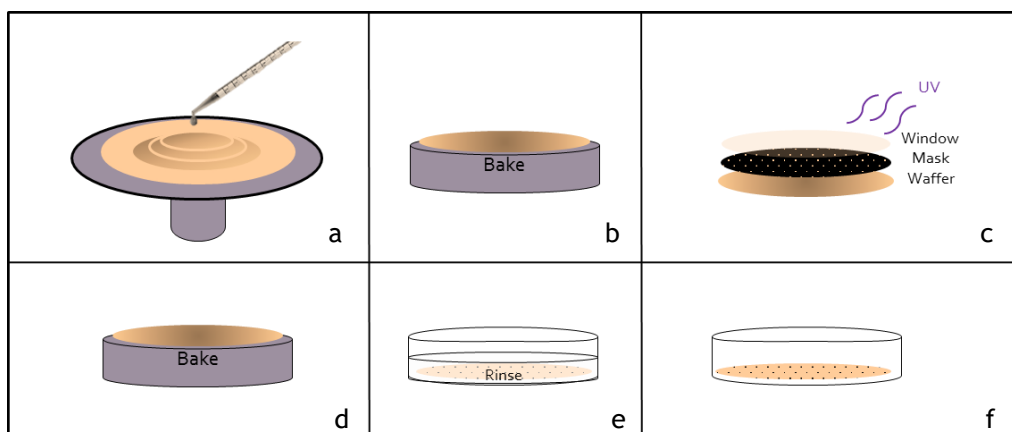


Figure 8 - Brief scheme of photolithography process. A) SU8 deposition on top of wafer placed in the spinning disk; b) First 5 minutes baking; c) window, mask and wafer assembly under UV curing; d) secondary baking; e) SU8 rinsing; f) Final master with desired pattern.

PDMS (Poly(dimethylsiloxane)) stamps, were developed with a ratio of 10:1 of the two initial supplied components: prepolymer and cross-linker. This mixture was then cast in the master petri-dish, placed in vacuum and further baked overnight at 80°C. On the day

after, cured stamps were cut in the desired shape and size, according to further applications.

3.3 Micropatterned POEGMA brushes

Micropatterned substrates for photoactivation preparation was based on previous stated techniques by Costa *et. al.* [141]. This 3-day process started with a polymerization phase. Gold covered substrates were stamped for 30 seconds with the thiol initiator w-mercaptoundecyl bromoisobutyrate inked on a PDMS stamp with a specific pattern (Figure 9) in order to create a self-assembled monolayer.

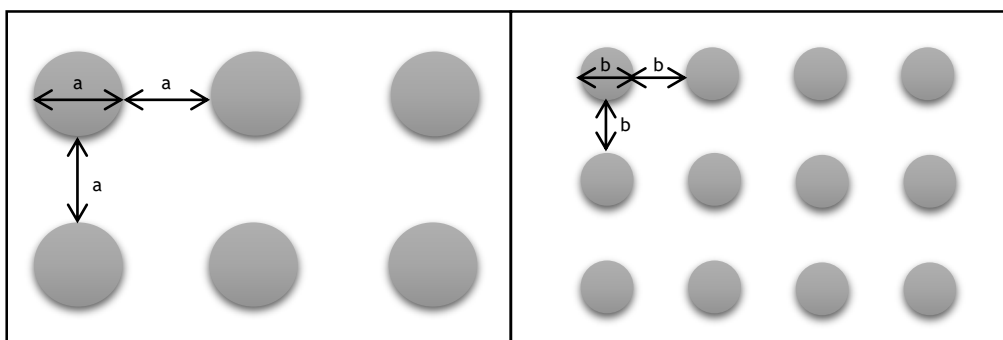


Figure 9 - Stamped patterns used during the present work with $a=400\ \mu\text{m}$ and $b=200\ \mu\text{m}$.

After that, the substrates were incubated for one hour at room temperature with a solution containing 12g of OEGMA (oligo(ethylene glycol) methacrylate ($MW_{\text{avg}}\ 360$)), 18mg of Cu(II)Br_2 , 320mg of Bipyr, 82mg of Cu(I)Cl and a ratio of Water/EtoH of 4:1, with the aim of performing an Atom Transfer Radical Polymerization. Before incubating the substrates in this solution, the same solution was stirred and degassed with N_2 , removing oxygen from the solution and turning the reaction quicker and more consistent. Once that incubation ended, brushes with an estimated 60 nm thickness were submitted to an overnight incubation, also at room temperature, with 510mg of DSC ($\text{N,N}'$ -disuccinimidyl carbonate, 0.1M), and 240 mg of DMAP (Dimethylamine pyridine, 0.1M) in 20 mL of DMF (N,N -dimethylformamide) in order to allow further reaction with primary amine of propargylamine. In the second day of procedure, all substrates were cleaned with DMF, water and 100% ethanol, followed by a second overnight incubation in a solution of DMF with 1% of propargylamine. This step led to the addition of a tripled-bonded alkyne group on the brushes allowing a future coupling of peptides when submitted to photoactivation. On the day after substrates were rinsed again with DMF, water and ethanol, being ready for further applications.

Photoactivation process based in thiol-ene and thio-yne reactions

Once developed, polymeric brushes were sterilized with 70% ethanol or under UV light, both for 30 minutes. After sterilization substrates were plated with different conditions depending on the format applied. 24 hours after cell seeding, photoactivation of brushes was performed by thiol-yne reactions. In order to do that, cell seeded substrates were cleaned with Phenol red-free DMEM and further incubated with different ratios of Irgacure 2959 (2-hydroxy-40-(2-hydroxyethoxy)-2-methylpropiophenone, PI; Sigma-Aldrich)/Peptide and placed under or over UV light ($k_{max}=365nm$). Irgacure 2959 was previously resuspended at 0.5% (w/v) in Phenol red free DMEM, letting to dissolve at 37°C overnight. List of used peptides include RGD (arginine-glycine-aspartic acid, CGGRGDSP), RGE (Arg-Gly-Glu-Ser, CGGRGESP) and RGD-BT (H-Cys-Gly-Gly-Arg-Gly-Asp-Ser-Pro-Lys-Biotin). UV exposition had 1 minute duration, with substrates being immediately washed after that time with Phenol free DMEM, followed by a second washing with DMEM.

3.4 Assay Assembly

Since the primary goal of this work was to create a new high throughput *in vitro* assay for cell migration a key step was to list all materials necessary to assemble the new desired format, followed by purchase, testing and optimization. For the 96 well plate approach, a new customized glass, 96 well plates without bottom, adhesive, containers and petri dishes were searched among several suppliers and resulted in a new design that is going to be described in the next chapter. However, along with this search, a new design emerged, possibly being cheaper and easier to manipulate. This new design had as a base a glass microscope slide with a 50 well silicone chamber and will also be further explained in the results section. Between procedures that went under optimization are: substrate sterilization, substrate incubation previous to cell plating, cell seeding densities applied (for all cell lines and two different patterns), photoactivation steps and peptide concentration applied.

3.5 Cell Culture

Four cell lines were used during the present work. Hela (epithelial cervical cancer cells), NIH3T3 (mouse fibroblasts), HCA2 (human epidermal fibroblasts) and MDA-MB231 (invasive epithelial breast cancer cells). Cell lines were maintained in Dulbecco's

Modified Eagles Medium (DMEM), supplemented with 1% of Pen/Strep and 10% of Fetal Bovine Serum. MCF-7 cells, a non-invasive epithelial breast cancer cell line, were cultured with the same medium supplemented with 0.01 mg/ml human recombinant insulin. Medium change was performed every 3 days for all cell lines.

Micropatterned substrates

For micropattern cell migration assays, all cell lines were plated in patterned substrates with specific cell densities according to each approach, as will be further described, for 24 hours until photoactivation and at least 24 hours after photoactivation, at 37°C in a 5% CO₂ atmosphere.

Scratch Assay

Scratch assays were performed in all listed cell lines. Using a 12 well plate, cells were plated with a density of 200 000 cells/well (approximately 52 600 cells/cm²) and were incubated at 37°C in a 5% CO₂ atmosphere for at least 24 hours, until cells reach a confluence of 80%. The next day, a scratch with a cross pattern was performed in each of the wells with a 200 µL pipette tip. At least 5 images of cell migration were acquired in each well at each time point (Figure 10).

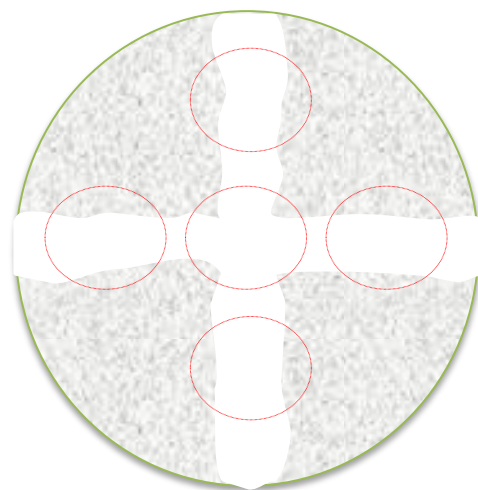


Figure 10 - Scratch assay example with red circles marking imaged sites of each assay.

Chosen time points were: 0, 4, 8 and 24 for HCA2 and NIH3T3; 0, 4, 24 and 48 for HeLa and MDA-MB231 and 0, 4, 8, and 24 hours after scratching for MCF-7. MDA-MB231 and MCF-7 migration was also tested after mitomycin C treatment. In this case cells were incubated with 40 µg/ml of mitomycin C for at least 3 hours before scratching.

Inhibitors Assay

Regarding the inhibitors assay, cells were incubated with 4 different inhibitors, each of them with 4 different concentrations (Table 4).

Table 4 - Final applied inhibitors and their concentration.

	Blebbistatin	Lantrunculin	Y27632	Nocodazole
Function affected	Myosin contractility	Actin polymerisation	Rho-kinase	Microtubules
C1	0	0	0	0
C2	0,5 nM	10 nM	100 nM	100 nM
C3	5 μ M	0,1 μ M	1 μ M	1 μ M
C4	25 μ M	0,5 μ M	5 μ M	5 μ M
C5	50 μ M	1 μ M	10 μ M	10 μ M

With these inhibitors, two kinds of experiments were performed, both of them using the 50 well silicone approach. The first experiment was performed by seeding the cells with a cell density of 2000 cells/well (approximately 1500 cells/cm²) in each of the 50 wells, with the silicone adhered on top of a normal glass microscope slide. After a 24 hours regular incubation, cells were incubated during one hour with each of the listed inhibitors. Once 1 hour was passed, cells were fixed, stained and imaged.

Regarding the other experiments, cells were plated in a gold covered glass microscope slide with a previous developed pattern (400 μ m diameter islands), using a cell density of 8000 cells/well (approximately 5 700 cells/cm²). 24 hours after plating, substrates were photoactivated. Since cells showed to be stressed after photoactivation, inhibitors incubation was only performed one hour after that same process. However, inhibitors were kept in the medium for the remaining 23 hours to assess the effects on migration.

3.6 Immunostaining

Immunostaining was performed with the solutions mentioned in section 3.1. In the first day of the procedure, samples fixed with 4% PFA and permeabilized for 10 minutes with triton. After permeabilization, samples were blocked for 30 minutes with blocking solution. Lastly, samples were incubated with primary antibody at 4°C overnight. After this incubation period, samples were washed with PBS and incubated with secondary antibodies and/or dyes for one hour. Once this incubation ended samples were washed with PBS and water, and small drops of Mowiol were placed over the sample before mounting a cover slip on the top of the sample allowing future microscope analysis. It is important to note that some samples were only stained with dyes, eliminating the necessity of the first overnight incubation.

3.7 Cell Imaging and Analysis

During this project three different microscopes were used. In the beginning, for the majority of the assembly optimization, a Nikon Eclipse inverted microscope with live image acquisition was used. However, besides that microscope, a Leica DM4000 manual epifluorescence microscope and an In Cell microscope were used.

For the image analysis several parameters were measured. Regarding the scratch assays, ImageJ® software was used to measure the area of the scratch. In order to calculate cell migration rates, the same area was divided by the length of the scratch. Image J was also used for cell migration assays in micropatterned substrates, where the area of the regions of islands without cells was measured and compared with the initial size of the same islands giving a percentage of wound closure after 24 hours. The last measure and results quantified with the help of image J were the brightness of photoactivated RGD-BT islands, giving the mean value of each of them along the slide. Besides Image J, Metamorph software was used to acquire cells with MM-Leica epifluorescence and an IN Cell Analyzer protocol started to become established with the aim of imaging and analysing automatically all the 50 wells of the 50 well silicone approach.

3.8 Statistical Analysis

Polymeric brushes brightness mean value and cell migration rates results were reported as the mean \pm standard deviation of one representative experiment of three or two independent experiments. Data was analysed with a one way analysis of variance (ANOVA) using the GraphPad® software.

Chapter 4 | Results

4.1 Optimization for new patterns and cells

As stated in chapter 3, the first phase of this project was to learn how to perform all related techniques. Moreover, since new patterns and cells were applied, an optimization process was accomplished during that training.

After choosing two different patterns, one with 200 μ m and another with 400 μ m islands, and four different cell lines, HeLa, MDA-Mb231, MCF-7 and HCA2, several steps were performed in order to optimize the technique. This optimization started using HeLa cells and both patterns. After applying the same conditions used in previous work with NIH 3T3 cells [141], results revealed that the cell density was too low for these patterns and HeLa cells. In order to improve cell density, the first modified step was the initiator inking. PDMS stamps with the desired pattern were usually cleaned with ethanol before stamping the gold surface and after being soaked with initiator. In this case, the cleaning step was omitted in an attempt to increase the initiator stamping on the surface. However, that did not lead to major differences.

The next step changed was substrate incubation. In the former approach it was usual to incubate the substrate with PBS after ethanol sterilization until cells seeding. In this case, an incubation of the substrate for at least 30 minutes with 10% serum before cell seeding showed to give rise to a more accurate pattern. At last, cell seeding time and density also needed optimization. After several attempts, the best result emerged with a cell seeding time of 30 minutes before washing. Cell seeding density was also reached for HeLa and for all other cell lines. In Figure 11 is possible to see the technique before and after optimization for HeLa cells in a 400 μ m islands pattern.

After HeLa cells, other 3 cell lines were plated on developed polymeric brushes: MDA-Mb231, MCF-7 and HCA2. HeLa, MDA-Mb231 and MCF-7 are all cancer cell lines, however they have different morphologies and features between them. First, HeLa cells, a cervical cancer cell line, show an epithelial morphology and a prominent nucleus surrounded by a triangular cytoplasmic geometry. Moreover they can migrate collectively and are one of

the most sensitive, displaying detachment and growth inhibition cell lines according to the surface where are plated [163]. By their turn, MDA-Mb231 are a breast adenocarcinoma cell line that show an elongated cytoplasm and migrate individually through the substrate. When cultured *in vitro* this epithelial-like morphology cell exhibit invasive properties [164]. The last cancer cell line tested was MCF-7. Even being also a breast adenocarcinoma cell line, these cells exhibit a different level of invasiveness when compared with MDA-Mb231 and a different morphology. When cultured *in vitro*, MCF-7 exhibit a round cytoplasm forming domes while proliferating, making them difficult to count. Moreover, they are also capable of migrating collectively [165]. Besides cancer cell lines, a fibroblast cell line was also tested. HCA2 are dermal fibroblasts established from a sigmoid colon adenocarcinoma that exhibit epithelial morphology [166].

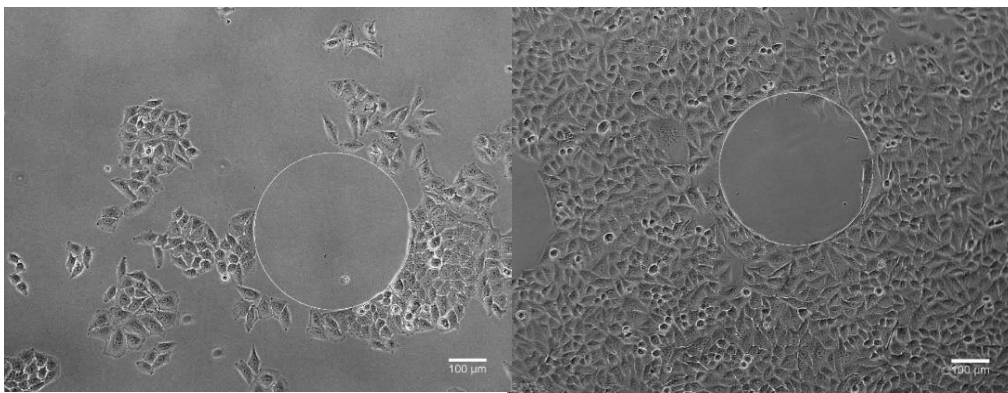
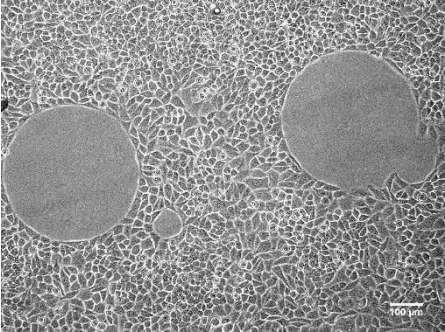
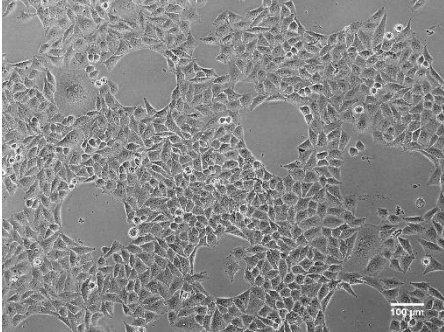


Figure 11 - 400µm islands with HeLa cells before (left) and after (right) optimization. Images were acquired 24 hours after cell seeding. Both scale bars are 100 µm.

In Figure 12 is possible to see all cell lines density optimized for each pattern. HeLa cell showed the same cell density as MCF-7 (600 000 cells/well for 400µm islands and 800 000 cells/well for 200µm islands) while MDA-Mb231 led to the same cell density as HCA2 (400 000 cells/well for 400µm islands and 600 000 cells/well for 200µm islands). The possibility of optimizing cell density for all four different cell lines increased the versatility of the developed technique.

	400µm	200µm
HeLa		
	600 000 cells/well 317 500 cells/cm ²	800 000 cells/well 420 000 cells/cm ²

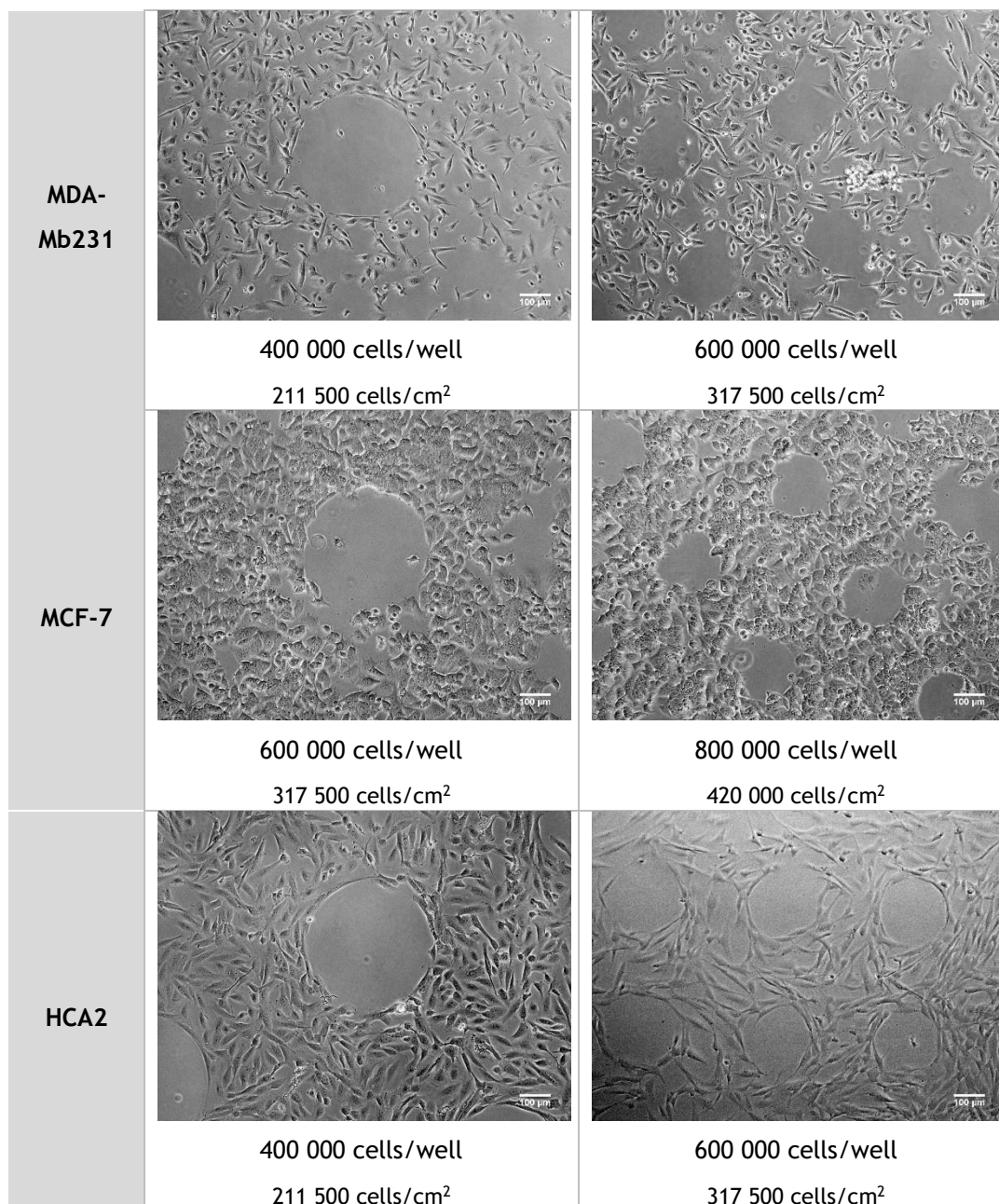


Figure 12 - Cell seeding density optimization for all four cell lines in both patterns. Images were acquired 24 hours after cell seeding. On the left is possible to see cells seeded in a 400µm islands pattern while on the right is possible to see cells seeded in a 200 µm islands pattern. All scale bars are 100µm. Cells/cm² ratio was calculated assuming a diameter of 1.55cm.

4.2 New assemblies design

After optimizing cell seeding for all four cell lines and both chosen patterns, new approaches were designed. In Figure 13 there is a scheme with all steps performed during the former approach. It is important to notice that after step d1) substrate incubation responsible for brush polymerization was performed in specific containers that could

carry 5 coverslips at a time. Regarding step e), coverslips are cut in 1cmx1cm squares with the help of a diamond tipped pen and placed in different wells with the aim of further applying different conditions between wells.

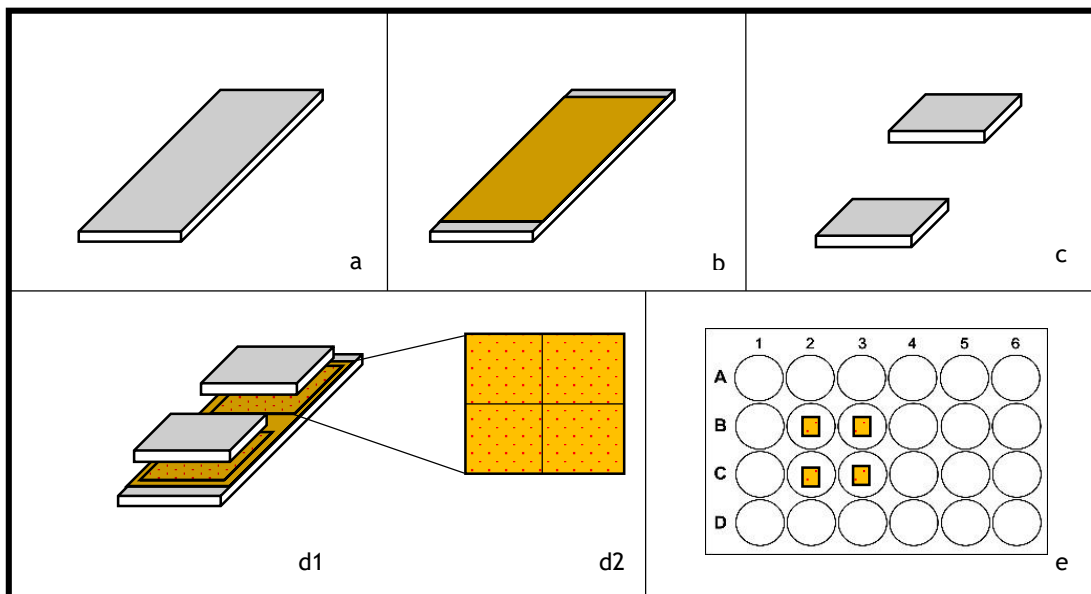


Figure 13 - Former approach. A) clean glass coverslip; b) gold covered coverslip; PDMS stamps with desire pattern; d1) microcontact printing - stamps soaked in initiator ink the reagent on the gold surface; d2) half of the coverslip cut in four squares; e) 1cmx1cm squares placed in a 24 well plate. The red dots represent the polymeric brushes islands.

To scale up micropattern synthesis, the initial idea was to use a 96 well plate without a bottom and further adhere a customized glass covered with gold, presenting the desire polymeric brush patterns. This approach is displayed in Figure 14.

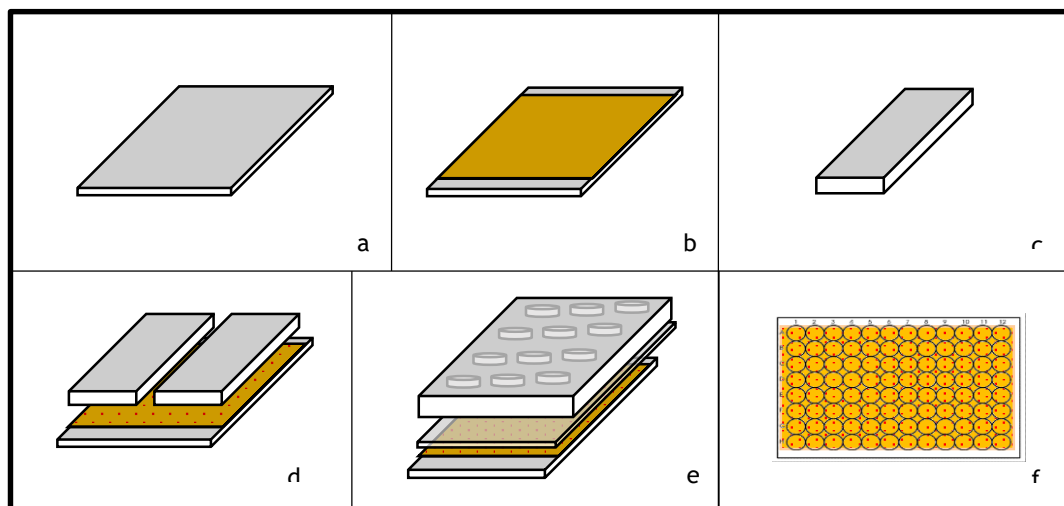




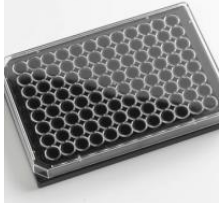


Figure 14 - 96 well plate approach. A) clean customized glass; b) glass covered with gold; c) PDMS stamp cut with the desire format in order to fit the glass; d) Microcontact printing - this step would require a perfect alignment of the stamps preventing polymeric brushes overlap; e) Scheme of different materials applied - plate, adhesive and patterned glass; f) customized glass attached to the plate and ready to use. The red dots represent the polymeric brushes islands.

Once the design was planned, the search for the ideal suppliers and materials started. There were five types of materials needed: customized glass, 96 well plate without bottom and with lid, nontoxic adhesive, square petri dishes for manipulation after micropatterning and overnight containers for micropatterning technique incubations. After an extensive search for suppliers the short list of chosen ones is presented in Table 5.

Table 5 - Chosen materials and suppliers, with description, for the 96 well-plate approach.

Material	Supplier	Description
<i>Overnight Containers</i>	 Brain Research Labs	Glass Staining Dish with Cover, 30 Slides 130 x 100 x 70mm
<i>Square Petri dishes</i>	 Fisher Scientific	Petri dish square with four vents polystyrene sterile 120mm
<i>Glass</i>	 Schott	D 263® T eco Thin Glass customized glass Dimensions: 0.7mm thickness +/- 0.5; 110mm +/- 0.5mm X 75mm +/- 0.5mm
<i>Adhesive</i>	 3M™	3M™ Scotch-Weld™ UV Adhesive
	 Adhesive Research	Product 90106 double faced tape
<i>96 Well Plate/Lid</i>	 Porvair	96 Well A-Plate Krystal glass bottom plate, black and transparent lid

After this extensive search, a new material emerged bringing new possibilities and a new approach. This material, a 50 well silicone from Grace Biolabs (Figure 16), motivated a new design also described in Figure 15.

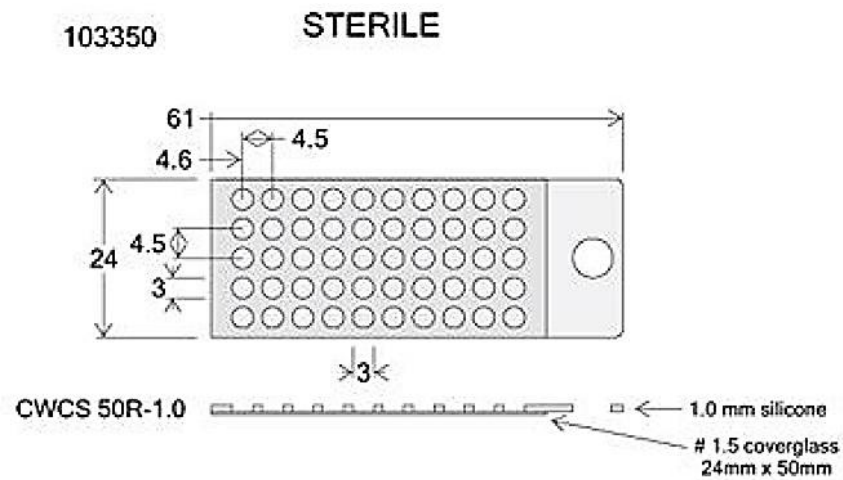


Figure 16 - Scheme view of the 50 well silicone from Grace Biolabs.

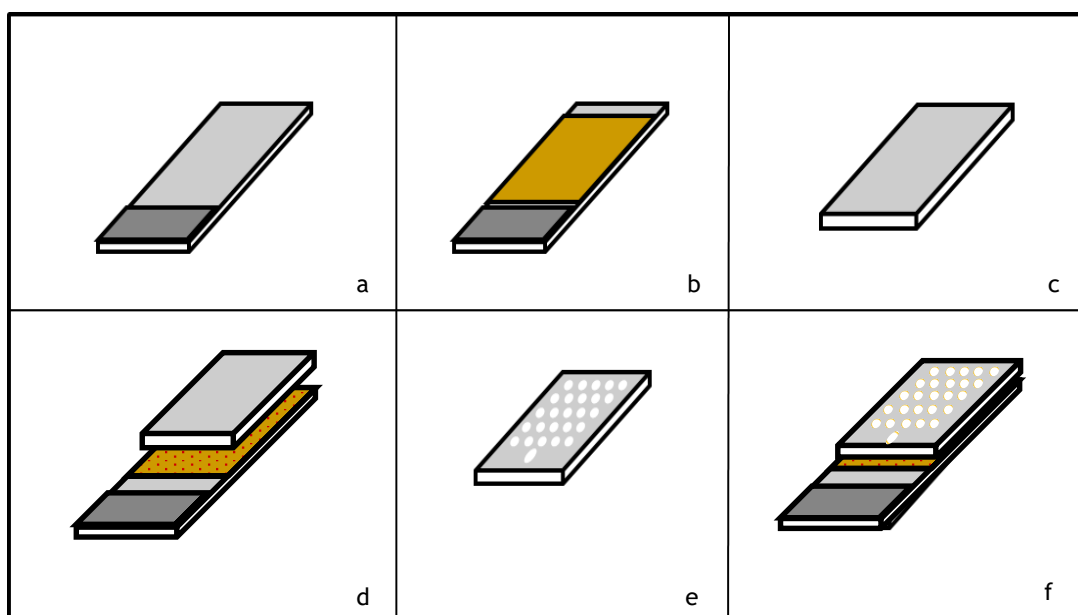


Figure 15 - 50 well silicone approach. A) cleaned microscope slide; b) gold covered microscope slide; c) PDMS stamp cut according to the size of the microscope slide; d) microcontact printing of the microscope slide; e) Reusable 50 well silicone; f) 50 well silicone placement under microscope slide with polymeric brushes. The red dots represent the polymeric brushes islands.

Since this approach involved less new materials and optimization when compared with the 96 well approach, further experiments were performed using it. All real formats are presented in Figure 17.

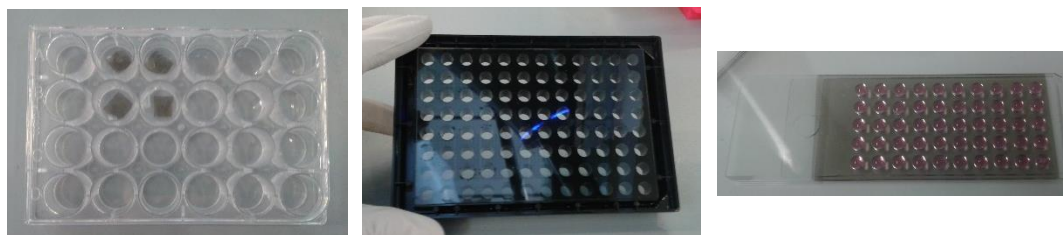


Figure 17 - Real formats of different approaches. At left is the former approach, 24 well-plate format, with 4 1cmx1cm squares disposed in 4 wells. In the centre is the 96 well-plate format upside down, showing the glass adhered to the bottom of the plate. At right is the 50 well-silicone approach with cells already plated in the wells.

4.3 50 Well silicone approach optimization

As shown in Figure 18, the 50 well silicone approach had similar a) b) c) and d) steps when comparing with the 24 well plate approach. The main difference applied in those steps were the glass, microscope slide instead of a coverslip, and stamping the entire surface at the same time instead of stamping in two separate times. The 50 well silicone is then manually placed above the microscope slide (Figure 15-f) for further cell seeding and assays performance. In the previous format, after placing each 1cmx1cm square in different wells, all substrates used to be sterilized with ethanol for 30 minutes allowing further cell seeding. However, in the 50 well silicone format two different sterilization processes were tested. Both with a 30 minute duration, substrates were sterilized with ethanol and under UV light. In order to understand if the UV could affect further processes, substrates were photoactivated with RGD-biotin (RGD-BT) and stained with FITC-SA. In Figure 18 both sterilizations are represented showing that none of them led major differences between brightness of photoactivated polymeric brushes.

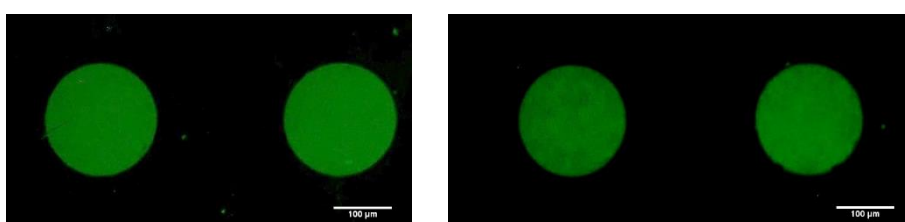


Figure 18 - Photoactivated substrates after ethanol (left) and UV (right) sterilization. Both photoactivation were performed with a 1mg/mL RGD-BT concentration. Both scale bars are

Since no difference in brightness were observed between both sterilisation processes, from then on, the adapted sterilization was the UV one.

Besides substrate sterilization, photoactivation process also needed optimization. Since the chosen glass for the 50 well approach had different features than the one used in the 24 well plate and previous photoactivation was performed placing the UV lamp

under the 24 well plate, two different assays were carried out to understand if the lamp position could have some influence on polymeric brush photoactivation. In Figure 19 is possible to notice that UV placement over polymeric brushes led to a more uniformed photoactivation than the UV placement under substrates. After those assays, brushes started to be photoactivated placing the UV above them.

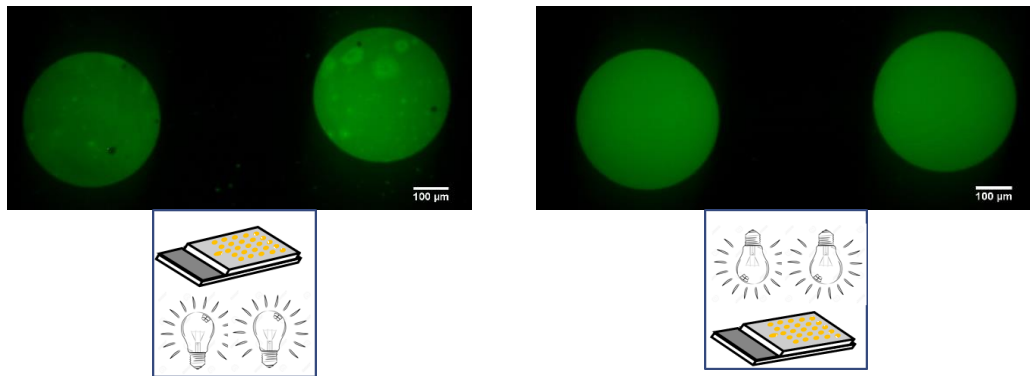


Figure 19 - UV position during polymeric brush photoactivation. UV light placed under (left) and above (right) substrates. Both photoactivations were performed with a 1mg/mL RGD-BT concentration. Both scale bars are 100µm.

After this initial optimization, a new assay was performed in order to understand the relation between RGD-BT concentration and polymer brush photoactivation. As shown in Figure 20, RGD-BT photoactivation showed a higher brightness mean value at a concentration of 2,5mg/mL with a high significance when compared with other concentration brightness mean value.

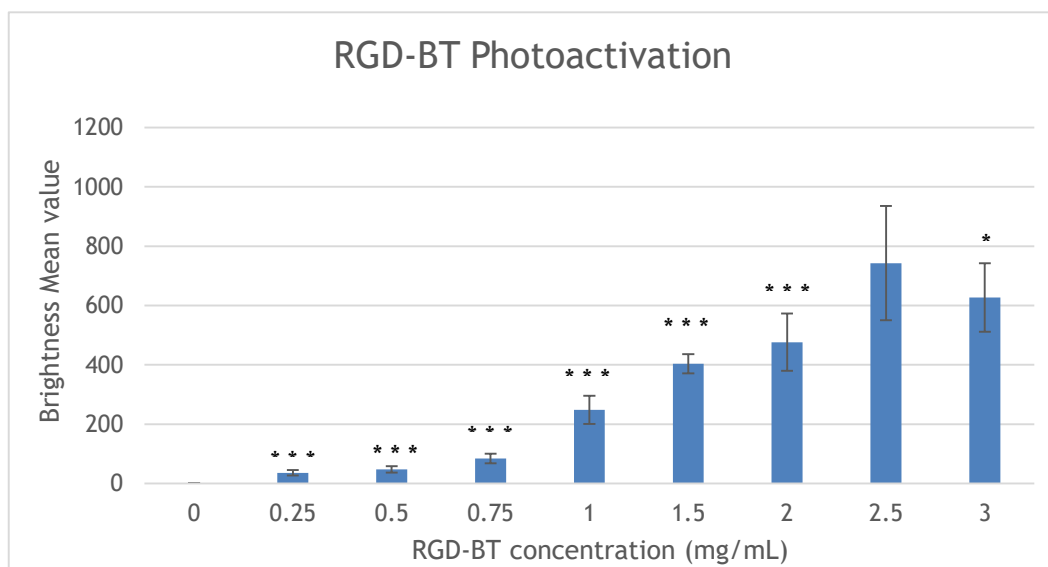


Figure 20 - Brightness mean value of 400 µm islands after photoactivation using 9 different RGD-BT concentrations. This trend was observed in 2 of 3 independent experiments. The other experiment showed a higher variance between 0 and 0.5 mg/mL. N=6-24 depending on the number of brushes present in each acquired image. Data sets are significant at different levels * $p < 0.05$, *** $p < 0.001$ when compared with 2,5 mg/mL RGD-BT concentration.

This experiment was performed in three independent times, being this results representative of two of those experiments. The third experiment as shown a higher brightness mean value for the 3mg/mL RGD-BT concentration.

With the aim of studying further the accuracy of the present method, other type of assays were performed. Using the same RGD-BT concentration in every well (2mg/mL), brightness mean value was acquired along a horizontal (Figure 21) and a vertical (Figure 22) line of the 50 well silicone.

In Figure 21 is possible to see that even with brightness mean values varying between 400 and 620, differences between each well show not to have higher significance, proving the consistency of the approach along a horizontal line of the 50 well silicone. However, in Figure 22, regarding vertical consistency, values showed that there were significant differences when comparing well four with wells 2 and 5, even with no significant differences when comparing well 1 with all other wells. All three independent experiments performed to evaluate vertical consistency of 50 well silicone approach show significant differences between pairs of wells. These results decrease the reliability and consistency of the approach.

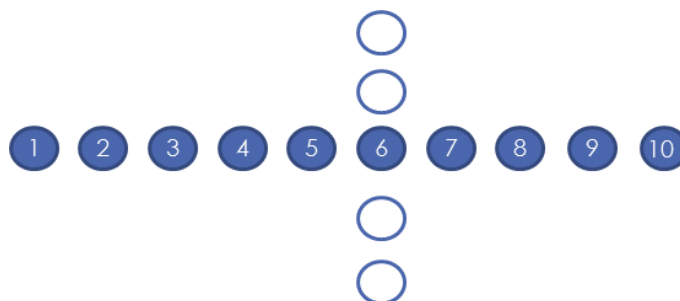
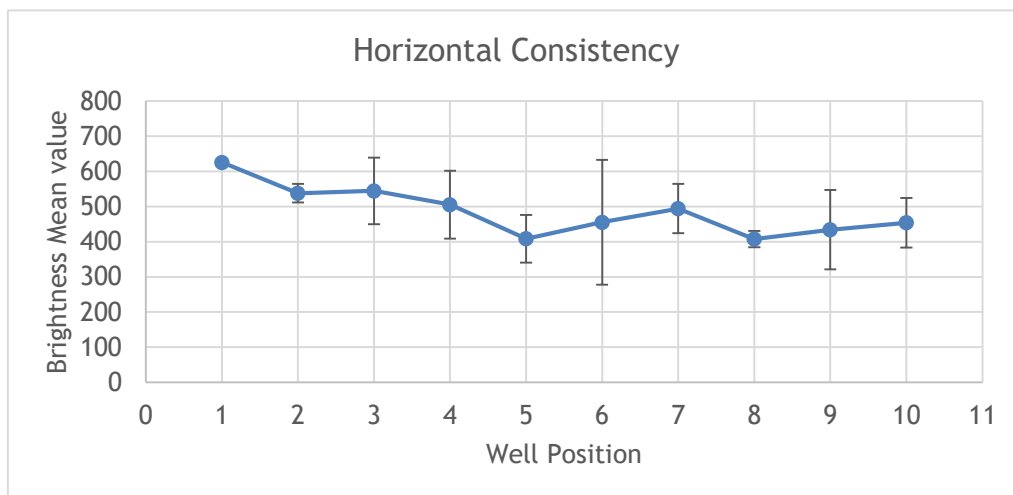


Figure 21 - Brightness mean value of 400 μm islands after photoactivation using a RGD-BT concentration of 2 mg/mL along a horizontal line of the 50 well silicone. This trend was observed in 3 independent experiments. This graph represents one of those experiments with $n=5$. The bottom figure represents the position of each well in the 50 well silicone. The P value between acquired results was 0.0793, considered not quite significant.

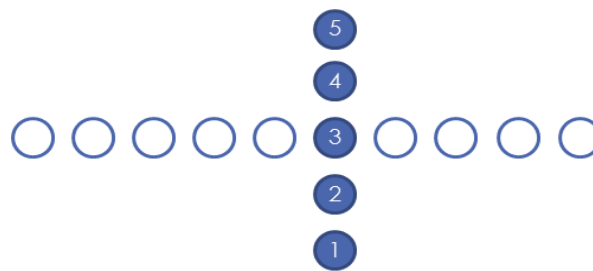
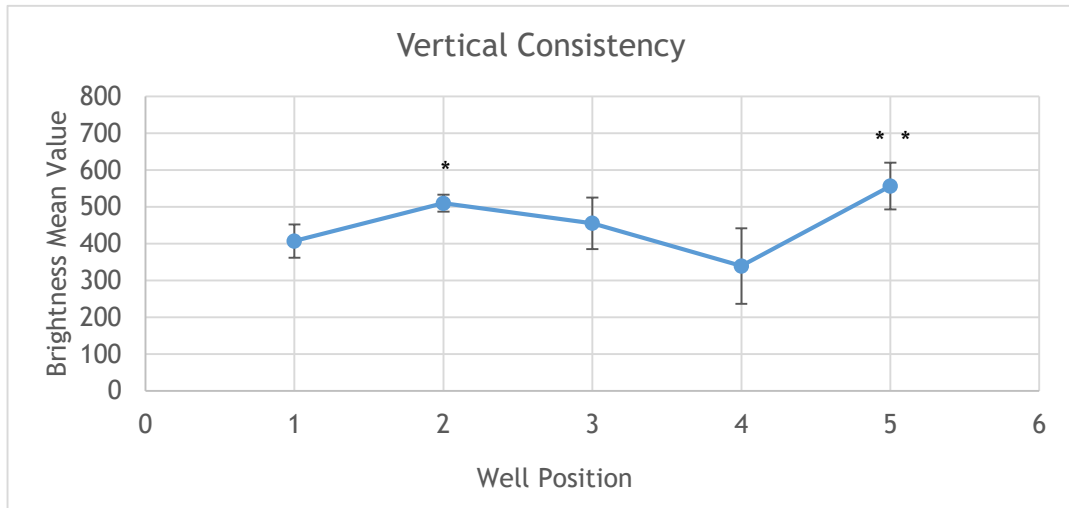


Figure 22 - Brightness mean value of 400 μ m pillars after photoactivation using a RGD-BT concentration of 2 mg/mL along a vertical line of the 50 well silicone. This trend was observed in 3 independent experiments. This graph represents one of those two experiments, with n=5. The bottom figure represents the position of each well in the 50 well silicone. The P of wells 2,3,4 and 5 when compared with well 1 was not significant, however, data sets are significant at different levels * p<0.05, ** p<0.01 when compared with well number 4.

The last assay performed with the aim of understanding the consistency of photoactivation linked the position of 400 μ m islands in each well with their corresponding brightness mean value. Figure 23 shows the result of this last assay. Performed in two independent experiments, the brightness mean value showed to be higher on central brushes of the well. This allowed the perception of which brushes of each well should be quantified in each of the further assays when using the present technique.

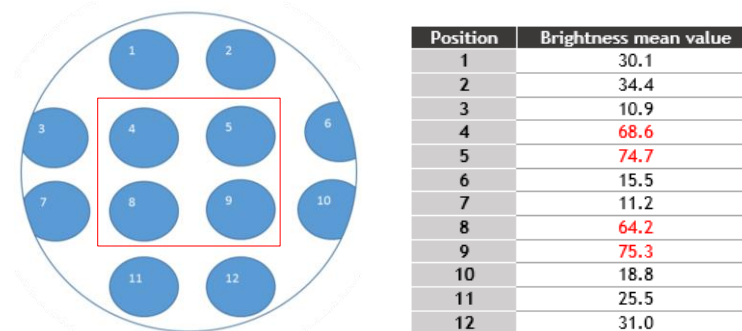


Figure 23 - Brightness mean value of 400 μ m islands according to their position in the well using a RGD-BT concentration of 2mg/mL. Marked with a red line is the region with the four highest values of brightness in contrast with the brushes of the same well. This trend was observed in 2 independent experiments, with an n=1 since brightness of each island was acquired as a whole.

After the brightness mean value measurements, an optimization of the cell seeding in the same approach was performed. Figure 24 shows both patterns after this optimization that led to a cell seeding density of 8000 cells/well ($113\,200\text{ cells/cm}^2$) for the $400\mu\text{m}$ islands and a cell seeding density of 10 000 cells/well ($141\,500\text{ cells/cm}^2$) for the $200\mu\text{m}$ islands. The possibility of optimizing HCA2 cell seeding density proved that this approach could be applied in further studies.

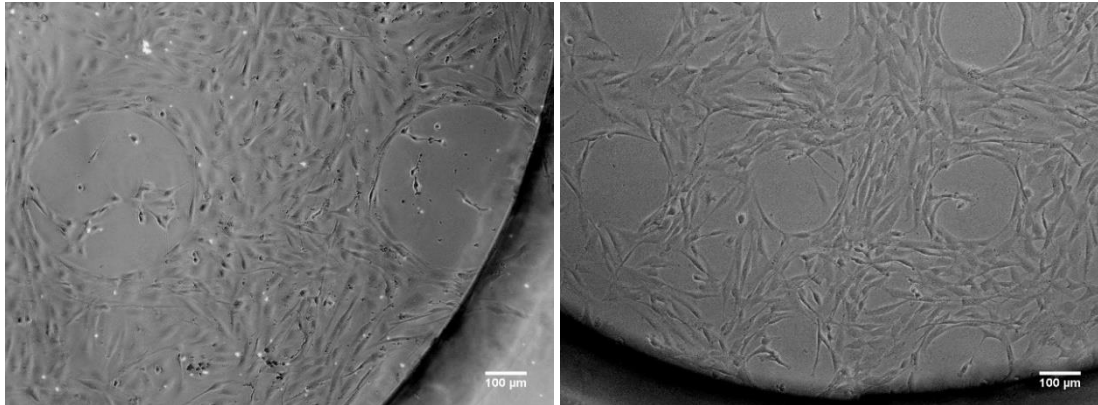


Figure 24 - $400\mu\text{m}$ (left) and $200\mu\text{m}$ (right) islands with cells after cell seeding optimization. Images were acquired 24 hours after cell seeding. Black lines in both images are the edge of the silicone wells. Both scale bars are $100\mu\text{m}$.

4.4 96 well plate approach optimization

During the 50 well silicone approach optimization, the 96 well plate approach also received some attention. As mentioned in Table 5, several materials were researched and tested. Excluding overnight containers and square petridishes, all other materials had to be tested. The first materials to be tested were the adhesives to adhere the glass to the plate. 3M™ Scotch-Weld™ UV Adhesive allowed the adhesion of the glass to the bottom of the plate and a further cell plating. However, the adhesive was toxic leading to the death of the majority of the cells (Figure 25-a). The second adhesive tested was a double faced tape. The wells were punched manually using a hammer, a puncher and a 96 well plate stencil. As it is possible to see in Figure 25-b, this adhesive showed to be non-toxic for the cells 24 hours after seeding allowing both correct adhesion of the glass to the plate and cell patterning. It is also important to notice that a cell seeding density optimization was performed leading to a value of 100 000 cells/well ($320\,000\text{ cells/cm}^2$, assuming a diameter of 0.630cm).

After these initial optimizations, the photoactivation reaction in the 96 well plate was tested using HCA2 cells and a RGD concentration of 2mg/mL is presented in Figure 26.

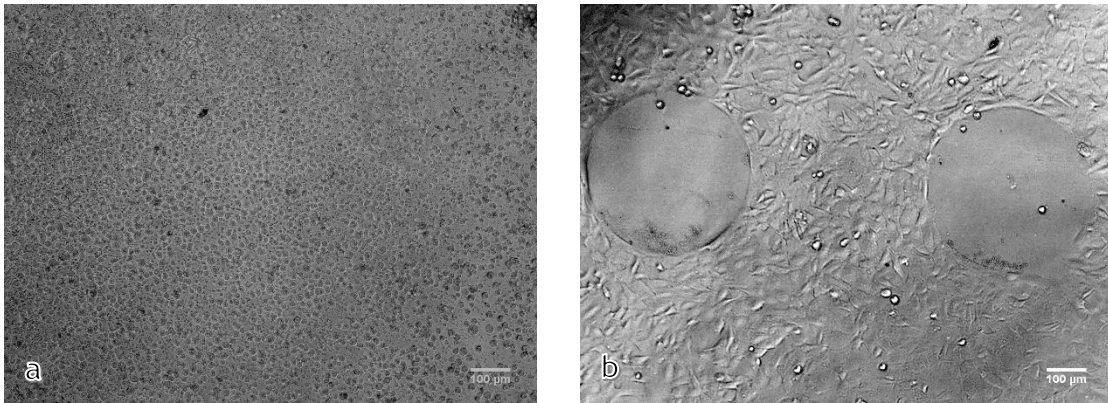


Figure 25 - HCA2 seeded in clean glass (a) and patterned glass (b) after substrate adhesion to the bottom of the 96 well plate using 3M™ Scotch-Weld™ UV Adhesive (a) and punched double faced tape (b). Images were acquired 24 hours after cell seeding. Both scale bars are 100 µm.

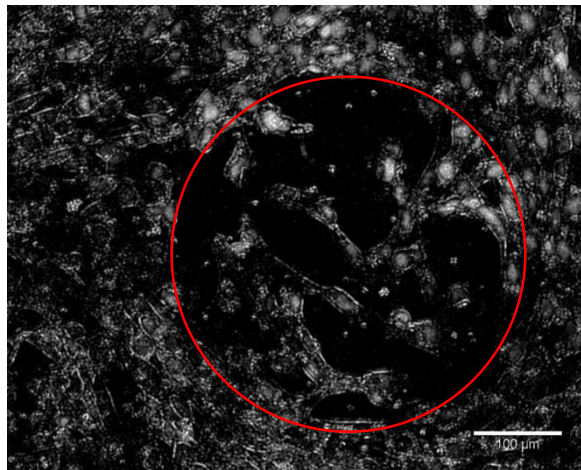


Figure 26 - HCA2 migration after polymeric brush photoactivation with a RGD concentration of 2 mg/mL, using the 96 well plate approach. A red line is marking one pillar coloured in black being closed by migrating cells. Scale bar is 100 µm.

4.5 Scratch assays

Cell migration of each cell line was tested using scratch assays in order to compare their different migration speeds and select which one could be used for further assay validation.

HeLa cells were first tested and compared with another cancer cell line, MDA-Mb231. As shown in Figure 27, MDA-Mb231 travelled a greater distance after 48 hours, which lead to a further comparison with another cell line.

MDA-Mb231 migration was then compared with another breast cancer cell line, MCF-7, as shown in Figure 28.

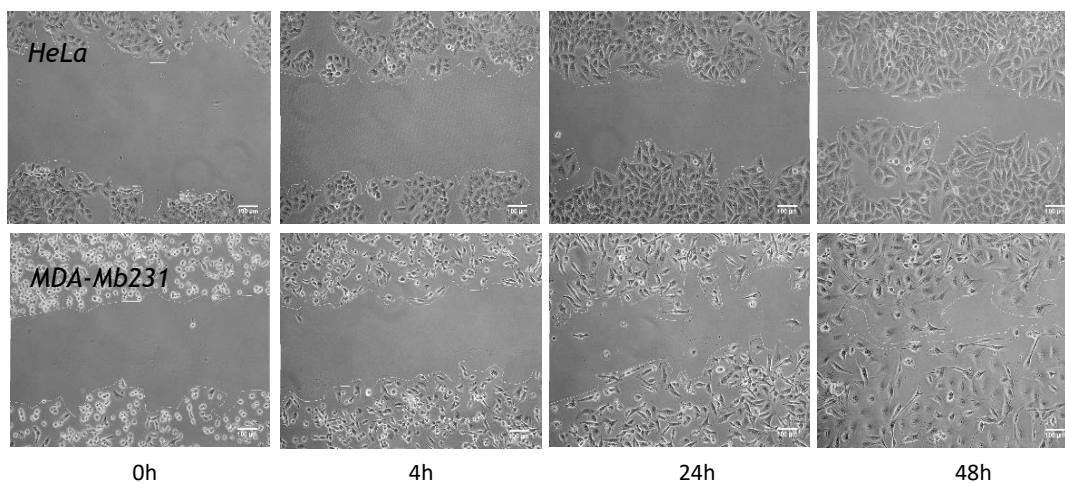
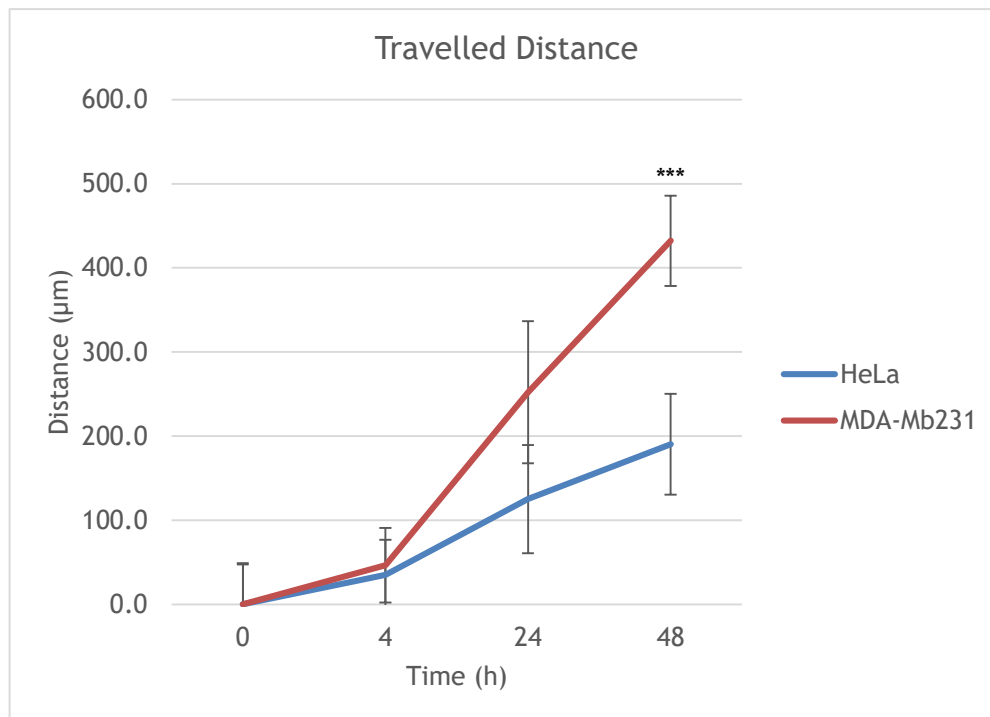


Figure 27 - HeLa cells migration compared with MDA-Mb231 cells after a scratch assay performance. Travelled distance were measured at 0, 4, 24 and 48 hours after scratching. Number of performed measurements (n) varied between 12 and 16 depending on the accuracy and measurability of each image scratch. All scale bars are 100µm. Differences between MDA-Mb231 and HeLa migration data sets are highly significant (***) $p < 0.001$).

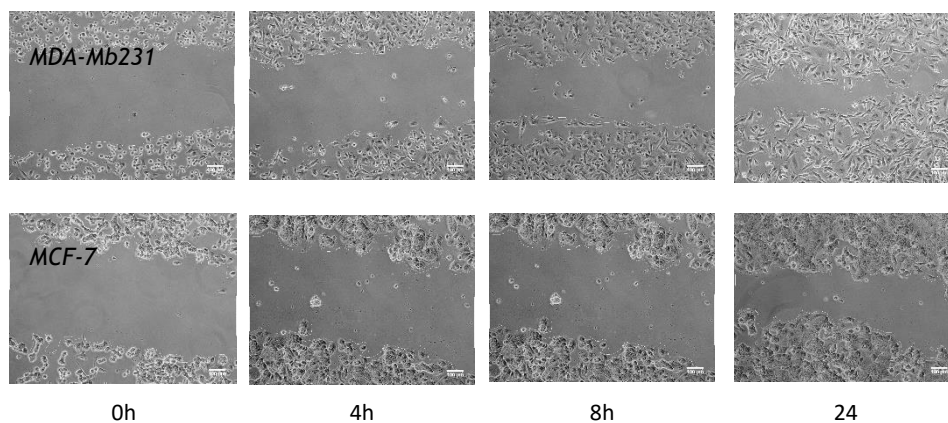
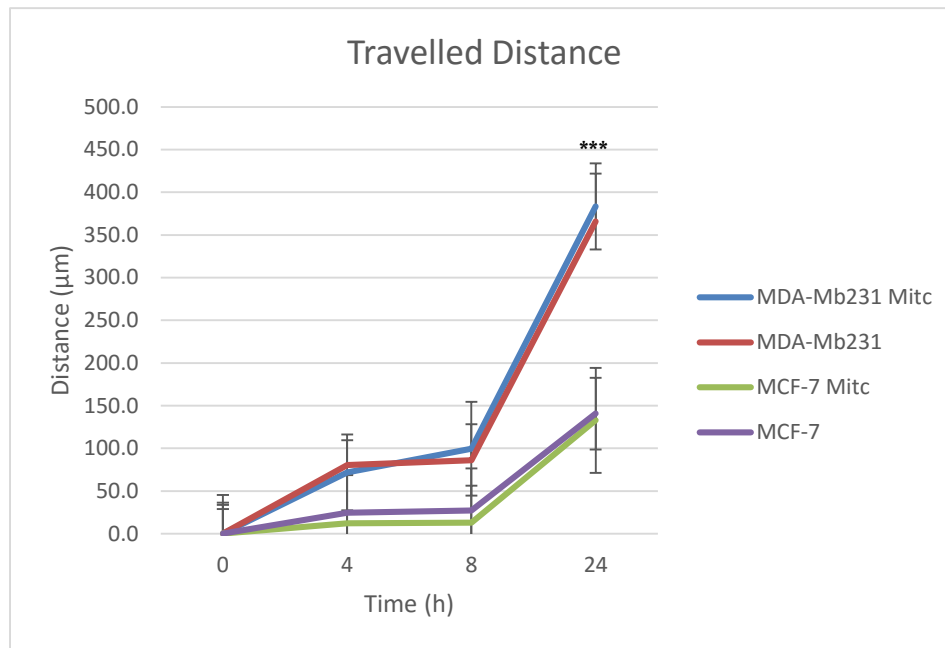


Figure 28 - Comparison between MDA-Mb231 and MCF-7 migration after a scratch assay performance. Travelled distances were measured at 0, 4, 8 and 24 hours after scratching, in cells treated and non-treated with mitomycin C. Number of performed measurements (n) varied between 12 and 16 for the non mitomycin c specimens and between 4 and 6 for the mitomycin specimens depending on the accuracy and measurability of each image scratch. Chosen images showed on top are examples of mitomycin C treated cells migration. Regarding significance, data sets showed no significance between mitomycin C treatment and no treatment in the same cell line and higher significance between results of different cell lines (***) $p < 0.001$). All scale bars are 100µm.

In this case, cells were also treated with mitomycin C, a DNA synthesis inhibitor, with the aim of understanding if cell proliferation could have some influence in wound closure. No higher differences were noticed between migration of cells treated and non-treated with mitomycin C. However a higher and significant difference was notice between migration of MDA-Mb231 and MCF-7.

Last scratch assay performed compared two different types of fibroblasts, NIH3T3 and HCA2. In Figure 29 is possible to see that HCA2 as a higher migration rate that NIH3T3

with significant differences at 8 hours after scratching but with no significant differences at 24 hours.

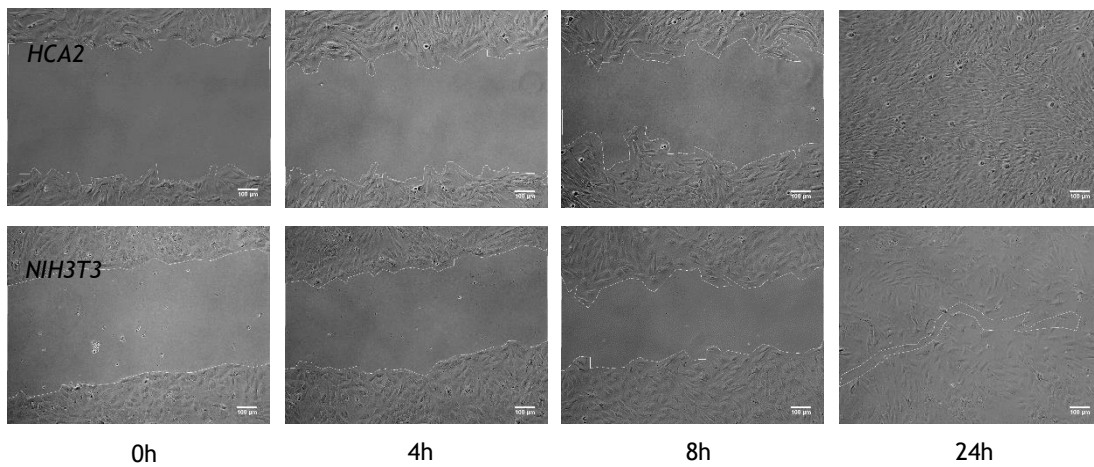
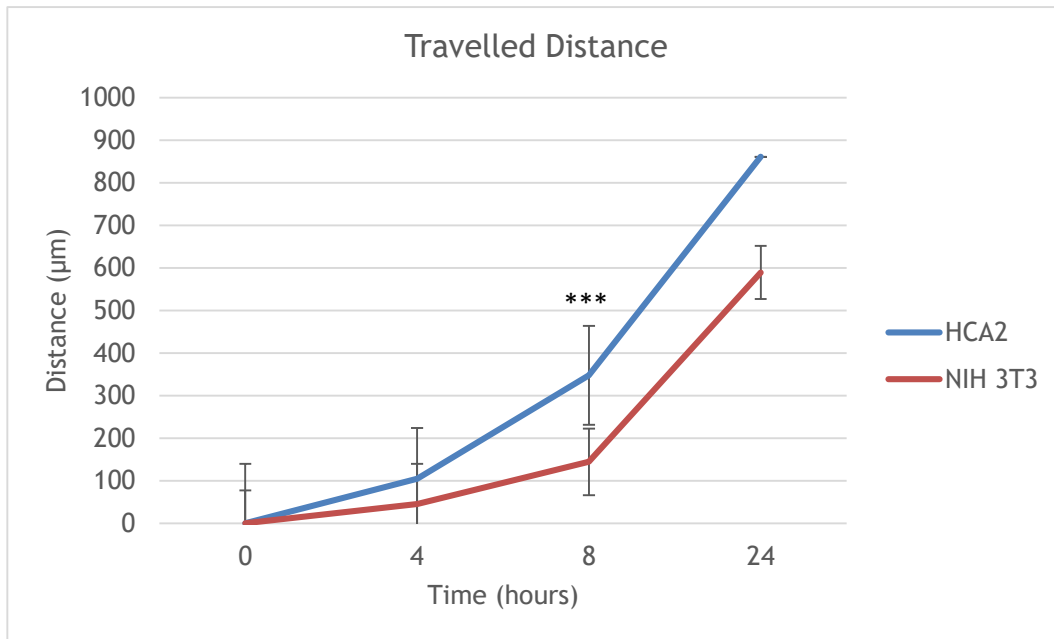


Figure 29 - Comparison between HCA2 and NIH3T3 migration after a scratch assay performance. Travelled distances were measured at 0, 4, 8 and 24 hours after scratching. Number of performed measurements (n) varied between 15 and 16 depending on the accuracy and measurability of each image scratch. There was a high statistical difference between both cell lines at 8 hours (***) but no statistical difference (ns $p > 0.05$) between both cell lines at 24 hours after scratching. All scale bars are 100µm.

At last, in order to compare all tested cell lines, Figure 30 integrates all listed assays in the same graph, comparing their migration with HCA2 migration. In this graph it is possible to notice, 24 hours after scratching, a significant difference in migration of HCA2 when compared with HeLa, MDA-Mb231 and MCF-7. After these experiments, HCA2 were the chosen cell line to use in all subsequent assays.

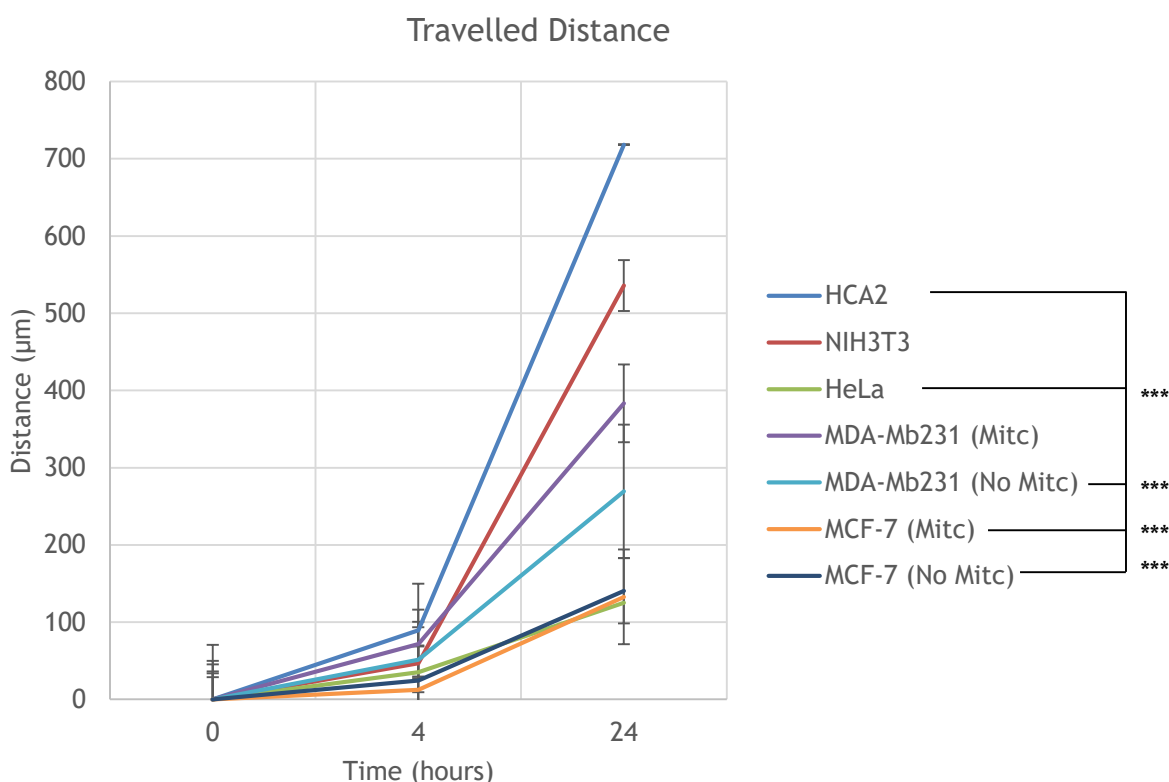


Figure 30 - All preformed scratch assays. Travelled distances were measured at 0, 4, and 24 hours after scratching. Number of performed measurements (n) varied between 5 and 16 depending on the accuracy and measurability of each image scratch. There was a high statistical difference between HCA2 cell line and HeLa, MDA-Mb231 (no mitc), and both MCF-7 lines, at 24 hours (** $p < 0.001$).

4.6 Cell migration in photoactivated polymeric brushes

For the present work, and having into consideration previous scratch assays, HCA2 seemed to be the best cell line to use since they showed good migration properties and to be reactive to substrate alterations. However, all other cell lines can be used in future studies increasing the usability of the system. After the cell line was chosen, 50 well silicone was the approach used to perform different types of assays.

The first assay performed using HCA2 cell line and 50 well silicone approach had the aim to show the relationship between RGD concentration and cell migration. Using the same range of RGD concentrations used in previous RGD-BT photoactivation assay, the percentage of the photoactivated area covered by cells was measured 24 hours after photoactivation. As it is possible to see in Figure 31, a significant difference on wound closure is present in all RGD concentrations when compared with 0 mg/mL. However, at higher concentrations (between 1 to 3 mg/mL), no significant differences were detected.

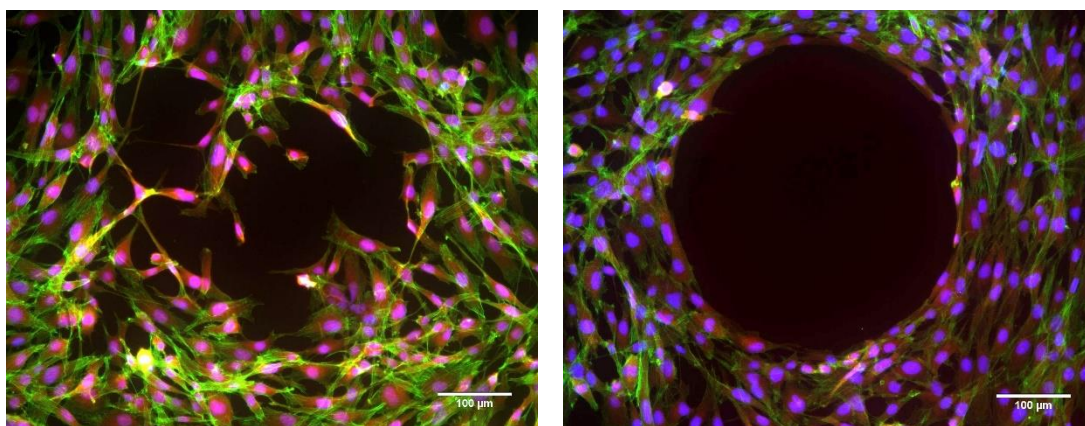
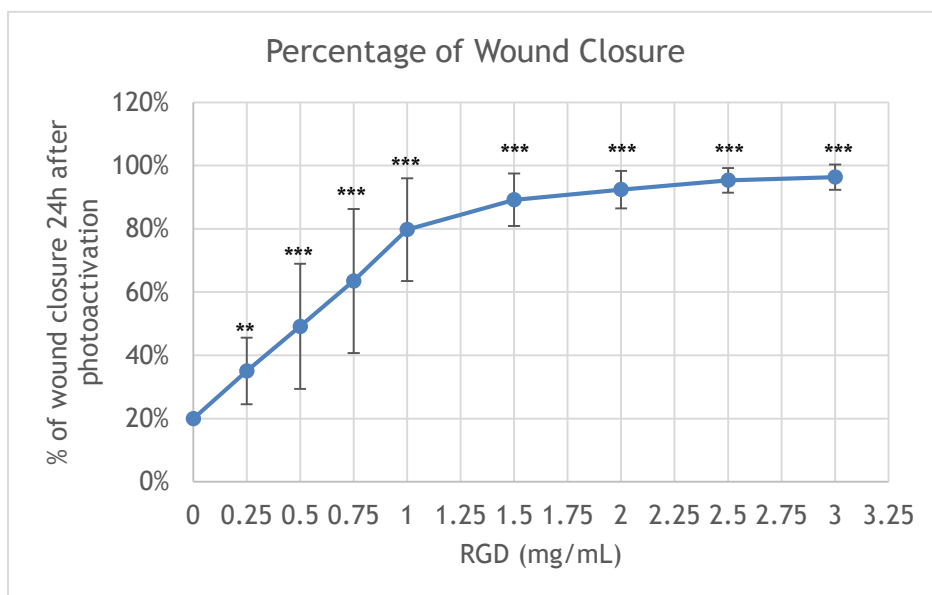


Figure 31 - Percentage of wound closure 24 hours after photoactivation. The wounds are 400 μm islands of polymeric brushes. This trend was observed in 2 of 3 independent experiments. This graph represents one of those two experiments. There was statistical significant difference (** $p < 0.01$ and *** $p < 0.001$) when comparing all RGD concentrations with 0 concentration. There were no statistical significant difference between pairs of data sets with concentrations between 1 to 3 mg/mL. $N = 6-12$ depending on the number of brushes present in each acquired image. Regarding the images, at left is an island photoactivated with 2mg/mL RGD being invaded by HCA2, where at right is the control a RGE (1mg/mL) photoactivated brush. Both images were acquired 24 hours after photoactivation. Cells cytoskeleton is stained with green while DNA is stained with blue.

It is also important to notice that three independent experiments were performed in order to establish a relation between RGD concentration and wound closure. However, only

two presented this trend. The third experiment was performed using RGD-BT instead of RGD allowing brushes staining but led to a different result with a significant difference only present in higher concentrations (between 2 to 3 mg/mL) when compared with 0mg/mL concentration.

The final assay performed using the 50 well silicone approach was the study of how cytoskeletal inhibitors can influence cell structures and wound closure. Cytoskeleton is one of the major regulators of cell migration. Due to that, analysis based in variations of its structure were used as proof of principle of the reliability of the system and its compatibility with different conditions and assays. Using four different inhibitors with five different concentrations each, cells were analysed seeded in clean glass (without pattern) and on micropatterned polymeric brushes. In the case of clean glass seeding, cells were incubated with different inhibitors at different concentrations during 1 hour. On the other hand, cells seeded on patterned substrates were incubated with inhibitors during 23 hours, starting 1 hour after photoactivation. Results for each inhibitor are presented between Figure 32 and Figure 35. It is important to notice that each assay was performed in 3 independent times, however, since it was impossible to image accurately those samples, only a qualitatively analysis was possible to perform.

Starting with Blebbistatin (Figure 32), at higher concentrations (C4 and C5), it is possible to notice a major difference in cells cytoskeleton, losing their integrity and becoming stretch and thinner. This trend is also possible to notice in right images, where cells seem to struggle more to invade 400 μ m islands.

In Figure 33, Latruculin also shows to have a major influence in cell structures at higher concentrations (C4 and C5) with both cytoskeleton and microtubules being fragmented and turning the cells rounded. However, at C4 it is still possible to see some migration (right image).

Regarding Y27632 effect (Figure 34), cells seem to present a fragmented cytoskeleton on their edges but capable of maintaining their general structure (left images). Comparing with their migration pattern, even maintaining an almost intact morphology, cell seem to stop migrating when a high concentration Y27632 inhibitor is applied.

At last, Nocodazole (Figure 35) seems to be really aggressive to cells. Its effects start to be present at concentration C3 with microtubules being partially fragmented. Nevertheless, cell cytoskeleton seem to be still mostly intact and cell migration seems to be completely absent only under C5 effect.

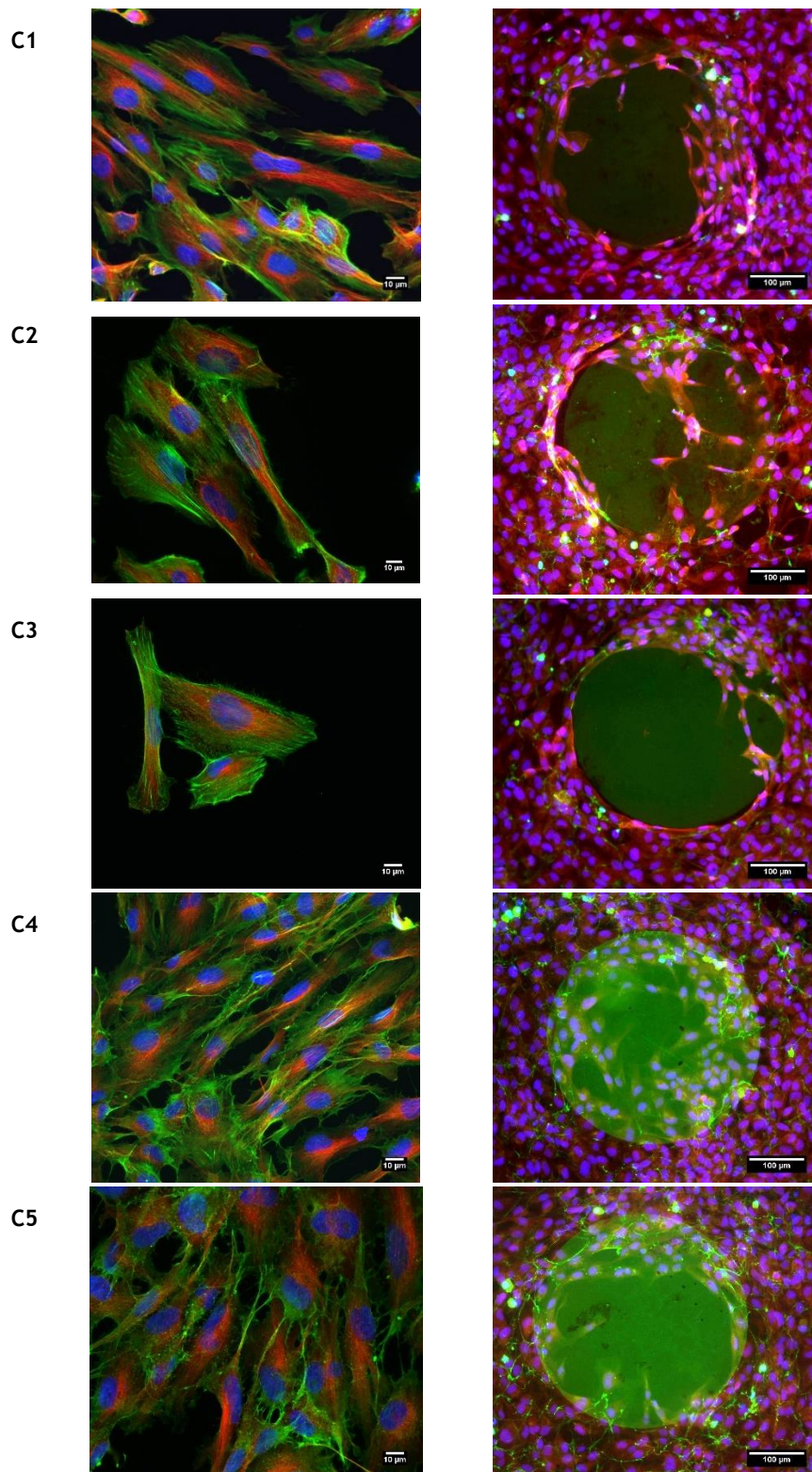


Figure 32 - Blebbistatin effect in cell structure when plated in glass (left) and polymeric brushes (right). Left images were acquired 24 hours after photoactivation with a RGD-BT concentration of 2mg/mL. Applied blebbistatin concentrations were: C1=0nM; C2=0.5nM; C3=5 μ M; C4=25 μ M and C5=10 μ M. Left scale bars are 10 μ m while right scale bars are 100 μ m. At left, cytoskeleton is stained with green, microtubules with red and DNA with blue. At right, POEGMA brushes are stained with green, cell cytoplasm with red and DNA with blue.

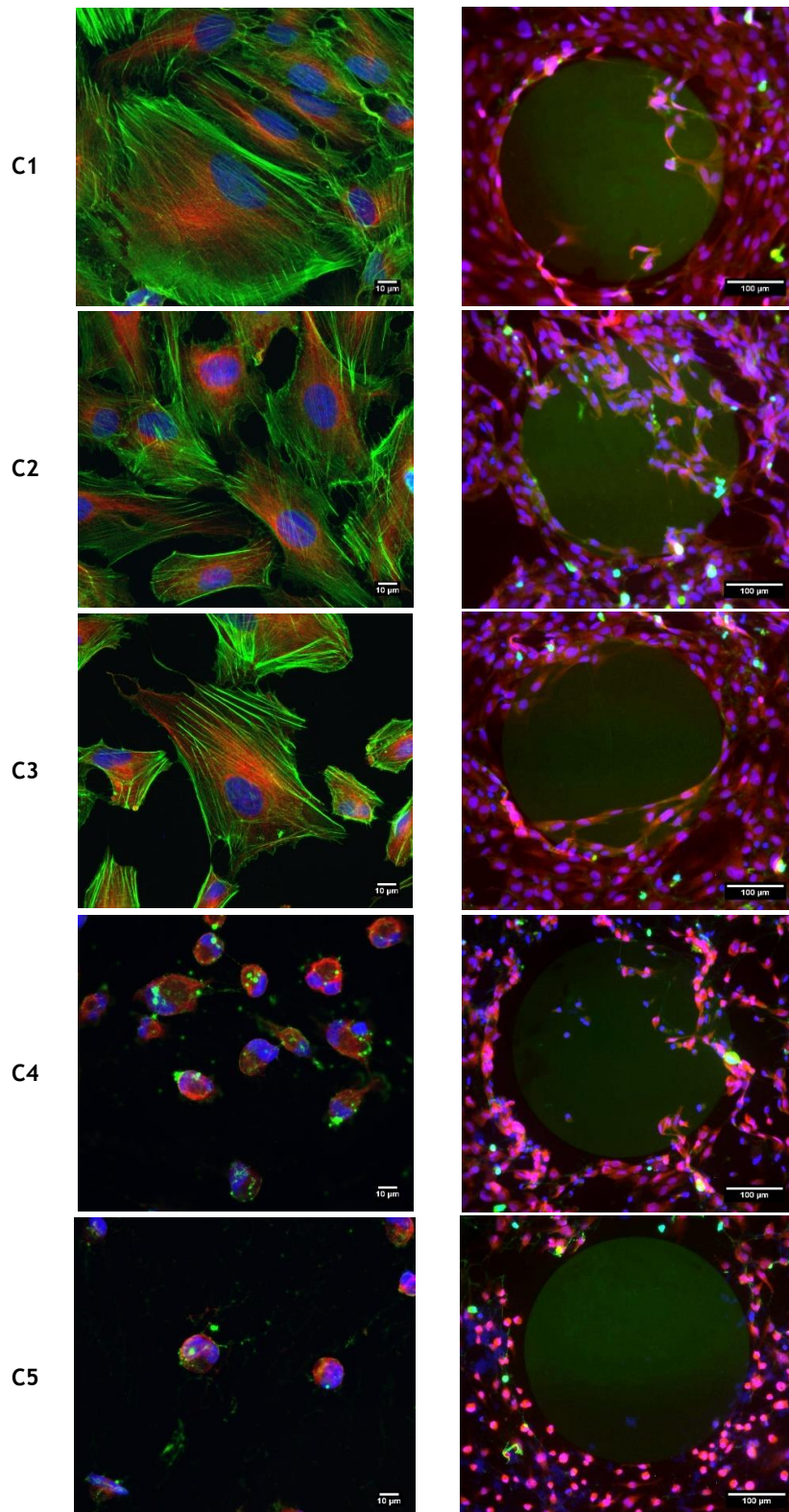


Figure 33 - Latrunculin effect in cell structure when plated in glass (left) and polymeric brushes (right). Left images were acquired 24 hours after photoactivation with a RGD-BT concentration of 2mg/mL. Applied Latrunculin concentrations were: C1=0nM; C2=100nM; C3=1µM; C4=25µM and C5=50µM. Left scale bars are 10µm while right scale bars are 100µm. At left, cytoskeleton is stained with green, microtubules with red and DNA with blue. At right, POEGMA brushes are stained with green, cell cytoplasm with red and DNA with blue.

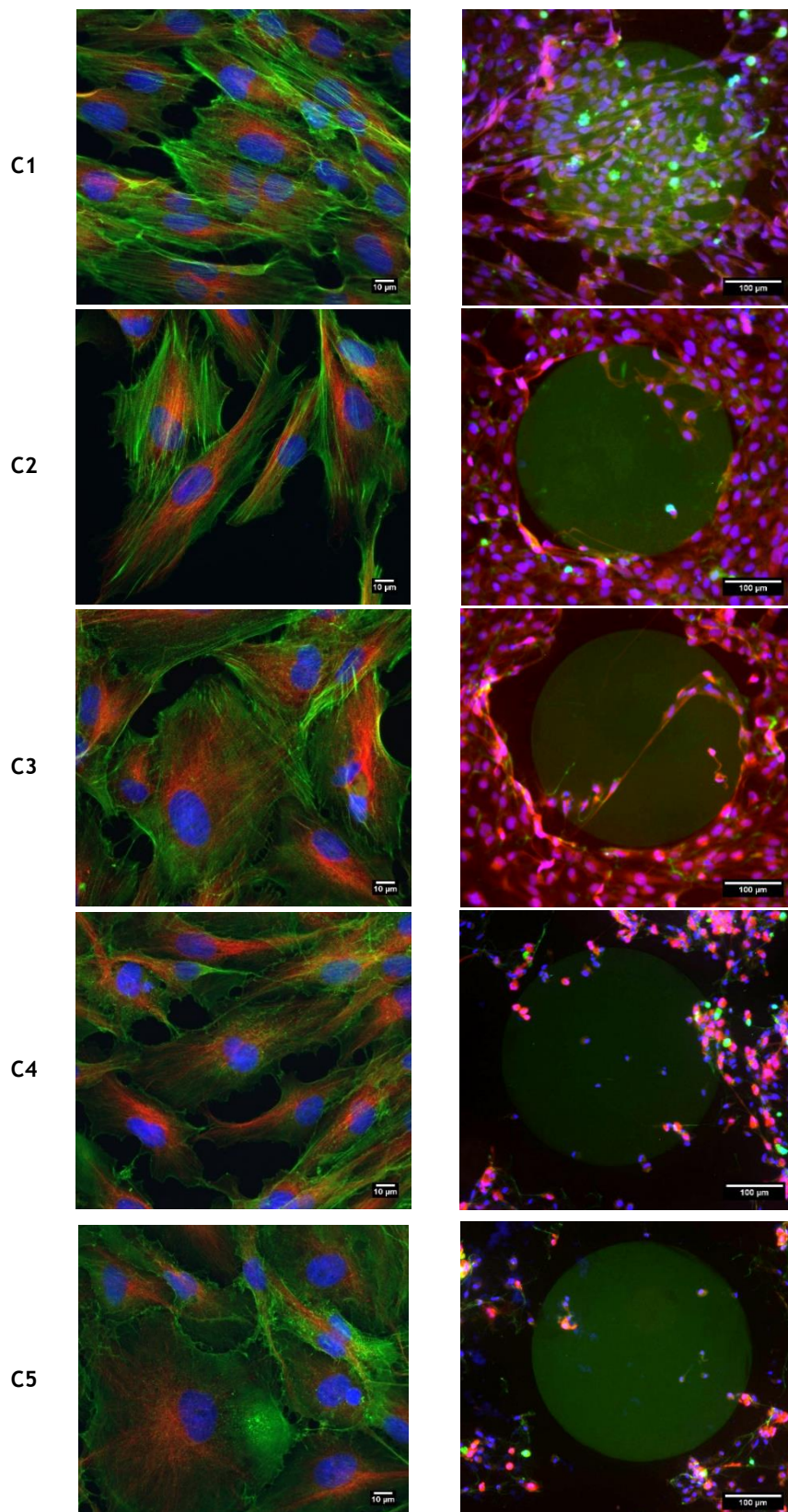


Figure 34 - Y27632 effect in cell structure when plated in glass (left) and polymeric brushes (right). Left images were acquired 24 hours after photoactivation with a RGD-BT concentration of 2mg/mL. Applied Y27632 concentrations were: C1=0 μ M; C2=100nM; C3=1 μ M; C4=5 μ M and C5=10 μ M. Left scale bars are 10 μ m while right scale bars are 100 μ m. At left, cytoskeleton is stained with green, microtubules with red and DNA with blue. At right, POEGMA brushes are stained with green, cell cytoplasm with red and DNA with blue.

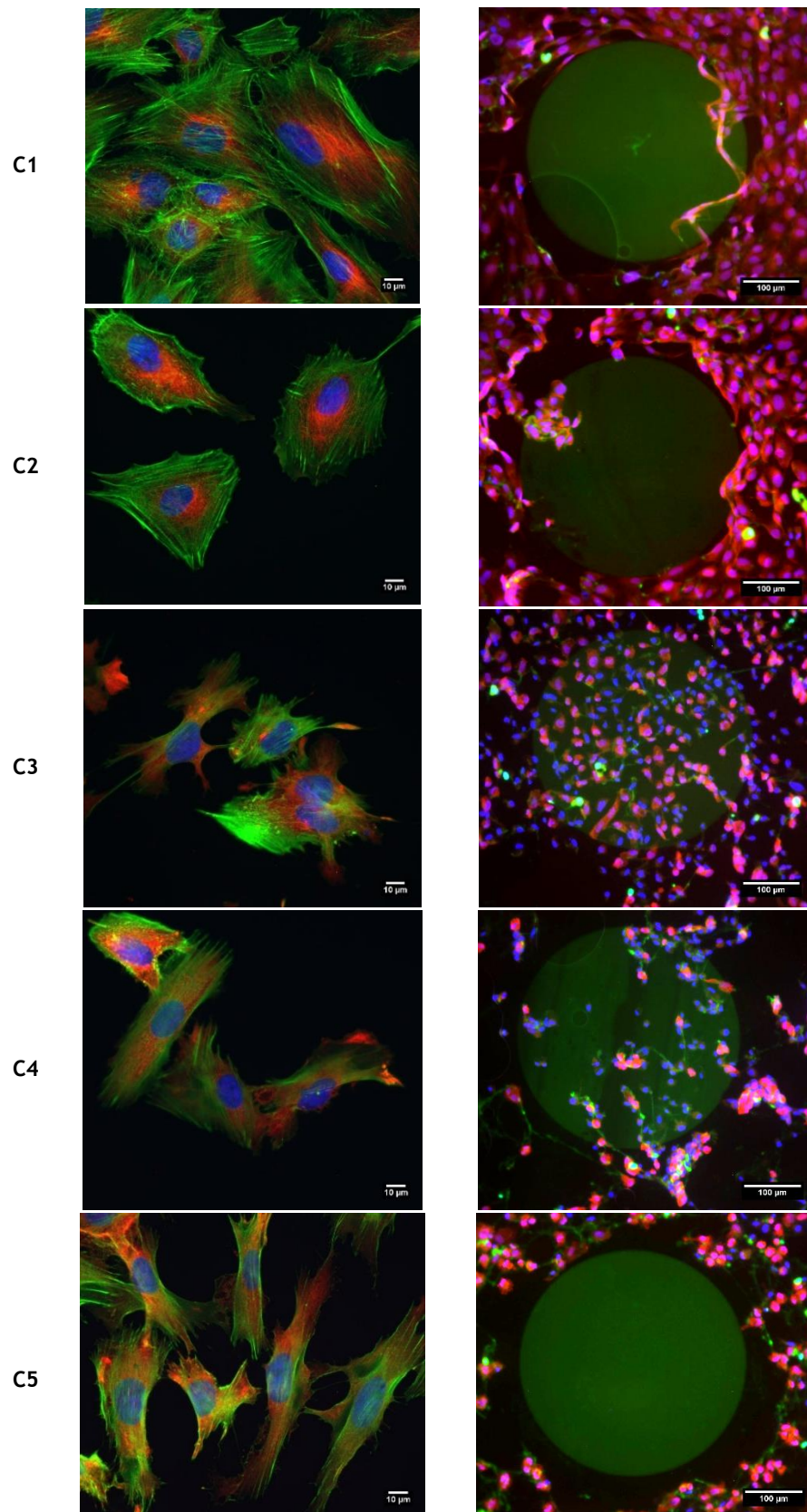


Figure 35 - Nocodazole effect in cell structure when plated in glass (left) and polymeric brushes (right). Left images were acquired 24 hours after photoactivation with a RGD-BT concentration of 2mg/mL. Applied Nocodazole concentrations were: C1=0nM; C2=10nM; C3=100nM; C4=500nM and C5=1μM. Left scale bars are 10μm while right scale bars are 100μm. At left, cytoskeleton is stained with green, microtubules with red and DNA with blue. At right, POEGMA brushes are stained with green, cell cytoplasm with red and DNA with blue.

4.7 InCell microscopy and analysis

The final phase of the present work focused on establishing an InCell microscope analysis protocol. InCell microscopy allows an automated acquisition of images from standardized well plate formats. However, since in the present work the techniques were performed using a manually placed 50 well silicone in a microscope slide, well position were subject to changes between assays. In order to solve that obstacle, certain measures started to be performed before the InCell acquisition. Figure 36 blue arrows represent the necessary measures to align each sample set for image acquisition.

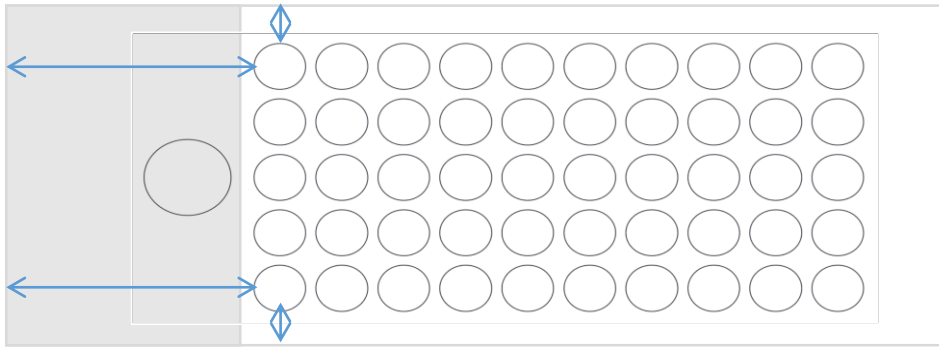


Figure 36 - Scheme of the 50 well silicone placed above the microscope slide. Blue arrows symbolize measures necessary to set up in cell microscope protocol acquisition.

Since each image of the well acquired with the InCell microscope would only capture one or half of an island, the protocol defined a 9 images acquisition per well. After that acquisition, with the help of InCell Analyzer, those 9 images were stitched together leading to an overall image and allowing a more accurate quantification of cell migration (Figure 37).

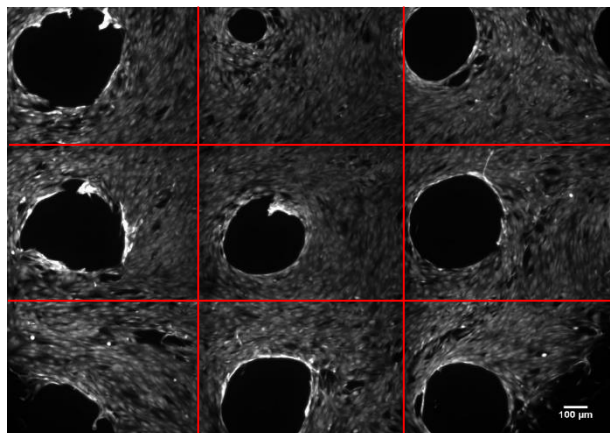


Figure 37 - Example of 9 acquired images of the same well after being stitched by the In Cell Analyzer software. Red lines mark previous borders of each individual image.

Regarding quantification processes, several attempts were performed as shown in Figure 38. In this figure is possible to see an original image acquired by the InCell microscope (top left). This image was acquired with the aim of measure wound closure. The attempts exemplified in the figures show the regions without cells (bottom left, yellow marks), region with higher brightness mean value corresponding to stained brushes and excluding other regions (bottom right, brushes are green while regions of no interest are red), and an overlap of both acquisitions (top right), where brushes region are marked with a green line and region without cells are marked with a yellow line. The main idea was to acquire a non-invaded area represented by the overlapped region. However, as it is possible to notice in Figure 38, marked regions are not completely accurate providing unviable results. This analysis is currently under optimization.

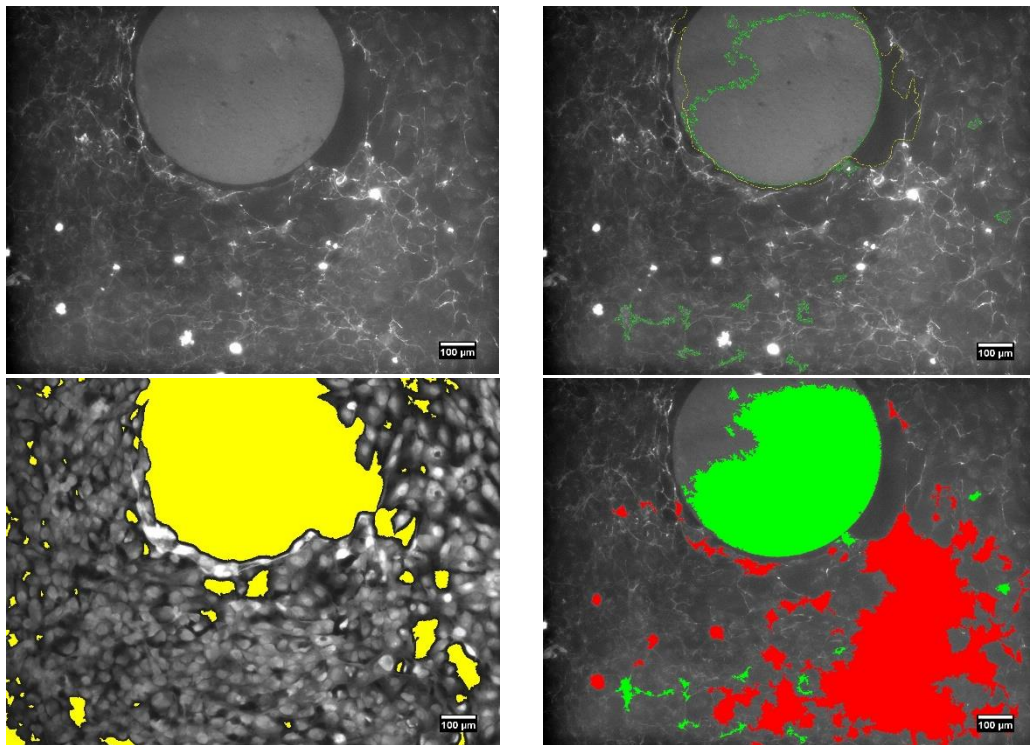


Figure 38 - InCell Analyzer Software general view (right top image) and examples of the several attempts performed in order to acquire the region of polymeric brushes islands. All scale bars are 100µm. Area without cells is colored with yellow, area with POEGMA brushes is colored with green and area without POEGMA brushes is colored with red.

Chapter 5 | Discussion

The present work had the aim of creating a new high throughput assay for *in vitro* cell migration studies mainly related with wound healing.

In a wound, collective cell migration is highly relevant. With preserved cell-cell junctions, cells travel collectively in 2-Dimensions as epithelial sheets across basal membranes [50]. Epithelial monolayers migrate with the aim of closing a tissue defect following the interface between the underlying substrate and cell-free space until the gap is closed [56]. Moreover cells also react to other contexts like pillars, substrate rigidity, tensile forces and micropatterned adhesion areas, altering their traction forces, differentiation, growth and apoptosis. Substrate dimension has some influence in migration too, leading cells to a dimensional preference detection during the process [57].

With the purpose of developing an *in vitro* assay capable of mimicking 2D wound healing *in vivo* processes and being replicated, a micropatterned polymeric brushes model was created. Micropatterning techniques are known for allowing a homogeneous functionalization of a given surface with the application of a desired pattern to it [143]. Gold was the chosen surface for this experiment giving a clean and fast patterning [167]. Regarding the polymer, POEGMA was the chosen one since allows an excellent reproducibility and control of micrometre sized features [142].

This work was based in previous developed technique by *Costa et. al.*, 2014, however additional optimization was performed for a new set up with a different cell line and different patterns. Those optimizations were necessary mostly because the pattern was the inverse of the original one and lead to hampered adhesion of cells. After trying different set ups it was possible to conclude that the optimal cell seeding density showed to be different between cells and patterns most likely due to the fact that all the cell lines studied had different morphologies and the available area for cells to adhere of 200 and 400 μ m islands was different.

After those initial optimizations three different approaches were described. In fact, the 24 well plate approach had some limitations like the reduced number of possible conditions per assay and some time consuming steps like cutting the substrates and

placing them individually in each well. Those limitations lead to the creation of two new approaches. Both of them showed advantages and disadvantages. Table 6 compares characteristics of all three approaches. It is possible to conclude, comparing the cost per reaction, that the 50 well silicone is the most affordable approach, however it is necessary to analyse other features besides the cost. As present in Table 6, and excluding the 24 well plate approach since it seems to have less advantages comparing with the other two, the 50 well silicone uses less reagent per reaction, the same materials used in the original approach and allows a total photoactivation of the wells. However, there are several big disadvantages with this approach. First, the hard manipulation of the wells turns the assay more vulnerable to errors caused by the researcher performing it, therefore is less reproducible. Moreover, since this project aims to create a high throughput assay capable of being automatically analysed, having samples with variable positions between different slides and the difficulty to prepare the samples for image acquisition are the main disadvantages of this approach. At last, the fact that all 50 wells have to be manipulated individually makes the technique time consuming and increases the possibility of damaging each reaction. Therefore this approach does not seem to solve the problem proposed. By its turn, the 96 well plate uses larger reagent volume, involves a higher price per reaction, still need optimization regarding adhesive application and has to be performed using a customized glass. However, the fact that it has standard measurements allowing direct analysis and the use of multichannel pipettes makes the approach more automatized and attractive. In fact, this automatized feature of the approach will decrease the influence of who is performing the assay. In addition, sample preparation for cell imaging is also different and less susceptible to damage increasing the possibilities of acquiring good results from samples.

Table 6 - Comparison between the three developed techniques.

Approach	Suppliers	Materials cost	Estimated Cost (Per Reaction)	Advantages	Disadvantages
24 well Plate	Sigma Aldrich (Glass and plate)	0,065£/glass 0,12£/plate	0,13£ (0,176€) per reaction (1 glass for 8 reactions and 1 plate for 24 reactions)	Easier to optimize since it is an already established approach	Only 20 wells can be photoactivated each time; Large volumes of reagents are used in each condition (500mL)
50 well silicone	Sigma Aldrich (Glass) Grace Biolabs (Silicone Well) Fisher Science (Square Petridish)	0,42£/glass 6,3£/silicone 0,58£/petri dish	0,033£ (0,0447€) per reaction (1 glass, 1 petri dish and 1 silicone for 50 reactions plus each)	Slides have the same size has former glasses; silicone wells are reusable; all wells can be photoactivated	Hard manipulation; Manual placement of silicones has high influence in automated microscopy;

			silicone can be reused ten times)	at the same time; small volume per reaction (10 μ L)	Possible cross over between wells; difficult mounting samples process for image acquisition
96 well plate	Schott (Customized Glass) Porvair (Plate and lid) Adhesive research (adhesive) BrainResearch (Container)	6,23 € /glass 2,65 € /plate 1,05 € /lid - Adhesive undefined - Container not added since it requires only an initial investment	0,104€ (0,141 €) per reaction (1 plate and 1 glass for 96 reactions)	Medium volume per reaction (100 μ L); Direct analysis by In Cell microscopy due to standard measures; Possibility to use multichannel pipette	Customized glass; adhesive manually punched; higher volumes for polymer brushes development; last column cannot be photoactivated

After this comparison is possible to consider that even being more expensive, the 96 well plate approach showed to be more promising and therefore its first optimizations were also performed after 50 well silicone optimizations were complete.

Moving now to the optimization itself, analysing Figure 18 it is possible to conclude that UV sterilization showed to have no effect on the polymeric chain structure. After that the standard ethanol sterilization was replaced by the UV one since this last one is less time consuming and decreases the number of manual manipulation in each well. In Figure 19, regarding the UV light placement it is possible to notice that RGD-BT photoactivation seems weaker with the light placed under the microscope slide. This could happened due to the higher thickness of the microscope slide used comparing with the thickness of previous applied coverslips. That thickness could influence the capacity of UV light to photoactivate polymeric brushes.

The RGD-BT photoactivation results show a saturation point for the brushes photoactivation around a concentration of 2,5 mg/mL. In fact, thiol-yne reaction requires free thiols so in this case all the thiols were probably coupled with the peptide at this concentration [141]. In higher concentrations like 3mg/mL, brightness mean value seemed to decrease, probably because with a higher amount of peptide the competition to couple in available thiols became more difficult to achieve or they could partially self-react. The reason why saturation point is much higher than the one showed in previous works is still not clearly understood. However, the fact that reagents were confined in a smaller space forming a dome could have a large influence as this results with the peptide accumulating on top of that same dome.

Horizontal and vertical consistency also showed some variations between well positions. Since the entire slide was placed under UV light inducing all wells to the same

UV intensity, those variations were directly related with wells manipulation. Hereupon, those results reflect that 50 wells are hard to manipulate and decreases technique reproducibility. The dome effects emerges again in Figure 23 As shown, four central patterns of each well seem to present a higher mean brightness value probably due to an accumulation of peptide in the centre of the well. From then on, all values started to be only acquired from the centre of the well.

At last, in Figure 24 it is possible to see the ideal cell seeding density. Besides that, it is possible to see that silicone wells can isolate cells within a given area (the border of the wells are visible) and that cells can reach and adhere to the surface until the edge covering the entire well. Moreover, even with the ideal cell seeding density and without photoactivating polymeric brushes, some cells seem to cross islands. This can be justified by resistive forces. Those forces are applied by the substrate and normally help balancing internal forces of cells that lead to pre-stress of adherent cells' cytoskeleton. With the redistribution of internal forces due to imposition of physical boundaries, cell remodeling is normally activated and further force sensitive cellular processes become active. In specific sites that adhesion is inhibited, cells are able cross that patterned regions by applying a higher contractile force [115] leading to the result present in Figure 24.

In 96 well plate approach, the double faced tape adhesive showed to be non-toxic (Figure 25) allowing the development of the technique. Even without quantitative results, analysing qualitatively Figure 25, is possible to notice that with a RGD concentration of 2mg/mL cells are able to migrate and invade polymeric brushes with 400 μ m islands.

Regarding the scratch assay, it is possible to see some differences between all different types of cell lines. In cancer cell lines, HeLa showed to be the one travelling a smaller distance probably because it is a less invasive cell line. Difference between MDA-Mb231 and MCF-7 were also noticed. MCF-7 showed to be slower than MDA-Mb231, probably because instead of migrating along the substrate, MCF-7 usually create vertical domes, delaying their migration process. Moreover, the mitomycin C treatment showed not to have a major influence in cell migration rate. In the case of fibroblasts, human fibroblasts showed to migrate faster than mouse fibroblasts (Figure 29). This result can be justified by the fact that HCA2 are a dermal fibroblast cell line derived from Human sigmoid colon adenocarcinoma, contrasting with NIH3T3, a mouse embryonic fibroblast cell line. Based on Figure 30 it is possible to conclude that HCA2 are the fastest cell line, between the ones analysed. It is important to notice that fibroblasts are part of the cell types responsible for dermal tissue regulation using integrins as communicators between cytoskeleton and ECM constituents, being easy to handle *in vitro* and giving reliable results related with cell migration and wound healing [90]. In wound healing fibroblasts are highly present in proliferative phase helping in neo-angiogenesis [5]. However, in chronic wounds, fibroblasts have a different morphology, migration capacities,

proliferation and responsiveness wounds [28]. Mechanical forces development and further creation of mechanical feedback loop between cells and their environment are some of the roles that fibroblasts play under wound site influence [8]. Those features related to HCA2 migration rate make it advantageous for assay development and validation.

After choosing the ideal cell line to test, a cell migration assay with photoactivated polymeric brushes was performed. In this assay, patterned islands act as microwounds and a relation between RGD concentration and wound closure was established. As shown in Figure 31, cell migration and wound closure seems to stabilize between 2mg/mL and 3mg/mL concentration. This result contrasts with the results shown in Figure 20. This difference between experiments can be justified by the fact that the utilized peptide was different in the first two wound closure experiments (RGD instead of RGD-BT). Moreover, brightness mean value only represents the coupling of peptide to polymeric brushes. In other words, the fact that a higher RGD concentration is present in brushes surface does not mean that cells integrins can sense more sequences and motivate a higher cell migration rate.

Regarding inhibitors assay, four different inhibitors were used. All of them showed to have an aggressive effect in higher concentrations. Blebbistatin is known for directly inhibiting myosin function very specifically [13]. In Figure 32, at higher concentrations it is possible to notice a difference in cell structure with cell cytoskeleton (green) turning thinner and stretched (C4 and C5 left images). By its turn, Latrunculin is known for its role in inhibiting actin polymerization. In fact, in Figure 33 is possible to see that at higher concentrations both cytoskeleton and microtubules lose their structure as fibroblasts replace their elongated morphology by a rounded one. Y27632, a Rho-kinase inhibitor, also show to have some influence at higher concentrations in cell cytoskeleton, since it is possible to notice a fragmentation pattern around cells. Lastly, Nocodazole, a microtubules inhibitor, lead to major differences in fibroblasts microtubules making them more agglomerated instead of aligned and stretched as before.

Is important to notice that inhibitors treatment when cells were plated in glass had the duration of one hour and, in the case of micropatterned surfaces, cells were treated with inhibitors during 23 hours (treatment started one hour after photoactivation until 24 hours after photoactivation were fulfilled). That 23 hours treatment was performed mostly because cells can restore their initial structures after inhibitor application.

All these differences were also visible when cells were plated in micropatterned surfaces as shown in right images of Figure 32 to Figure 35. However, after 3 independent experiments using 5 different concentrations of the 4 different inhibitors, wound closure could not be quantified and related to cell inhibitors concentration. This happened mostly because several manipulation steps had an influence in final image acquisition. Besides

wells could be easily scratched during manipulation, mounting media and cover slip coverage for further image acquisition show to highly damage samples. This damaging was mostly due to the peeling of cells placed under the islands to its borders. Moreover, it is possible to see along all images placed at left in Figure 32 to Figure 35 that even being acquired with the same intensity and being photoactivated with the same RGD-BT concentration, islands show different brightness revealing a high variability between wells. These results reflect some of the 50 well silicone approach and the need of further optimizations. Moreover, they also bring new potential advantages of the 96 well format since this seem to be a more optimized approach.

The final results of the present work were related with InCell Microscopy acquisition. As stated along section 4.7, the major difficulty of 50 well silicone approach is the variance of sample position between assays. Besides that disadvantage, in terms of image analysis, other obstacles emerged. First, as already stated in this chapter, mounting samples process for image acquisition showed to damage samples making it impossible to perform further quantifications. Moreover, brightness mean values seemed to be difficult to acquire mostly because FITC-SA signal was weak in the presence of cells and could be indistinct from the image background.

During the next and final chapter of the present work some conclusions and future improvements are suggested in an attempt of opposing these problems.

Chapter 6 | Concluding Remarks and Future Work

Wound healing is a complex, regenerative process essential for human survival and typically triggered when an injury occurs. In the case of skin this process is especially important since as the largest organ of the body it performs a wide range of fundamental and physiological functions. Chronic wounds emerge as a result of a failure during the wound healing phases [26]. This disorder is currently a major problem for health care systems, affecting millions of individuals and costing billions to all countries around the world [41]. Most previous studies related with wound healing and chronic wounds have been performed using animals since the associated processes are complex and dynamic would be better understood has a whole. However, according to Great Britain 2012 statistics, this use of animals in research has reached a very high number of experiments, some of them non-successful, resulting in a lot of animals used in vain. Moreover, wound healing in animals has different features when compared with human wound healing, potentially making animal research less relevant [168].

The present work was developed with the aim of creating new *in vitro* high throughput strategies for cell migration and wound healing studies in an attempt to reduce animals in research and provide more reliable data about those processes.

For that purpose, two different formats were designed, based in a previously established technique by *Costa et. al.*, 2014.

The first approach, 50 well silicone format, was optimized for many of its key parameters. The first steps to be optimized were the sterilization process, which ended up being performed by UV, and the UV lamp placement during photoactivation that showed to be more efficient when the lamp was placed above the samples. Brightness mean value for different RGD-BT concentration was also quantified giving 2,5 mg/mL as the concentration responsible for the highest mean value. Moreover, photoactivation consistency along a horizontal line, along a vertical line and along different positions on the same well was also tested. Those results showed that the format had some faults (like only the four central patterns showed high photoactivation values), but they also showed that it could be used in further studies as there were no high significant differences in

horizontal and vertical consistency between different wells when compared with the first position.

Regarding cell optimization, after four cell lines (HeLa, MDA-Mb231, MCF-7 and HCA2) migration rates were evaluated by a scratch wound assay, the chosen cell line to apply in further studies was HCA2. Cell seeding density for this human fibroblast cell line was optimized for two different patterns using the 50 well silicone approach.

After cell choice, two different assays using the 50 well silicone approach were performed. The first assay tried to establish a relation between wound closure percentage and RGD concentration. In this assay cells showed to migrate more when submitted to high concentrations of peptide. In a second assay, four different inhibitors with five different concentrations were applied to HCA2 after submitting patterns to photoactivation. This assay helped reveal some other faults in the 50 well silicone approach since final samples could not be quantified completely.

With these results it was possible to conclude that HCA2 were a good cell line for the current work since their migration rates were very high when compared with other cell lines, they react to different RGD concentrations and showed differences in cell structures between different inhibitors and different inhibitors concentration appliance. Regarding the 50 well silicone approach, it was shown in principle that this technique can be used to study cell migration. However, some few aspects still need further optimisation in order to become ready to carry out high content screens. Those optimisations are mainly related with the final processes of samples preparation for image acquisition. In order to improve that acquisition, a new mounting media should be tested, with the aim of decreasing cell detachment from the substrates, and a higher concentration of FITC-SA should be used. This last step will allow a higher brightness mean value of the brushes and a more accurate analysis by InCell analyzer. Once the image acquisition problem is solved, InCell analysis protocol should also be completed.

Regarding the 96 well plate approach, some optimizations were performed like materials assembly, adhesive toxicity and cell seeding density. Further optimizations include automating adhesive punching, since doing it manually is time consuming, and perform RGD-BT assays similar to the ones performed in the 50 well silicone approach. Moreover, even exhibiting standard measures between samples, an InCell acquisition protocol should be also created. Once the InCell analysis protocol is set up for 50 well silicone approach, the same protocol can be applied to images acquired from the 96 well plate. Other features that should be further studied are the storage of each approach and related life-time of developed substrates.

Both approaches showed to be promising in the field of wound healing, creating new possibilities for *in vitro* studies, at low costs and higher reproducibility.

The 50 well silicone approach has more manipulation challenges than the 96 well plate approach, however since it requires small volumes of reagents and materials, it could be the ideal approach when performing certain screenings with rare or expensive reagents.

By its turn, the 96 well plate approach allows more results per experiment and a more automated process.

Future works using both developed approaches include wound healing assays using different cell lines or even different peptides. In fact, several different conditions can be applied. One is bacterial colonization which is often associated chronic wound keys [18]. Different mechanical stimulus can also be applied, like negative pressure, resembling negative pressure treatments in chronic wounds [169]. In addition to regular cell migration, another approach is to study healing reverse mechanisms like excessive healing and scar formation. By performing a comparison between low healing profiles and excessive healing perhaps new discoveries could emerge, creating new research pathways.

Since the technique showed to be reliable for several types of cell lines, it could also be applied for the study of other cellular and biological processes than wound healing, such as for the development of siRNA libraries with the aim of identifying key genes, or even for drug testing.

References

- [1] J. Bensouillah, "Aromadermatology: Aromatherapy in the Treatment and Care of Common Skin Conditions," in *Aromadermatology*, Paperback, 2006, pp. 1-11.
- [2] C. Fathke, L. Wilson, K. Shah, B. Kim, A. Hocking, R. Moon, and F. Isik, "Wnt signaling induces epithelial differentiation during cutaneous wound healing.," *BMC Cell Biol.*, vol. 7, p. 4, Jan. 2006.
- [3] S. MacNeil, "Biomaterials for tissue engineering of skin," *Mater. Today*, vol. 11, no. 5, pp. 26-35, May 2008.
- [4] S. Enoch and D. J. Leaper, "Basic science of wound healing," *Surg.*, vol. 26, no. 2, pp. 31-37, Feb. 2008.
- [5] S. Schreml, R.-M. Szeimies, L. Prantl, M. Landthaler, and P. Babilas, "Wound healing in the 21st century.," *J. Am. Acad. Dermatol.*, vol. 63, no. 5, pp. 866-81, Nov. 2010.
- [6] S. Enoch, J. E. Grey, and K. G. Harding, "ABC of wound healing: Recent advances and emerging treatments," *British Medical Journal*, vol. 332, no. 7547, pp. 962-965, 2006.
- [7] J. A. Flegg, H. M. Byrne, M. B. Flegg, and D. L. S. McElwain, "Wound healing angiogenesis: the clinical implications of a simple mathematical model.," *J. Theor. Biol.*, vol. 300, pp. 309-16, May 2012.
- [8] G. L. Rolin, D. Binda, M. Tissot, C. Viennet, P. Saas, P. Muret, and P. Humbert, "In vitro study of the impact of mechanical tension on the dermal fibroblast phenotype in the context of skin wound healing.," *J. Biomech.*, vol. 47, no. 14, pp. 3555-3561, Sep. 2014.
- [9] J. J. Tomasek, G. Gabbiani, B. Hinz, C. Chaponnier, and R. A. Brown, "Myofibroblasts and mechano-regulation of connective tissue remodelling.," *Nat. Rev. Mol. Cell Biol.*, vol. 3, no. 5, pp. 349-63, May 2002.
- [10] R. Ogawa, S. Akaishi, C. Huang, T. Dohi, M. Aoki, Y. Omori, S. Koike, K. Kobe, M. Akimoto, and H. Hyakusoku, "Clinical Applications of Basic Research that Shows Reducing Skin Tension Could Prevent and Treat Abnormal Scarring: The Importance of Fascial/Subcutaneous Tensile Reduction Sutures and Flap Surgery for Keloid and Hypertrophic Scar Reconstruction," *J. Nippon Med. Sch.*, vol. 78, no. 2, pp. 68-76, 2011.
- [11] F. Rippke, V. Schreiner, and H. J. Schwanitz, "The acidic milieu of the horny layer: New findings on the physiology and pathophysiology of skin pH," *American Journal of Clinical Dermatology*, vol. 3, no. 4, pp. 261-272, 2002.
- [12] F. H. Silver, L. M. Siperko, and G. P. Seehra, "Review Mechanobiology of force transduction in dermal tissue," pp. 3-23, 2003.
- [13] S. L. Edwards, "Tissue viability: understanding the mechanisms of injury and repair.," *Nursing standard (Royal College of Nursing (Great Britain) : 1987)*, vol. 21, no. 13, 2006.
- [14] B. Hinz, G. Celetta, J. J. Tomasek, G. Gabbiani, and C. Chaponnier, "Alpha-smooth muscle actin expression upregulates fibroblast contractile activity.," *Mol. Biol. Cell*, vol. 12, no. 9, pp. 2730-2741, Sep. 2001.

- [15] P.-J. Wipff, D. B. Rifkin, J.-J. Meister, and B. Hinz, "Myofibroblast contraction activates latent TGF-beta1 from the extracellular matrix.," *J. Cell Biol.*, vol. 179, no. 6, pp. 1311-23, Dec. 2007.
- [16] T. M. Freyman, I. V Yannas, Y. S. Pek, R. Yokoo, and L. J. Gibson, "Micromechanics of fibroblast contraction of a collagen-GAG matrix.," *Exp. Cell Res.*, vol. 269, no. 1, pp. 140-53, Sep. 2001.
- [17] R. M. Farahani and L. A. DiPietro, "Microgravity and the implications for wound healing.," *Int. Wound J.*, vol. 5, no. 4, pp. 552-61, Oct. 2008.
- [18] T. R. Dargaville, B. L. Farrugia, J. A. Broadbent, S. Pace, Z. Upton, and N. H. Voelcker, "Sensors and imaging for wound healing: a review.," *Biosens. Bioelectron.*, vol. 41, pp. 30-42, Mar. 2013.
- [19] P. Martin, "Wound healing--aiming for perfect skin regeneration.," *Science*, vol. 276, no. 5309, pp. 75-81, Apr. 1997.
- [20] R. Agha, R. Ogawa, G. Pietramaggiore, and D. P. Orgill, "A review of the role of mechanical forces in cutaneous wound healing.," *J. Surg. Res.*, vol. 171, no. 2, pp. 700-8, Dec. 2011.
- [21] J. Kluwe, A. Mencin, and R. F. Schwabe, "Toll-like receptors, wound healing, and carcinogenesis.," *J. Mol. Med. (Berl.)*, vol. 87, no. 2, pp. 125-38, Feb. 2009.
- [22] P. Huebener and R. F. Schwabe, "Regulation of wound healing and organ fibrosis by toll-like receptors.," *Biochim. Biophys. Acta*, vol. 1832, no. 7, pp. 1005-17, Jul. 2013.
- [23] J. Walburn, K. Vedhara, M. Hankins, L. Rixon, and J. Weinman, "Psychological stress and wound healing in humans: a systematic review and meta-analysis.," *J. Psychosom. Res.*, vol. 67, no. 3, pp. 253-71, Sep. 2009.
- [24] J. Hardwicke, D. Schmaljohann, D. Boyce, and D. Thomas, "Epidermal growth factor therapy and wound healing – past, present and future perspectives," *Surg.*, vol. 6, no. 3, pp. 172-177, Jun. 2008.
- [25] G. Turgut, A. Ozcan, O. Sümer, N. Yeşiloğlu, and L. Baş, "Reconstruction of complicated scalp defect via skin traction.," *J. Craniofac. Surg.*, vol. 20, no. 1, pp. 263-4, Jan. 2009.
- [26] G. S. Lazarus, "Definitions and guidelines for assessment of wounds and evaluation of healing," *Arch. Dermatol.*, vol. 130, no. 4, pp. 489-493, Apr. 1994.
- [27] T. A. Mustoe, K. O'Shaughnessy, and O. Kloeters, "Chronic wound pathogenesis and current treatment strategies: a unifying hypothesis.," *Plast. Reconstr. Surg.*, vol. 117, no. 7 Suppl, p. 35S-41S, Jun. 2006.
- [28] N. S. Greaves, K. J. Ashcroft, M. Baguneid, and A. Bayat, "Current understanding of molecular and cellular mechanisms in fibroplasia and angiogenesis during acute wound healing.," *J. Dermatol. Sci.*, vol. 72, no. 3, pp. 206-17, Dec. 2013.
- [29] M. Turns, "The diabetic foot: An overview of assessment and complications," *British Journal of Nursing*, vol. 20, no. 15 SUPPL. 2011.
- [30] O. Z. Lerman, R. D. Galiano, M. Armour, J. P. Levine, and G. C. Gurtner, "Cellular dysfunction in the diabetic fibroblast: Impairment in migration, vascular endothelial

- growth factor production, and response to hypoxia," *Am. J. Pathol.*, vol. 162, no. 1, pp. 303-312, 2003.
- [31] J. M. Smiell, T. J. Wieman, D. L. Steed, B. H. Perry, A. R. Sampson, and B. H. Schwab, "Efficacy and safety of becaplermin (recombinant human platelet-derived growth factor-BB) in patients with nonhealing, lower extremity diabetic ulcers: a combined analysis of four randomized studies.," *Wound Repair Regen.*, vol. 7, no. 5, pp. 335-346, 1999.
- [32] S. S. Scherer, G. Pietramaggiore, J. C. Mathews, M. J. Prsa, S. Huang, and D. P. Orgill, "The mechanism of action of the vacuum-assisted closure device.," *Plast. Reconstr. Surg.*, vol. 122, no. 3, pp. 786-97, Sep. 2008.
- [33] A. Kasuya and Y. Tokura, "Attempts to accelerate wound healing," *J. Dermatol. Sci.*, Nov. 2014.
- [34] G. D. Winter, "Formation of the scab and the rate of epithelisation of superficial wounds in the skin of the young domestic pig. 1962.," *J. Wound Care*, vol. 4, no. 8, pp. 366-367; discussion 368, 1995.
- [35] V. Banks, S. Bale, K. Harding, and E. F. Harding, "Evaluation of a new polyurethane foam dressing.," *J. Wound Care*, vol. 6, no. 6, pp. 266-269, 1997.
- [36] J. Shepherd, P. Sarker, S. Rimmer, L. Swanson, S. MacNeil, and I. Douglas, "Hyperbranched poly(NIPAM) polymers modified with antibiotics for the reduction of bacterial burden in infected human tissue engineered skin.," *Biomaterials*, vol. 32, no. 1, pp. 258-67, Jan. 2011.
- [37] M. Matsusaki and M. Akashi, "Novel functional biodegradable polymer IV: pH-sensitive controlled release of fibroblast growth factor-2 from a poly(gamma-glutamic acid)-sulfonate matrix for tissue engineering.," *Biomacromolecules*, vol. 6, no. 6, pp. 3351-6, Jan. 2005.
- [38] J. Schaubert and R. L. Gallo, "Antimicrobial peptides and the skin immune defense system.," *J. Allergy Clin. Immunol.*, vol. 122, no. 2, pp. 261-6, Aug. 2008.
- [39] C. K. Sen, G. M. Gordillo, S. Roy, R. Kirsner, L. Lambert, T. K. Hunt, F. Gottrup, G. C. Gurtner, and M. T. Longaker, "Human skin wounds: a major and snowballing threat to public health and the economy.," *Wound Repair Regen.*, vol. 17, no. 6, pp. 763-71, Jan. 2009.
- [40] J. Posnett and P. . Franks, "The burden of chronic wounds in the UK," *Nurs. Times*, vol. 104, no. 3, pp. 44-45, 2008.
- [41] S. Coles, "Footwear and offloading for patients with diabetes.," *Nurs. Times*, vol. 104, no. 3, pp. 40-43, 2008.
- [42] J. Posnett, "The Resource Impact of Wounds on Health-care Providers in Europe," *J. Wound Care*, vol. 18, no. 4, 2009.
- [43] H. Blaser, S. Eisenbeiss, M. Neumann, M. Reichman-Fried, B. Thisse, C. Thisse, and E. Raz, "Transition from non-motile behaviour to directed migration during early PGC development in zebrafish.," *J. Cell Sci.*, vol. 118, no. Pt 17, pp. 4027-4038, Sep. 2005.
- [44] S. P. Palecek, J. C. Loftus, M. H. Ginsberg, D. A. Lauffenburger, and A. F. Horwitz, "Integrin-ligand binding properties govern cell migration speed through cell-substratum adhesiveness.," *Nature*, vol. 385, no. 6616, pp. 537-540, Feb. 1997.

- [45] A. Huttenlocher, R. R. Sandborg, and A. F. Horwitz, "Adhesion in cell migration.," *Curr. Opin. Cell Biol.*, vol. 7, no. 5, pp. 697-706, Oct. 1995.
- [46] H. Birkedal-Hansen, "Proteolytic remodeling of extracellular matrix.," *Curr. Opin. Cell Biol.*, vol. 7, no. 5, pp. 728-735, Oct. 1995.
- [47] A. Aman and T. Piotrowski, "Cell migration during morphogenesis," *Dev. Biol.*, vol. 341, no. 1, pp. 20-33, 2010.
- [48] G. Charras and E. Paluch, "Blebs lead the way: how to migrate without lamellipodia," *Nat Rev Mol Cell Biol*, vol. 9, no. 9, pp. 730-736, Sep. 2008.
- [49] J. P. Thiery, "Epithelial-mesenchymal transitions in tumour progression.," *Nat. Rev. Cancer*, vol. 2, no. 6, pp. 442-454, Jun. 2002.
- [50] N. Kramer, A. Walzl, C. Unger, M. Rosner, G. Krupitza, M. Hengstschläger, and H. Dolznig, "In vitro cell migration and invasion assays.," *Mutat. Res.*, vol. 752, no. 1, pp. 10-24, Jan. 2013.
- [51] J.-P. Thiery, K. Chua, W. J. Sim, and R. Huang, "Epithelial mesenchymal transition during development in fibrosis and in the progression of carcinoma.," *Bull. Cancer*, vol. 97, no. 11, pp. 1285-1295, Nov. 2010.
- [52] C. Chang, "Motile chondrocytes from newborn calf: migration properties and synthesis of collagen II," *Osteoarthr. Cartil.*, vol. 11, no. 8, pp. 603-612, Aug. 2003.
- [53] R. J. Petrie, A. D. Doyle, and K. M. Yamada, "Random versus directionally persistent cell migration.," *Nat. Rev. Mol. Cell Biol.*, vol. 10, no. 8, pp. 538-549, 2009.
- [54] A. Haeger, K. Wolf, M. M. Zegers, and P. Friedl, "Collective cell migration: guidance principles and hierarchies.," *Trends Cell Biol.*, Jun. 2015.
- [55] M. Théry, V. Racine, M. Piel, A. Pépin, A. Dimitrov, Y. Chen, J.-B. Sibarita, and M. Bornens, "Anisotropy of cell adhesive microenvironment governs cell internal organization and orientation of polarity.," *Proc. Natl. Acad. Sci. U. S. A.*, vol. 103, no. 52, pp. 19771-6, Dec. 2006.
- [56] E. Anon, X. Serra-Picamal, P. Hersen, N. C. Gauthier, M. P. Sheetz, X. Trepat, and B. Ladoux, "Cell crawling mediates collective cell migration to close undamaged epithelial gaps.," *Proc. Natl. Acad. Sci. U. S. A.*, vol. 109, no. 27, pp. 10891-6, Jul. 2012.
- [57] S. S. Chang, W. Guo, Y. Kim, and Y. Wang, "Guidance of cell migration by substrate dimension.," *Biophys. J.*, vol. 104, no. 2, pp. 313-21, Jan. 2013.
- [58] C. Feng, Y. Cheng, and P. G. Chao, "The influence and interactions of substrate thickness, organization and dimensionality on cell morphology and migration.," *Acta Biomater.*, vol. 9, no. 3, pp. 5502-10, Mar. 2013.
- [59] P. Friedl and D. Gilmour, "Collective cell migration in morphogenesis, regeneration and cancer.," *Nat. Rev. Mol. Cell Biol.*, vol. 10, no. 7, pp. 445-457, Jul. 2009.
- [60] G. Reig, E. Pulgar, and M. L. Concha, "Cell migration: from tissue culture to embryos.," *Development*, vol. 141, no. 10, pp. 1999-2013, 2014.
- [61] A. a Khalil and P. Friedl, "Determinants of leader cells in collective cell migration.," *Integr. Biol. (Camb)*, vol. 2, no. 11-12, pp. 568-574, 2010.

- [62] J. Kolega, M. S. Shure, W. T. Chen, and N. D. Young, "Rapid cellular translocation is related to close contacts formed between various cultured cells and their substrata.," *J. Cell Sci.*, vol. 54, no. July 2015, pp. 23-34, 1982.
- [63] P. Haas and D. Gilmour, "Chemokine signaling mediates self-organizing tissue migration in the zebrafish lateral line.," *Dev. Cell*, vol. 10, no. 5, pp. 673-680, May 2006.
- [64] D. Vestweber, "Cadherins in tissue architecture and disease," *J. Mol. Med.*, vol. 93, no. 1, pp. 5-11, 2015.
- [65] R. Bruzzone, T. W. White, and D. L. Paul, "Connections with connexins: the molecular basis of direct intercellular signaling.," *Eur. J. Biochem.*, vol. 238, no. 1, pp. 1-27, May 1996.
- [66] B. DeFranco, B. Nickel, Baty, J. Martinez, V. Gay, V. Sandulache, D. Hackam, and S. Murray, "Migrating Cells Retain Gap Junction Plaque Structure and Function," *Cell communication & adhesion*, 2008. [Online]. Available: http://www.tandfonline.com/doi/full/10.1080/15419060802198298#.VeLXt_ZVikp. [Accessed: 30-Aug-2015].
- [67] X. Wang, L. He, Y. I. Wu, K. M. Hahn, and D. J. Montell, "Light-mediated activation reveals a key role for Rac in collective guidance of cell movement in vivo.," *Nat. Cell Biol.*, vol. 12, no. 6, pp. 591-597, 2010.
- [68] T. Das, K. Safferling, S. Rausch, N. Grabe, H. Boehm, and J. P. Spatz, "A molecular mechanotransduction pathway regulates collective migration of epithelial cells," *Nat. Cell Biol.*, vol. 17, no. February, 2015.
- [69] R. Farooqui and G. Fenteany, "Multiple rows of cells behind an epithelial wound edge extend cryptic lamellipodia to collectively drive cell-sheet movement.," *J. Cell Sci.*, vol. 118, no. Pt 1, pp. 51-63, 2005.
- [70] N. Dodge Zantek and M. S. Kinch, "Analysis of cell migration," in *Methods in Cell Biology*, vol. 63, Elsevier, 2001, pp. 549-559.
- [71] M. Fronza, B. Heinzmann, M. Hamburger, S. Laufer, and I. Merfort, "Determination of the wound healing effect of Calendula extracts using the scratch assay with 3T3 fibroblasts.," *J. Ethnopharmacol.*, vol. 126, no. 3, pp. 463-7, Dec. 2009.
- [72] R. Pankov, Y. Endo, S. Even-Ram, M. Araki, K. Clark, E. Cukierman, K. Matsumoto, and K. M. Yamada, "A Rac switch regulates random versus directionally persistent cell migration.," *J. Cell Biol.*, vol. 170, no. 5, pp. 793-802, Aug. 2005.
- [73] K. M. Stroka, Z. Gu, S. X. Sun, and K. Konstantopoulos, "Bioengineering paradigms for cell migration in confined microenvironments.," *Curr. Opin. Cell Biol.*, vol. 30C, pp. 41-50, Oct. 2014.
- [74] A. Al-Kilani, O. de Freitas, S. Dufour, and F. Gallet, "Negative feedback from integrins to cadherins: a micromechanical study.," *Biophys. J.*, vol. 101, no. 2, pp. 336-44, Jul. 2011.
- [75] J. Labat-Robert, "Cell-Matrix interactions, the role of fibronectin and integrins. A survey.," *Pathol. Biol. (Paris)*, vol. 60, no. 1, pp. 15-9, Feb. 2012.
- [76] K. Yamada, "Integrin transmembrane signaling and cytoskeletal control," *Curr. Opin. Cell Biol.*, vol. 7, no. 5, pp. 681-689, 1995.

- [77] M. A. Arnaout, S. L. Goodman, and J.-P. Xiong, "Structure and mechanics of integrin-based cell adhesion.," *Curr. Opin. Cell Biol.*, vol. 19, no. 5, pp. 495-507, Oct. 2007.
- [78] A. Beauvais-Jouneau and J.-P. Thiery, "Multiple roles for integrins during development," *Biol. Cell*, vol. 89, no. 1, pp. 5-11, Mar. 1997.
- [79] R. O. Hynes, "Integrins Bidirectional, Allosteric Signaling Machines," *Cell*, vol. 110, no. 6, pp. 673-687, Sep. 2002.
- [80] A. M. Mercurio, I. Rabinovitz, and L. M. Shaw, "The alpha 6 beta 4 integrin and epithelial cell migration.," *Curr. Opin. Cell Biol.*, vol. 13, no. 5, pp. 541-5, 2001.
- [81] P. Moreno-Layseca and C. H. Streuli, "Signalling pathways linking integrins with cell cycle progression.," *Matrix Biol.*, vol. 34, pp. 144-53, Feb. 2014.
- [82] E. H. J. Danen and A. Sonnenberg, "Integrins in regulation of tissue development and function.," *J. Pathol.*, vol. 201, no. 4, pp. 632-641, 2003.
- [83] I. K. Gipson, S. Spurr-Michaud, A. Tisdale, J. Elwell, and M. A. Stepp, "Redistribution of the hemidesmosome components alpha 6 beta 4 integrin and bullous pemphigoid antigens during epithelial wound healing.," *Exp. Cell Res.*, vol. 207, no. 1, pp. 86-98, Jul. 1993.
- [84] B. Geiger, A. Bershadsky, R. Pankov, K. M. Yamada, and B. G. Correspondence, "Transmembrane extracellular matrix- cytoskeleton crosstalk," *Nat. Rev. Mol. Cell Biol.*, vol. 2, no. November, pp. 793-805, 2001.
- [85] E. Zamir and B. Geiger, "Molecular complexity and dynamics of cell-matrix adhesions.," *J. Cell Sci.*, vol. 114, no. Pt 20, pp. 3583-3590, 2001.
- [86] R. Zaidel-bar, S. Itzkovitz, A. Ma, R. Iyengar, and B. Geiger, "Functional atlas of the integrin adhesome," vol. 9, no. 8, 2007.
- [87] F. N. Kenny and J. T. Connelly, "Integrin-mediated adhesion and mechano-sensing in cutaneous wound healing," *Cell Tissue Res.*, pp. 571-582, 2014.
- [88] X. Chen and B. M. Gumbiner, "Crosstalk between different adhesion molecules," *Curr. Opin. Cell Biol.*, vol. 18, no. 5, pp. 572-578, 2006.
- [89] H. Yano, Y. Mazaki, K. Kurokawa, S. K. Hanks, M. Matsuda, and H. Sabe, "Roles played by a subset of integrin signaling molecules in cadherin-based cell-cell adhesion.," *J. Cell Biol.*, vol. 166, no. 2, pp. 283-95, Jul. 2004.
- [90] J. A. Schiro, B. M. C. Chan, W. T. Roswit, P. D. Kassner, A. P. Pentland, M. E. Hemler, A. Z. Eisen, and T. S. Kupper, "Integrin $\alpha 2 \beta 1$ (VLA-2) mediates reorganization and contraction of collagen matrices by human cells," *Cell*, vol. 67, no. 2, pp. 403-410, Oct. 1991.
- [91] T. Fujimura, S. Moriwaki, G. Imokawa, and Y. Takema, "Crucial role of fibroblast integrins alpha2 and beta1 in maintaining the structural and mechanical properties of the skin.," *J. Dermatol. Sci.*, vol. 45, no. 1, pp. 45-53, Jan. 2007.
- [92] C. M. Niessen, M. H. van der Raaij-Helmer, E. H. Hulsman, R. van der Neut, M. F. Jonkman, and a Sonnenberg, "Deficiency of the integrin beta 4 subunit in junctional epidermolysis bullosa with pyloric atresia: consequences for hemidesmosome formation and adhesion properties.," *J. Cell Sci.*, vol. 109 (Pt 7, pp. 1695-1706, 1996.

- [93] H. Gardner, A. Broberg, A. Pozzi, M. Laato, and J. Heino, "Absence of integrin $\alpha 1\beta 1$ in the mouse causes loss of feedback regulation of collagen synthesis in normal and wounded dermis.," *J. Cell Sci.*, vol. 112 (Pt 3, pp. 263-272, 1999.
- [94] J. Chen, T. G. Diacovo, D. G. Grenache, S. A. Santoro, and M. M. Zutter, "The $\alpha 2$ Integrin Subunit-Deficient Mouse," *Am. J. Pathol.*, vol. 161, no. 1, pp. 337-344, Jul. 2002.
- [95] B. K. Pilcher, J. A. Dumin, B. D. Sudbeck, S. M. Krane, H. G. Welgus, and W. C. Parks, "The activity of collagenase-1 is required for keratinocyte migration on a type I collagen matrix.," *J. Cell Biol.*, vol. 137, no. 6, pp. 1445-1457, Jun. 1997.
- [96] G. Szulgit, R. Rudolph, A. Wandel, M. Tenenhaus, R. Panos, and H. Gardner, "Alterations in fibroblast $\alpha 1\beta 1$ integrin collagen receptor expression in keloids and hypertrophic scars," *J. Invest. Dermatol.*, vol. 118, no. 3, pp. 409-415, 2002.
- [97] R. S. Sawhney, M. M. Cookson, Y. Omar, J. Hauser, and M. G. Brattain, "Integrin $\alpha 2$ -mediated ERK and calpain activation play a critical role in cell adhesion and motility via focal adhesion kinase signaling: identification of a novel signaling pathway.," *J. Biol. Chem.*, vol. 281, no. 13, pp. 8497-8510, 2006.
- [98] N. V. Bukoreshtliev, K. Haase, and A. E. Pelling, "Mechanical cues in cellular signalling and communication," *Cell Tissue Res.*, vol. 352, no. 1, pp. 77-94, 2013.
- [99] P. A. Janmey and R. T. Miller, "Mechanisms of mechanical signaling in development and disease.," *J. Cell Sci.*, vol. 124, no. Pt 1, pp. 9-18, 2011.
- [100] M.-F. Carlier, J. Pernier, P. Montaville, S. Shekhar, and S. Kühn, "Control of polarized assembly of actin filaments in cell motility," *Cell. Mol. Life Sci.*, 2015.
- [101] A. J. Ridley, M. A. Schwartz, K. Burridge, R. A. Firtel, M. H. Ginsberg, G. Borisy, J. T. Parsons, and A. R. Horwitz, "Cell migration: integrating signals from front to back.," *Science*, vol. 302, no. 5651, pp. 1704-1709, Dec. 2003.
- [102] K. Suffoletto, N. Ye, F. Meng, D. Verma, and S. Z. Hua, "Intracellular forces during guided cell growth on micropatterns using FRET measurement.," *J. Biomech.*, vol. 48, no. 4, pp. 627-35, Feb. 2015.
- [103] A. B. Jaffe and A. Hall, "Rho GTPases: biochemistry and biology.," *Annu. Rev. Cell Dev. Biol.*, vol. 21, pp. 247-269, 2005.
- [104] K. Rottner, A. Hall, and J. V. Small, "Interplay between Rac and Rho in the control of substrate contact dynamics," *Curr. Biol.*, vol. 9, no. 12, pp. 640-51, Jun. 1999.
- [105] M. Amano, M. Ito, Y. Fukata, K. Chihara, T. Nakano, Y. Matsuura, and K. Kaibuchi, "Phosphorylation and Activation of Myosin by Rho-associated," *J. Biol. Chem.*, vol. 271, pp. 20246-20249, 1996.
- [106] W. M. Petroll and M. Miron-Mendoza, "Mechanical interactions and crosstalk between corneal keratocytes and the extracellular matrix.," *Exp. Eye Res.*, vol. 133, pp. 49-57, Apr. 2015.
- [107] R. Fernandez-Gonzalez, S. de M. Simoes, J.-C. Röper, S. Eaton, and J. A. Zallen, "Myosin II Dynamics Are Regulated by Tension in Intercalating Cells," *Dev. Cell*, vol. 17, no. 5, pp. 736-743, Nov. 2009.

- [108] J. M. Leerberg, G. A. Gomez, S. Verma, E. J. Moussa, S. K. Wu, R. Priya, B. D. Hoffman, C. Grashoff, M. A. Schwartz, and A. S. Yap, "Tension-sensitive actin assembly supports contractility at the epithelial zonula adherens.," *Curr. Biol.*, vol. 24, no. 15, pp. 1689-99, Aug. 2014.
- [109] A. M. Shewan, M. Maddugoda, A. Kraemer, S. J. Stehbens, S. Verma, E. M. Kovacs, and A. S. Yap, "Myosin 2 is a key Rho kinase target necessary for the local concentration of E-cadherin at cell-cell contacts.," *Mol. Biol. Cell*, vol. 16, no. 10, pp. 4531-42, Oct. 2005.
- [110] A. M. Ross, Z. Jiang, M. Bastmeyer, and J. Lahann, "Physical aspects of cell culture substrates: Topography, roughness, and elasticity," *Small*, vol. 8, no. 3, pp. 336-355, 2012.
- [111] B. R. Brückner and A. Janshoff, "Elastic properties of epithelial cells probed by atomic force microscopy," *Biochim. Biophys. Acta - Mol. Cell Res.*, Jul. 2015.
- [112] C. G. Galbraith, K. M. Yamada, and M. P. Sheetz, "The relationship between force and focal complex development.," *J. Cell Biol.*, vol. 159, no. 4, pp. 695-705, 2002.
- [113] A. Das, "A critical pull to polarize the cell.," *Biophys. J.*, vol. 107, no. 2, pp. 285-6, Jul. 2014.
- [114] J.-L. Maître, H. Berthoumieux, S. F. G. Krens, G. Salbreux, F. Jülicher, E. Paluch, and C.-P. Heisenberg, "Adhesion functions in cell sorting by mechanically coupling the cortices of adhering cells.," *Science*, vol. 338, no. 6104, pp. 253-6, Oct. 2012.
- [115] O. M. Rossier, N. Gauthier, N. Biais, W. Vonnegut, M.-A. Fardin, P. Avigan, E. R. Heller, A. Mathur, S. Ghassemi, M. S. Koeckert, J. C. Hone, and M. P. Sheetz, "Force generated by actomyosin contraction builds bridges between adhesive contacts.," *EMBO J.*, vol. 29, no. 6, pp. 1055-68, Mar. 2010.
- [116] N. Ye, D. Verma, F. Meng, M. W. Davidson, K. Suffoletto, and S. Z. Hua, "Direct observation of α -actinin tension and recruitment at focal adhesions during contact growth.," *Exp. Cell Res.*, vol. 327, no. 1, pp. 57-67, Sep. 2014.
- [117] I. Thievensen, P. M. Thompson, S. Berlemont, K. M. Plevock, S. V. Plotnikov, A. Zempljic-Harpf, R. S. Ross, M. W. Davidson, G. Danuser, S. L. Campbell, and C. M. Waterman, "Vinculin-actin interaction couples actin retrograde flow to focal adhesions, but is dispensable for focal adhesion growth.," *J. Cell Biol.*, vol. 202, no. 1, pp. 163-77, Jul. 2013.
- [118] E. F. Woodham and L. M. Machesky, "Polarised cell migration: intrinsic and extrinsic drivers.," *Curr. Opin. Cell Biol.*, vol. 30, pp. 25-32, Oct. 2014.
- [119] S. J. Habib, B.-C. Chen, F.-C. Tsai, K. Anastassiadis, T. Meyer, E. Betzig, and R. Nusse, "A localized Wnt signal orients asymmetric stem cell division in vitro.," *Science*, vol. 339, no. 6126, pp. 1445-8, Mar. 2013.
- [120] P. A. Coulombe, "Wound epithelialization: accelerating the pace of discovery.," *J. Invest. Dermatol.*, vol. 121, no. 2, pp. 219-230, Aug. 2003.
- [121] L. G. Johnson, "Applications of imaging techniques to studies of epithelial tight junctions.," *Adv. Drug Deliv. Rev.*, vol. 57, no. 1, pp. 111-21, Jan. 2005.

- [122] S. Delabarre, C. Claudon, and F. Laurent, "Influence of several extracellular matrix components in primary cultures of bovine mammary epithelial cells," *Tissue Cell*, vol. 29, no. 1, pp. 99-106, Feb. 1997.
- [123] P. B. van Wachem, C. M. Vreeriks, T. Beugeling, J. Feijen, a Bantjes, J. P. Detmers, and W. G. van Aken, "The influence of protein adsorption on interactions of cultured human endothelial cells with polymers.," *J. Biomed. Mater. Res.*, vol. 21, no. 6, pp. 701-18, Jun. 1987.
- [124] F. Tatin, A. Taddei, A. Weston, E. Fuchs, D. Devenport, F. Tissir, and T. Makinen, "Planar cell polarity protein Celsr1 regulates endothelial adherens junctions and directed cell rearrangements during valve morphogenesis.," *Dev. Cell*, vol. 26, no. 1, pp. 31-44, Jul. 2013.
- [125] X. You, "Regulation of migration of primary prostate epithelial cells by secreted factors from prostate stromal cells," *Exp. Cell Res.*, vol. 288, no. 2, pp. 246-256, Aug. 2003.
- [126] D. W. Williams, H. Wu, J.-E. Oh, C. Fakhar, M. K. Kang, K.-H. Shin, N.-H. Park, and R. H. Kim, "2-Hydroxyethyl methacrylate inhibits migration of dental pulp stem cells.," *J. Endod.*, vol. 39, no. 9, pp. 1156-60, Sep. 2013.
- [127] B. Rees, S. W. Spiekstra, M. Carfi, K. Ouwehand, C. A. Williams, E. Corsini, J. D. McLeod, and S. Gibbs, "Inter-laboratory study of the in vitro dendritic cell migration assay for identification of contact allergens.," *Toxicol. In Vitro*, vol. 25, no. 8, pp. 2124-34, Dec. 2011.
- [128] H. Yang, X. Gou, Y. Wang, T. M. Fahmy, A. Y.-H. Leung, J. Lu, and D. Sun, "A Dynamic Model of Chemoattractant-Induced Cell Migration," *Biophys. J.*, vol. 108, no. 7, pp. 1645-1651, Apr. 2015.
- [129] G. S. Kijanka, I. K. Dimov, R. Burger, and J. Ducrée, "Real-time monitoring of cell migration, phagocytosis and cell surface receptor dynamics using a novel, live-cell opto-microfluidic technique.," *Anal. Chim. Acta*, vol. 872, pp. 95-9, May 2015.
- [130] D. Lehnert, B. Wehrle-Haller, C. David, U. Weiland, C. Ballestrem, B. a Imhof, and M. Bastmeyer, "Cell behaviour on micropatterned substrata: limits of extracellular matrix geometry for spreading and adhesion.," *J. Cell Sci.*, vol. 117, no. Pt 1, pp. 41-52, 2004.
- [131] A. Kumar and G. Whitesides, "Features of gold having micrometer to centimeter dimensions can be formed through a combination of stamping with an elastomeric stamp and an alkanethiol 'ink' followed by chemical etching," vol. 4, pp. 2002-2004, 1993.
- [132] A. Olivier, F. Meyer, J.-M. Raquez, P. Damman, and P. Dubois, "Surface-initiated controlled polymerization as a convenient method for designing functional polymer brushes: From self-assembled monolayers to patterned surfaces," *Prog. Polym. Sci.*, vol. 37, no. 1, pp. 157-181, Jan. 2012.
- [133] M. Krishnamoorthy, S. Hakobyan, M. Ramstedt, and J. E. Gautrot, "Surface-Initiated Polymer Brushes in the Biomedical Field: Applications in Membrane Science , Biosensing , Cell Culture , Regenerative Medicine and Antibacterial Coatings," *Chem. Rev.*, vol. 114, pp. 10976-11026, 2014.

- [134] N. Singh, X. Cui, T. Boland, and S. M. Husson, "The role of independently variable grafting density and layer thickness of polymer nanolayers on peptide adsorption and cell adhesion.," *Biomaterials*, vol. 28, no. 5, pp. 763-771, Mar. 2007.
- [135] H. Ma, J. Hyun, P. Stiller, and a. Chilkoti, "'Non-Fouling' Oligo(ethylene glycol)-Functionalized Polymer Brushes Synthesized by Surface-Initiated Atom Transfer Radical Polymerization," *Adv. Mater.*, vol. 16, no. 4, pp. 338-341, 2004.
- [136] S. Tugulu and H.-A. Klok, "Stability and nonfouling properties of poly(poly(ethylene glycol) methacrylate) brushes under cell culture conditions.," *Biomacromolecules*, vol. 9, no. 3, pp. 906-12, Mar. 2008.
- [137] S. Kouvroukoglou, "Endothelial cell migration on surfaces modified with immobilized adhesive peptides," *Biomaterials*, vol. 21, no. 17, pp. 1725-1733, Sep. 2000.
- [138] Y. Cao, "BIOFUNCTIONALIZATION AND SURFACE STUDIES OF SEMICONDUCTOR MATERIALS FOR SENSING DEVICE FABRICATION," no. May, 2013.
- [139] A. B. Lowe, "Thiol-yne 'click'/coupling chemistry and recent applications in polymer and materials synthesis and modification," *Polymer (Guildf.)*, vol. 55, no. 22, pp. 5517-5549, Oct. 2014.
- [140] C. Y. Zhou, H. Wu, and N. K. Devaraj, "Rapid access to phospholipid analogs using thiol-yne chemistry," *Chem. Sci.*, vol. 6, no. 7, pp. 4365-4372, 2015.
- [141] P. Costa, J. E. Gautrot, and J. T. Connelly, "Directing cell migration using micropatterned and dynamically adhesive polymer brushes.," *Acta Biomater.*, vol. 10, no. 6, pp. 2415-22, Jun. 2014.
- [142] J. E. Gautrot, B. Trappmann, F. Ocegüera-Yanez, J. Connelly, X. He, F. M. Watt, and W. T. S. Huck, "Exploiting the superior protein resistance of polymer brushes to control single cell adhesion and polarisation at the micron scale.," *Biomaterials*, vol. 31, no. 18, pp. 5030-41, Jun. 2010.
- [143] P. Calcagnile, L. Blasi, F. Rizzi, A. Quattieri, A. Athanassiou, E. Gogolides, and M. De Vittorio, "Parylene C Surface Functionalization and Patterning with pH- Responsive Microgels," 2014.
- [144] H. Lee, J. Pietrasik, S. S. Sheiko, and K. Matyjaszewski, "Stimuli-responsive molecular brushes," *Prog. Polym. Sci.*, vol. 35, no. 1-2, pp. 24-44, Jan. 2010.
- [145] A. M. Telford, L. Meagher, V. Glattauer, T. R. Gengenbach, C. D. Easton, and C. Neto, "Micropatterning of polymer brushes: grafting from dewetting polymer films for biological applications.," *Biomacromolecules*, vol. 13, no. 9, pp. 2989-96, Oct. 2012.
- [146] J. T. Connelly, J. E. Gautrot, B. Trappmann, D. W.-M. Tan, G. Donati, W. T. S. Huck, and F. M. Watt, "Actin and serum response factor transduce physical cues from the microenvironment to regulate epidermal stem cell fate decisions.," *Nat. Cell Biol.*, vol. 12, no. 7, pp. 711-718, 2010.
- [147] H.-Y. Chin, D. Wang, and D. K. Schwartz, "Dynamic Molecular Behavior on Thermoresponsive Polymer Brushes," *Macromolecules*, p. 150626085406005, 2015.
- [148] S. Weis, T. T. Lee, A. del Campo, and A. J. García, "Dynamic cell-adhesive microenvironments and their effect on myogenic differentiation.," *Acta Biomater.*, vol. 9, no. 9, pp. 8059-66, Sep. 2013.

- [149] J. Kim and R. C. Hayward, "Mimicking dynamic in vivo environments with stimuli-responsive materials for cell culture.," *Trends Biotechnol.*, vol. 30, no. 8, pp. 426-39, Aug. 2012.
- [150] I. Adanja, O. Debeir, V. Mégalizzi, R. Kiss, N. Warzée, and C. Decaestecker, "Automated tracking of unmarked cells migrating in three-dimensional matrices applied to anti-cancer drug screening," *Exp. Cell Res.*, vol. 316, pp. 181-193, 2010.
- [151] J. Huth, M. Buchholz, J. M. Kraus, K. Mølhav, C. Gradinaru, G. V. Wichert, T. M. Gress, H. Neumann, and H. a. Kestler, "TimeLapseAnalyzer: Multi-target analysis for live-cell imaging and time-lapse microscopy," *Comput. Methods Programs Biomed.*, vol. 104, pp. 227-234, 2011.
- [152] R. Bise, T. Kanade, Z. Yin, and S. Huh, "Automatic cell tracking applied to analysis of cell migration in wound healing assay," *2011 Annu. Int. Conf. IEEE Eng. Med. Biol. Soc.*, pp. 6174-6179, 2011.
- [153] A. Chakraborty and A. K. Roy-Chowdhury, "Context aware spatio-temporal cell tracking in densely packed multilayer tissues," *Med. Image Anal.*, vol. 19, no. 1, pp. 149-163, Jan. 2015.
- [154] M. Cicconet, M. Gutwein, K. C. Gunsalus, and D. Geiger, "Label free cell-tracking and division detection based on 2D time-lapse images for lineage analysis of early embryo development," *Comput. Biol. Med.*, vol. 51, pp. 24-34, 2014.
- [155] O. Debeir, V. Mégalizzi, N. Warzée, R. Kiss, and C. Decaestecker, "Videomicroscopic extraction of specific information on cell proliferation and migration in vitro," *Exp. Cell Res.*, vol. 314, no. 16, pp. 2985-2998, 2008.
- [156] M. Möller, M. Burger, P. Dieterich, and A. Schwab, "A framework for automated cell tracking in phase contrast microscopic videos based on normal velocities," *J. Vis. Commun. Image Represent.*, vol. 25, pp. 396-409, 2014.
- [157] S. R. Ghaemi, F. J. Harding, B. Delalat, S. Gronthos, and N. H. Voelcker, "Exploring the mesenchymal stem cell niche using high throughput screening.," *Biomaterials*, vol. 34, no. 31, pp. 7601-15, Oct. 2013.
- [158] S. Eun Chung, J. Kim, D. Yoon Oh, Y. Song, S. Hoon Lee, S. Min, and S. Kwon, "One-step pipetting and assembly of encoded chemical-laden microparticles for high-throughput multiplexed bioassays.," *Nat. Commun.*, vol. 5, p. 3468, 2014.
- [159] M. B. Oliveira, "High-throughput screening for integrative biomaterials design: exploring advances and new trends," vol. 32, no. 12, pp. 627-636, 2014.
- [160] V. P. Patel, "Tracking Migrating Cells with MetaMorph® Software," vol. 1, no. 4, pp. 17-20, 2009.
- [161] G. H. L. Sciences, "IN Cell Analyzer HCA Systems," 2014. [Online]. Available: <http://www.gelifesciences.com/webapp/wcs/stores/servlet/catalog/en/GELifeSciences-pt/brands/in-cell-analyzer/>. [Accessed: 20-May-2005].
- [162] Microchem, "SU-8 2000 Permanent Epoxy Negative Photoresist." 2010.
- [163] A. G. Clark, K. Dierkes, and E. K. Paluch, "Monitoring actin cortex thickness in live cells.," *Biophys. J.*, vol. 105, no. 3, pp. 570-80, Aug. 2013.

- [164] G. M. Nagaraja, M. Othman, B. P. Fox, R. Alsaber, C. M. Pellegrino, Y. Zeng, R. Khanna, P. Tamburini, a Swaroop, and R. P. Kandpal, "Gene expression signatures and biomarkers of noninvasive and invasive breast cancer cells: comprehensive profiles by representational difference analysis, microarrays and proteomics.," *Oncogene*, vol. 25, no. 16, pp. 2328-2338, 2006.
- [165] J. F. Gierthy, D. W. 2nd Lincoln, K. E. Roth, S. S. Bowser, J. A. Bennett, L. Bradley, and H. W. Dickerman, "Estrogen-stimulation of postconfluent cell accumulation and foci formation of human MCF-7 breast cancer cells.," *J. Cell. Biochem.*, vol. 45, no. 2, pp. 177-187, Feb. 1991.
- [166] S. C. Kirkland and I. G. Bailey, "Establishment and characterisation of six human colorectal adenocarcinoma cell lines.," *Br. J. Cancer*, vol. 53, no. 6, pp. 779-785, 1986.
- [167] R. S. Kane, S. Takayama, E. Ostuni, D. E. Ingber, and G. M. Whitesides, "Patterning proteins and cells using soft lithography.," *Biomaterials*, vol. 20, no. 23-24, pp. 2363-76, Dec. 1999.
- [168] S. W. Volk and M. W. Bohling, "Comparative wound healing—Are the small animal veterinarian's clinical patients an improved translational model for human wound healing research?," *Wound Repair Regen.*, vol. 21, no. 3, pp. 372-381, 2013.
- [169] X. Li, J. Liu, Y. Liu, X. Hu, M. Dong, H. Wang, and D. Hu, "Negative pressure wound therapy accelerates rats diabetic wound by promoting aogenesis," vol. 8, no. 3, pp. 3506-3513, 2015.
- [170] G. Moreno-Bueno, H. Peinado, P. Molina, D. Olmeda, E. Cubillo, V. Santos, J. Palacios, F. Portillo, and A. Cano, "The morphological and molecular features of the epithelial-to-mesenchymal transition," *Nat. Protoc.*, vol. 4, no. 11, pp. 1591-1613, Oct. 2009.
- [171] P. J. Brescia and P. Banks, "Investigation of Cell Migration using a High Density Cell Exclusion Assay and Automated Microplate Imager." BioTek, 2013.
- [172] T. M. Keenan and A. Folch, "Biomolecular gradients in cell culture systems.," *Lab Chip*, vol. 8, no. June 2000, pp. 34-57, 2008.